Half-metallic ferromagnets

Katsnelson, M. I.; Irkhin, V. Yu.; Chioncel, L.; Lichtenstein, A. I.; de Groot, R. A.

Published in:
Reviews of Modern Physics

DOI:
10.1103/RevModPhys.80.315

Publication date:
2008

Half-metallic ferromagnets: From band structure to many-body effects

M. I. Katsnelson*

Institute for Molecules and Materials, Radboud University of Nijmegen, NL-6525 ED Nijmegen, The Netherlands

V. Yu. Irkhin

Institute of Metal Physics, 620041 Ekaterinburg, Russia

L. Chioncel

Institute of Theoretical Physics, Graz University of Technology, A-8010 Graz, Austria and Department of Physics, University of Oradea, 410087 Oradea, Romania

A. I. Lichtenstein

Institute of Theoretical Physics, University of Hamburg, 20355 Hamburg, Germany

R. A. de Groot

Institute for Molecules and Materials, Radboud University of Nijmegen, The Netherlands and Zernicke Institute for Advanced Materials, NL-9747 AG Groningen, The Netherlands

(Published 1 April 2008)

A review of new developments in theoretical and experimental electronic-structure investigations of half-metallic ferromagnets (HMFs) is presented. Being semiconductors for one spin projection and metals for another, these substances are promising magnetic materials for applications in spintronics (i.e., spin-dependent electronics). Classification of HMFs by the peculiarities of their electronic structure and chemical bonding is discussed. The effects of electron-magnon interaction in HMFs and their manifestations in magnetic, spectral, thermodynamic, and transport properties are considered. Special attention is paid to the appearance of nonquasiparticle states in the energy gap, which provide an instructive example of essentially many-body features in the electronic structure. State-of-the-art electronic calculations for correlated *d*-systems are discussed, and results for specific HMFs (Heusler alloys, zinc-blende structure compounds, CrO_2, and Fe_3O_4) are reviewed.

DOI: 10.1103/RevModPhys.80.315 PACS number(s): 71.20.Be, 75.50.Cc, 71.10.Fd, 73.20.At

CONTENTS

*M.Katsnelson@science.ru.nl

I. INTRODUCTION

Twenty-five years ago the unusual magneto-optical properties of several Heusler alloys motivated the study of their electronic structure. This yielded an unexpected result: Some of these alloys showed the properties of metals as well as insulators at the *same* time in the *same* material, depending on the spin direction. This property was given the name of half-metallic magnetism (de Groot, Mueller, v. Engen, *et al.*, 1983). Although it is not exactly clear how many half metals are known to exist at this moment, half-metallic magnetism as a phenomenon has been generally accepted. Formally the expected 100% spin polarization of charge carriers in a half-metallic ferromagnet (HMF) is a hypothetical situation that can be approached only in the limit of vanishing temperature and by neglecting spin-orbital interactions. However, at low temperatures (as compared with the Curie temperature, which exceeds 1000 K for some HMFs) and minor spin-orbit interactions, a half metal deviates so markedly from a normal material that the treatment as a special category of materials is justified. The confusion about the number of well-established half metals originates from the fact that there is no "smoking gun" experiment to prove or disprove half metallicity. The most direct measurement is spin-resolved positron annihilation (Hanssen and Mijnarends, 1986), but this is a tedious, expensive technique requiring dedicated equipment. NiMnSb is the only proven HMF so far to the precision of the experiment, which was better than one-hundredth of an electron (Hanssen *et al.*, 1990). This number also sets the scale for concerns about temperature-induced depolarization and spin-orbit effects, detrimental for half metallicity.

The half metallicity in a specific compound should not be confused with the ability to pick up 100% polarized electrons from a HMF. The latter process involves electrons crossing a surface or interface into some medium where their degree of spin polarization is analyzed. This is clearly not an intrinsic materials property. The richness but also the complications of surfaces and interfaces are still not fully appreciated.

Because of these experimental complications, it is not surprising that electronic-structure calculations continue to play an important role in the search for new HMFs, as well as in the introduction of new concepts like half-metallic antiferromagnetism. However, electronic-structure calculations have weaknesses as well. Most of the calculations are based on density-functional theory (DFT) in the local-density or generalized gradient approximation. It is well known that these methods underestimate the band gap for many semiconductors and insulators, typically by 30%. It has been assumed that these problems do not occur in half metals since their dielectric response is that of a metal. This assumption was disproved recently. A calculation on the HMF $La_{0.7}Sr_{0.3}MnO_3$ employing the *GW* approximation (which gives a correct description of band gaps in many semiconductors) leads to a half-metallic band gap 2 eV in excess of the DFT value (Kino *et al.*, 2003). The consequences of this result are potentially dramatic: If it were valid in half-metallic magnetism in general, it would imply that many of the materials showing band gaps in DFT-based calculations of insufficient size to encompass the Fermi energy are actually true half metals. Clearly more work is needed in this area.

The strength of a computational approach is that it does not need samples: calculations can be performed even for nonexistent materials. But, in such an endeavor, a clear goal should be kept in mind. Certainly, computational studies can help in the design of new materials, but the interest is not so much in finding exotic physics in materials that have no chance of ever being realized. Such studies can serve didactical purposes, in which case they will be included in this review. However, the main focus will be devoted to materials that either exist or are (meta)stable enough to have a fair chance of realization.

This review will cover half metals and will not discuss the area of magnetic semiconductors. Some overlap exists, however. The older field of magnetic semiconductors started with semiconductors like the europium monochalcogenides and cadmium-chromium chalcogenides (Nagaev, 1983). Later, the focus changed to the so-called diluted magnetic semiconductors (Delves and Lewis, 1963). These are regular (i.e., III-V or II-VI) semiconductors, where magnetism is introduced by partial substitution of the cation by some (magnetic) 3*d* transition element. The resulting Curie temperatures remained unsatisfactory, however. The next step in the development was the elimination of the nonmagnetic transition element altogether. HMFs could be realized in this way, provided that the remaining transition-metal pnictides could be stabilized in the zinc-blende or related structures. The review will treat not the (diluted) mag-

netic semiconductors as such, but some aspects of metastable zinc-blende HMFs.

HMFs form quite a diverse collection of materials with different chemical and physical properties, and even the origins of the half metallicity can be quite distinct. For this reason, the origin of the band gap must be discussed in terms of two ingredients that define a solid: the crystal structure and the chemical composition. Two aspects are of importance in this context. The first one is "strong magnetism" versus "weak magnetism." In a strong magnet, the magnetic moment will not increase if the exchange splitting is hypothetically increased. Thus the size of the magnetic moment is not determined by the strength of the exchange interaction, but is limited instead by the availability of electron states. In practice, this implies that either the minority-spin subshell(s) responsible for the magnetism is (are) empty or the relevant majority channel(s) is (are) completely filled. In the case of weak magnetism, the magnetic moment is determined by a subtle compromise between the energy gain of an increase in magnetic moment (the exchange energy) and the (band) energy that the increase of the magnetic moment costs. To avoid misunderstanding, we emphasize that this definition of weak and strong magnets differs from that used by Moriya (1985) and most theoretical work on itinerant-electron magnetism. According to Moriya, strong magnets are those with well-defined magnetic moments, which means, for example, Curie-Weiss behavior of the wave-vector-dependent magnetic susceptibility $\chi(\mathbf{q},T)$ in the whole Brillouin zone. In this sense, all HMFs containing Mn ions are strong magnets. However, within this group of materials, we may introduce a finer classification based on the sensitivity of the magnetic moment to small variations of parameters.

All combinations of weak or strong magnetism with majority- or minority-spin band gaps are known today. Thus weak magnets with minority-spin band gaps are found in the Heusler alloys and artificial zinc blendes; examples of weak magnets with majority-spin gaps are the double perovskites and magnetite. The colossal-magnetoresistance materials, as well as chromium dioxide, are examples of strongly magnetic half metals with minority-spin band gaps, while the anionogenic ferromagnets such as rubidium sesquioxide are examples of strongly magnetic half metals with a majority-spin band gap.

An interesting and relatively new development is the work on half-metallic sulfides. The HMF state in oxides with the spinel structure is relatively rare. The prime example, of course, is magnetite. However, any substitution into the transition-metal sublattice leads almost invariably to a Mott insulating state, like the one in magnetite itself below the Verwey transition at 120 K. On the other hand, electrons in sulfides are substantially less well correlated. Hence a wealth of substitutions is possible in order to optimize properties, design half-metallic ferromagnets or antiferromagnets, and so on, without the risk of losing the metallic properties for the second spin direction as well. There is a price to be paid, however: Since the cation-cation distances are larger in sulfides, the Curie and Néel temperatures are lower than in oxides. Nevertheless, the work on half-metallic sulfides deserves much attention.

In all metallic ferromagnets, the interaction between conduction electrons and spin fluctuation is of crucial importance for physical properties. In particular, the scattering of charge carriers by magnetic excitations determines the transport properties of itinerant magnets (temperature dependences of resistivity, magnetoresistivity, thermoelectric power, anomalous Hall effect, etc.). From this point of view, HMFs, as well as ferromagnetic semiconductors, differ from "normal" metallic ferromagnets by the absence of spin-flip (one-magnon) scattering processes. This difference is also important for magnetic excitations since there is no Stoner damping, and spin waves are well defined in the whole Brillouin zone, as in magnetic insulators (Auslender and Irkhin, 1984a; Irkhin and Katsnelson, 1994).

Electron-magnon interaction also modifies considerably the electron energy spectrum in HMFs. These effects occur both in the usual ferromagnets and in HMFs. However, the peculiar band structure of HMFs (the energy gap for one spin projection) results in important consequences. In generic itinerant ferromagnets, the states near the Fermi level are quasiparticles for both spin projections. In contrast, in HMFs, an important role is played by incoherent [nonquasiparticle (NQP)] states that occur near the Fermi level in the energy gap (Irkhin and Katsnelson, 1994). The appearance of the NQP states in the work of Edwards and Hertz (1973) and Irkhin and Katsnelson (1983) is one of the most interesting correlation effects typical of HMFs. The origin of these states is connected with "spin-polaron" processes: Spin-down low-energy electron excitations, which are forbidden for HMFs in the one-particle picture, turn out to be possible as a superposition of spin-up electron excitations and virtual magnons. The density of the NQP states vanishes at the Fermi level but increases greatly at an energy scale of the order of the characteristic magnon frequency $\bar{\omega}$. These states are important for spin-polarized electron spectroscopy (Irkhin and Katsnelson, 2005a, 2006), nuclear magnetic resonance (NMR) (Irkhin and Katsnelson, 2001), and subgap transport in ferromagnet-superconductor junctions (Andreev reflection) (Tkachov *et al.*, 2001). The density of NQP states was calculated from first principles for a prototype HMF, NiMnSb (Chioncel, Katsnelson, de Groot, *et al.*, 2003), as well as for other Heusler alloys (Chioncel, Arrigoni, Katsnelson, *et al.*, 2006), zinc-blende structure compounds (Chioncel *et al.*, 2005; Chioncel, Mavropoulos, Lezaic, *et al.*, 2006), and CrO_2 (Chioncel *et al.*, 2007). Figure 1 shows the NQP contribution to the density of states.

Therefore, HMFs are interesting conceptually as a class of materials which may be convenient to treat many-body solid-state physics that cannot be described by band theory. It is usually accepted that many-body effects lead only to renormalization of the quasiparticle parameters in the sense of Landau's Fermi liquid (FL)

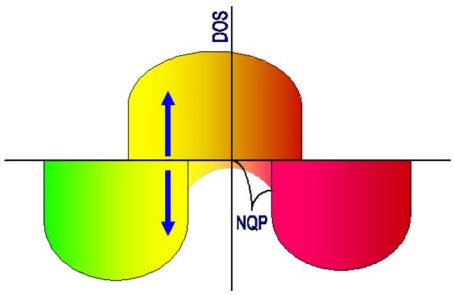

FIG. 1. (Color online) Density of nonquasiparticle states for half-metallic ferromagnets, possessing the gap in the minority spin channel. NQP states are the dominant many-body feature around E_F in comparison with other mean-field effects, such as spin-orbit or noncollinearity, as discussed.

theory, the electronic liquid being qualitatively similar to the electron gas (see, e.g., Nozieres, 1964). On the other hand, NQP states in HMFs are not described by the FL theory. As an example of highly unusual properties of the NQP states, we mention that they can contribute to the T-linear term in the electron heat capacity (Irkhin *et al.*, 1989, 1994; Irkhin and Katsnelson, 1990), even though their density at E_F is zero at temperature $T=0$ K. Some developments concerning the physical effects of NQP states in HMFs are considered in this review.

II. CLASSES OF HALF-METALLIC FERROMAGNETS

A. Heusler alloys and zinc-blende structure compounds

In this section, we treat HMFs with the Heusler $C1_b$ and $L2_1$ structures. Although not Heusler alloys in the strict sense, artificial half metals in the zinc-blende structure will also be discussed because of their close relation with the Heusler $C1_b$ alloys. The zinc-blende structure has a face-centered-cubic (fcc) Bravais lattice with a basis of $(0,0,0)$ and $(1/4,1/4,1/4)$, the two species coordinating each other tetrahedrally. The Heusler $C1_b$ structure consists of the zinc-blende structure with additional occupation of the $(1/2,1/2,1/2)$ site. Atoms at the latter position, as well as those at the origin, are tetrahedrally coordinated by the third constituent, which itself has a cubic coordination consisting of two tetrahedra. The Heusler $L2_1$ structure is obtained by additional occupation of the $(3/4,3/4,3/4)$ site by the same element already present at $(1/4,1/4,1/4)$. This results in the occurrence of an inversion center that is not present in the zinc-blende and Heusler $C1_b$ structures. This difference has important consequences for the half-metallic band gaps. The electronic structure of the Heusler alloys was reviewed recently by Galanakis and Mavropoulos (2007).

1. Heusler $C1_b$ alloys

Interest in fast, nonvolatile mass storage memory sparked much activity in the area of magneto-optics in general, and the magneto-optic Kerr effect (MOKE) specifically, at the beginning of the 1980s. All existing magnetic solids were investigated, leading to a record MOKE rotation of 1.27° for PtMnSb (van Engen *et al.*, 1983). The origin of these properties remained an unsolved problem, however. This formed the motivation to study the electronic structure of the isoelectronic Heusler $C1_b$ compounds NiMnSb, PdMnSb, and PtMnSb, and the subsequent discovery of half-metallic magnetism. Interestingly enough, there seems still to be no consensus on the origin of the magneto-optical properties. The original simple and intuitive explanation (de Groot, 1991) was complementary to the production of spin-polarized electrons by optical excitation in III-V semiconductors. In that case, the top of the valence band is split by the spin-orbit coupling, and the photoexcitation of electrons from the very top of the band by circularly polarized light leads to 50% spin polarization. In contrast, excitations from a valence band are possible for only one of the two components of circular light, as in the case of PtMnSb; this should result in a strong difference of the refraction and absorption for the two opposite polarizations. In PtMnSb, this difference is maximal for visible light, and for NiMnSb the maximum of off-diagonal optical conductivity is shifted to the ultraviolet region. The main contribution to this shift comes from scalar relativistic interactions in the final state (Wijngaard *et al.*, 1989), which are much weaker for Ni than for Pt due to the difference in nuclear charge. Further, the magneto-optical properties of the Heusler alloys were calculated by Antonov *et al.* (1997) in good agreement with experimental data, but the physical explanation was not provided. Recently, Chadov *et al.* (2006) demonstrated that the agreement between the calculated and experimental values for the Kerr rotation and ellipticity in NiMnSb can be improved further by taking into account correlation effects within the so-called local-density approximation plus dynamical mean-field theory (LDA+DMFT) approach (see Sec. IV.A).

Since NiMnSb is the most studied HMF (at least within the Heusler $C1_b$ structures), we concentrate on it here. The origin of its half-metallic properties has an analogy with the electronic structure of III-V zinc-blende semiconductors. Given the magnetic moment of $4\mu_B$, manganese is trivalent for the minority-spin direction and antimony is pentavalent. The Heusler $C1_b$ structure is the zinc-blende one with an additional site $(1/2,1/2,1/2)$ being occupied. The role of nickel is both to supply Mn and Sb with the essential tetrahedral coordination and to stabilize MnSb in the cubic structure (MnSb in the zinc-blende structure is half metallic, but not stable). Thus a proper site occupancy is essential: nickel has to occupy the double tetrahedrally coordinated site (Helmholdt *et al.*, 1984; Orgassa *et al.*, 1999). The similarity in chemical bonding between NiMnSb and zinc-blende semiconductors also explains why it is a weak magnet, as discussed in the Introduction: the presence of occupied manganese minority d states is essen-

tial for the band gap. These states play the same role as the metal *p* states in zinc-blende semiconductors, a situation that is possible only because of the absence of inversion symmetry. The similarity of chemical bonding in Heusler and zinc-blende structures in the original paper (de Groot, Mueller, v. Engen, *et al.*, 1983) was illustrated by "removing the nickel *d* states from the Hamiltonian." This has led to considerable confusion. Actually, the coupling ofmanganese and antimony states through nondiagonal matrix elements of the nickel *d* states was maintained in this calculation.

Several explanations of the band gap have been given in terms of a Ni-Mn interaction only (Galanakis *et al.*, 2002a). While this interaction is certainly present, it is not sufficient to explain the band gap in NiMnSb. These analyses are based on calculations for NiMnSb excluding the antimony, but keeping the volume fixed. This is a highly inflated situation with a volume more than twice the equilibrium one (Egorushkin *et al.*, 1983). Under expansion, bandwidths in metals decrease, leading eventually to a Mott insulating state. But even before this transition, a band gap appears simply due to inflation. This is not a hypothetical scenario: a solid as simple as elemental lithium becomes a half-metallic ferromagnet under expansion (Min *et al.*, 1986), yet there is no evidence for half-metallic magnetism under equilibrium conditions for this element. Also, it is not clear from these considerations why NiMnSb is half metallic only in the case of tetrahedrally coordinated manganese. Probably the chemical bonding in relation to the band gap is best summarized by Kübler (2000): a nickel-induced Mn-Sb covalent interaction.

Surfaces of NiMnSb do not show 100% spin polarization as determined by positron annihilation for the bulk (Bona *et al.*, 1985; Soulen *et al.*, 1999); part of the reason is their tendency to show surface segregation of manganese (Ristoiu *et al.*, 2000). Also, surfaces of NiMnSb are quite reactive and are easily oxidized. But, even without contaminations, none of the surfaces of NiMnSb is genuinely half metallic (de Wijs and de Groot, 2001; Galanakis, 2003). This is just another example of the sensitivity of half-metallic properties in NiMnSb to the correct crystal structure. But this does not necessarily imply that *interfaces* of NiMnSb with, for example, semiconductors cannot be completely spin polarized. For example, it was shown that, at the 111*b* interface of NiMnSb with CdS or InP, the HMF properties are completely conserved if semiconductors are anion terminated at the interface (de Wijs and de Groot, 2001). This anion-antimony bond may look exotic, but such a coordination is quite common in minerals like costobite and paracostobite (minerals are stable on a geological time scale). No experimental verification is available at present, partly because experimentalists tend to prefer the easier 100 surfaces in spite of the fact that calculations show that no half-metallic properties are possible there.

Several photoemission measurements have been reported on NiMnSb (Correa *et al.*, 2006) as well as the closely related PtMnSb (Kisker *et al.*, 1987). We concentrate on the latter because it is the first angular-resolved measurement using single-crystalline samples. Good agreement with the calculated band structure was obtained. This is a remarkable result. In calculations based on density-functional theory, the eigenvalues depend on the occupation. These occupations deviate from the ground state in a photoemission experiment. To very good precision, the dependence of the eigenvalues on the occupation numbers is given by the Hubbard parameter U. The consequence is that the effective U value in alloys like NiMnSb and PtMnSb is much smaller than, e.g., in Ni metal, where photoemission experiments indicate a satellite structure related to the so-called Hubbard bands (Lichtenstein *et al.*, 2001).

The transport properties of NiMnSb have been studied extensively (Otto *et al.*, 1989; Hordequin *et al.*, 2000; Borca *et al.*, 2001); a theoretical discussion of transport properties in HMFs is given in Sec. III.I. At low temperatures, the temperature dependence of the resistivity follows a T^2 law; however, this is absent in thin films (Moodera and Mootoo, 1994). At around 90 K, a transition takes place, beyond which the temperature dependence is $T^{1.65}$. The nature of this phase transition is unknown. One possibility is that it is the effect of thermal excitations, if the Fermi energy is positioned close to the top of the valence band or the bottom of the conduction band. For example, in the latter case, thermal excitations are possible from the metallic majority-spin direction to empty states in the conduction band of the minority-spin direction. Such, excitation reduces the magnetic moment, which in turn will reduce the exchange splitting, resulting in an even greater reduction in the energy difference between the Fermi energy and the bottom of the conduction band. This positive feedback will lead to a collapse of the half-metallic properties at a certain temperature. An analogous situation exists for E_F close to the valence-band maximum. Numerical simulations indicate that this scenario is highly unlikely in the case of NiMnSb because of its unusually low density of states at the Fermi energy. Another explanation has been put forward based on the crossing of a magnon and a phonon branch at an energy corresponding to 80 K (Hordequin, Lelivre-Bernab, and Pierre, 1997; Hordequin, Pierre, and Currat, 1997). It is unclear how this phonon-magnon interaction influences the electronic properties of NiMnSb.

Local magnetic moments have been studied experimentally as a function of temperature with polarized neutron scattering. The manganese moment decreases slightly with increasing temperature from $3.79\mu_B$ at 15 K to $3.55\mu_B$ at 260 K, while the nickel moment remains constant at $0.19\mu_B$ in the same temperature range. On the other hand, magnetic circular dichroism shows a reduction of both the manganese and nickel moments around 80 K. Borca *et al.* (2001) concluded that, at the phase transition, the coupling of the manganese and nickel moments is lost. A computational study (Lezaic *et al.*, 2006) showed vanishing of the moment of nickel at

the transition temperature. None of these anomalies is reflected in the spontaneous magnetization (Otto *et al.*, 1989) of bulk NiMnSb.

Two Heusler $C1_b$ alloys exist, isoelectronic with NiMnSb: PdMnSb and PtMnSb. Their electronic structures are very similar, but we discuss the differences. The calculated DFT band structure for PdMnSb is not half metallic. The minority-spin direction does show a band gap very similar to that of NiMnSb but the Fermi energy intersects the top of the valence band. Reliable calculations (e.g., based on the *GW* approximation) are needed to settle the issue of whether or not PdMnSb is half metallic. PtMnSb is very similar to NiMnSb, the largest differences being in the empty states just above the Fermi energy. The direct band gap (at the Γ point) in PtMnSb is between the triplet top of the valence band (neglecting spin-orbit interactions) and a totally symmetric singlet state. This singlet state is positioned at much higher energy in NiMnSb. These differences have been attributed to the much stronger mass-velocity and Darwin terms in platinum (Wijngaard *et al.*, 1989). Platinum does not carry a magnetic moment in PtMnSb. Consequently, no 90 K anomaly as in NiMnSb is to be expected and none has been reported to date.

Now consider whether half metals in the Heusler $C1_b$ structure exist when other than isoelectronic elements are substituted for Ni in NiMnSb. Since NiMnSb is a weak magnet, substitutions can be made only with elements reducing the total magnetic moment if the half-metallic properties are to be maintained. Thus cobalt, iron, manganese, and chromium will be considered. The case of Co was studied by Kübler (1984). The half-metallic properties are conserved; consequently, the magnetic moment is reduced to $3\mu_B$. Calculations on FeMnSb (de Groot *et al.*, 1986), MnMnSb (Wijngaard *et al.*, 1992), as well as CrMnSb (de Groot, 1991) all show the preservation of the half-metallic properties. In the case of FeMnSb, this implies a reduction of the total magnetic moment per formula unit to $2\mu_B$, which is an unusually small moment to be shared by iron and manganese. It is possible because FeMnSb orders *antiferromagnetically*. Thus the $2\mu_B$ total magnetic moment corresponds to the difference between the moments of iron and manganese rather than to their sum as implied by ferromagnetic ordering. This way of preserving a band gap (energetically favorable from a chemical-bonding point of view) while maintaining a sizable magnetic moments (favorable for the exchange energy) determines the magnetic ordering here. Both of these effects are usually larger than the exchange-coupling energies. The antiferromagnetic ordering is maintained in MnMnSb with a total moment of $1\mu_B$. In the case of CrMnSb, the antiferromagnetic coupling leads to a half-metallic solution with a zero net moment. This is a really exotic state of matter. It is genuinely half metallic, implying 100% spin polarization of the conduction electrons, yet it lacks a net magnetization (de Groot, 1991). The stability of such a solution depends sensitively on the balance between the energy gain of the band gap and the energy gain due to the existence of magnetic moments: if the first one dominates, a nonmagnetic semiconducting solution will be more stable (remember that the two spin directions are isoelectronic here).

In reality, the situation is more complex. CoMnSb does exist, but it crystallizes in a tetragonal superstructure with Co partially occupying the empty sites (Senateur *et al.*, 1972). The magnetic moments deviate from the ones expected for a half-metallic solution. FeMnSb does not exist, but part of the nickel can be substituted by iron. Up to 10%, the Heusler $C1_b$ structure is maintained, from 75% to 95% a structure comparable with CoMnSb is stable, and between 10% and 75% both phases coexist (de Groot *et al.*, 1986). MnMnSb exists, orders antiferromagnetically, and has a net moment of $1\mu_B$. It does not crystallize in the Heusler $C1_b$ structure and consequently is not half metallic. CrMnSb exists, is antiferromagnetic at low temperatures, and shows a transition at room temperature to a ferromagnetic phase.

A different substitution is the replacement of Mn by another transition metal. An interesting substitution is a rare-earth element *R*. Because of the analogy of half metals with $C1_b$ structure and III-V semiconductors, one expects Ni*R*Sb compounds to be nonmagnetic semiconductors.

Several of these compounds do exist in the $C1_b$ structure. Some examples are Sc, Y, and heavy rare-earth elements from the second half of the lanthanide series. All of them are indeed semiconductors (Pierre *et al.*, 1999; Pierre and Karla, 2000). Doping of NiMnSb by rare-earth elements has been suggested as a way to improve the finite-temperature spin polarization in NiMnSb. These substitutions do not influence the electronic band structure much (see also Sec. V.A.2), the band gap for the minority-spin direction remaining completely intact. However, the random substitution of nonmagnetic (Y, Sc) or very different (Ho–Lu) magnetic elements for manganese will modify the magnon spectrum (Attema *et al.*, 2004; Chioncel, 2004). This could be beneficial in increasing spin polarization in some temperature ranges.

2. Half metals with zinc-blende structure

The Curie temperatures of diluted magnetic semiconductors remain somewhat disappointing. A solution is to replace all the main group metals by transition metals. But there is a heavy price to be paid: These systems can be prepared only as metastable states—if at all—on a suitable chosen substrate. An alternative way to come to the same conclusion is to consider Heusler $C1_b$ alloys with larger band gaps. This is most easily accomplished by replacement of the antimony with arsenic or phosphorus. No stable Heusler $C1_b$ alloys exist with these lighter pnictides, however. An alternative is to try to grow them as metastable systems on a suitable chosen substrate. This makes nickel superfluous, since it fails in the case of lighter pnictides to play the role it does so well in NiMnSb. The bottleneck in this quest is not so

much in predicting systems that are good half metals, but in designing combinations of half metals and substrates that are metastable enough to have a chance of being realized experimentally.

Shirai *et al.* (1998) were the first to relate concentrated magnetic semiconductors with half-metallic magnets in their study of MnAs in the zinc-blende structure. The experimental realization indeed showed an increase of the Curie temperature: 400 K was reported for CrAs grown on GaAs. Xie, Xu, Liu, *et al.* (2003) calculated the stability of all 3*d* transition-metal chalcogenides in the zinc-blende structure with respect to the ground-state structure. Chromium telluride and selenide, as well as vanadium telluride, are good half metals that are stable toward tetrahedral and rhombohedral distortions. Zhao and Zunger (2005) considered the stability of an epitaxial layer as a function of the lattice parameter of the substrate, allowing for relaxation in the growth direction. The result is that, while the bulk zinc-blende phase is always unstable with respect to the (equilibrium) NiAs structure, there exist lattice constants for which the epitaxial zinc-blende phase is more stable than the epitaxial nickel arsenide structure. This is realized (computationally) for half-metallic CrSe.

An alternative to the concentrated III-V magnetic semiconductors is given by δ-doped III-V semiconductors. Here the magnetic properties are not introduced by a more or less homogeneous replacement of main group metals by magnetic transition metals. Instead, a very thin transition-metal layer is sandwiched between undoped III-V semiconductor materials (Nazmul *et al.*, 2002). The result is a clear increase in Curie temperature (Chiba *et al.*, 2003). This is not unrelated to the interface half metallicty introduced earlier (de Groot, 1991).

3. Heusler $L2_1$ alloys

The crystal structure of the Heusler $L2_1$ alloys is closely related to that of the $C1_b$ alloys. In the $L2_1$ structure, the $(1/2,1/2,1/2)$ position, empty in the $C1_b$ structure, is occupied by the same element that occupies the $(0,0,0)$ position. The similarity in structure suggests a similarity in interactions and physical properties, but, on the contrary, the interactions and physical properties of the two classes are actually quite distinct. The introduction of the fourth atom in the unit cell introduces an inversion center in the crystal structure. The band gap in the $C1_b$ compounds resulted from an interaction very similar to that in III-V semiconductors, where the manganese t_{2g} d electrons play the role of the p electrons in the III-V semiconductor. This is no longer possible in the presence of an inversion center. Consequently, bandwidths are reduced and usually Van Hove singularities occur in the vicinity of the Fermi energy. The smaller bandwidth leads to several (pseudo)gaps. Correlation effects are expected to become more observable here.

Another difference is the occurrence of defects. Experimentally it was noted that "the strong effect of cold work on Heusler alloys ($L2_1$ structure) contrasts with almost unobservable effects in the $C1_b$ structure alloy NiMnSb" (Schaf *et al.*, 1983). But here also there are indications that defects that destroy the band gap are energetically less favorable.

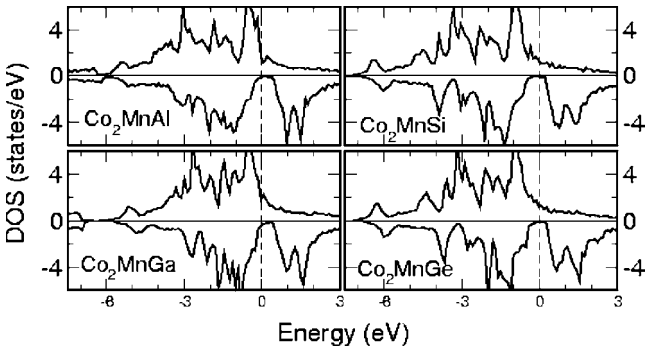

FIG. 2. DOS for the Co_2MnZ compounds with Z=Al, Si, Ge, Sn (Galanakis *et al.*, 2006).

Experimental work goes back to Heusler in the beginning of the last century. The motivation for his work was the possibility of preparing magnetic alloys from nonmagnetic elements (Heusler, 1903). (A material was considered magnetic in that period only if it possessed a spontaneous net magnetization.) More recently, the work of Ziebeck and Webster on neutron-diffraction investigations (Ziebeck and Webster, 1974) deserves mention as well as the NMR work by the Orsay group of Campbell.

The first band-structure calculations were by Ishida and co-workers (Ishida *et al.*, 1976a, 1976b, 1980, 1982), and by Kuebler, Williams, and Sommers (Kübler *et al.*, 1983). The latter contains a clue to half-metallic properties in the $L2_1$ compounds. The authors remark the following: "The minority-state densities at the Fermi energy for ferromagnetic Co_2MnAl and Co_2MnSn nearly vanish. This should lead to peculiar transport properties in these two Heusler alloys."

Calculations that explicitly addressed the question of half-metallic properties in the full Heusler alloys appeared not earlier than 1995 (Fujii *et al.*, 1995; Ishida *et al.*, 1995). A systematic study of the electronic structure of Heusler $L2_1$ compounds was undertaken by Galanakis, Dederichs, and Papanikolaou (Galanakis *et al.*, 2002b). That work also reviews half-metallic magnetism in full Heusler compounds upto 2002. For this reason, we refer to it for details and concentrate on subsequent developments here. (See Fig. 2.)

The Heusler $L2_1$ compounds have a unique position in the spectrum of half metals because of their Curie temperatures. High Curie temperatures are important in the application of half metals at finite temperature, since many of the depolarization mechanisms scale with the reduced temperature T/T_C. The Curie temperatures here approach 1000 K, Co_2MnSn shows a Curie temperature of 829 K, the germanium analog 905 K, while Co_2MnSi was a record holder for some time with a Curie temperature of 985 K (Brown *et al.*, 2000). A further increase was realized in Co_2FeSi. Experimentally an integer magnetic moment of $6\mu_B$ and a Curie temperature

of 1100 K were found (Wurmehl *et al.*, 2005). This result was not reproduced in calculations employing the LDA approximation. The magnetic moment of $6\mu_B$ could only be reproduced by the application of U in excess of 7.5 eV. This is an unusually high value and alternative explanations should also be considered. The question of lattice defects has been studied. On the basis of neutron diffraction, Co-Fe disorder can be excluded, but no data are available for the degree of Fe-Si interchange. Calculation of the magnetic saturation moment as a function of the iron-silicon disorder seems a logical next step in the understanding of this fascinating compound.

Whereas the investigations of the bulk electronic structures of full Heusler alloys have advanced comparably to those of half Heusler alloys, the situation with respect to the preservation of half-metallic properties at surfaces and interfaces still lags behind. Two important results were obtained recently. One result is the preservation of half-metallic properties of a Co_2MnSi (001) surface provided it is purely manganese terminated. This is the only surface of this half metal showing this property (Hashemifar *et al.*, 2005).

No genuine half-metallic interfaces between full Heusler alloys and semiconductors have been reported yet, but the results for $Co_2CrAl/GaAs$ look promising. For a (110) interface, a spin polarization of ≈90% was obtained (Nagao *et al.*, 2004). Although this is clearly not a genuine half-metallic interface, it should provide a good basis to analyze why half-metallic behavior is lost at an interface, in analogy with the successful work in the $C1_b$ case.

An interesting development in half-metallic magnetism is in electron-deficient full Heusler alloys. Reduction of the number of valence electrons to 24 per formula unit leads to either a nonmagnetic semiconductor or a half-metallic antiferromagnet. But, remarkably enough, the reduction of the number of valence electrons can be continued here, reentering a range of half-metals but now with a band gap for the majority-spin direction. This is best exemplified for the case of Mn_2VAl. It is a half-metallic ferrimagnet as calculated with the generalized gradient exchange-correlation potential (Weht and Pickett, 1999). Half metals with a band gap for the majority-spin direction rarely occur. The search for new candidates should be strongly supported.

B. Strongly magnetic half metals with minority-spin gap

1. Chromium dioxide

Chromium dioxide is the only metallic oxide of chromium. It orders ferromagnetically with a Curie temperature of about 390 K. Its half-metallic state was discovered by band-structure calculations (Schwarz, 1986; Matar *et al.*, 1992). The origin of the half metallicity is straightforward: in an ionic picture, chromium is in the form of a Cr^{4+} ion. The two remaining d electrons occupy the majority d states. The crystal-field splitting is that of a (slightly) deformed octahedron. The valence band for the majority-spin direction is 2/3 filled, hence the metallic properties. The minority-spin d states are at a significant higher energy due to the exchange splitting. For this reason, the Fermi level falls in a band gap between the (filled) oxygen $2p$ states and the (empty) chromium d states. Thus the HMF properties of chromium dioxide are basically properties of chromium and its valence and, as long as the crystal-field splitting is not changed too drastically, the half-metallic properties are conserved. This implies that the influence of impurities should not be dramatic, and a number of surfaces retain the half metallicity of the bulk. As a matter of fact, all the surfaces of low index are half metallic, with the possible exception of one of the (101) surfaces (van Leuken and de Groot, 1995; Attema *et al.*, 2006). Although initial measurements did not confirm these expectations (Kämper *et al.*, 1987), they were confirmed later by experiments with tunneling (Bratkovsky, 1997) and Andreev reflection (Ji *et al.*, 2001) on well-characterized surfaces. Recently, the flow of a triplet-spin supercurrent was realized in CrO_2 sandwiched between two superconducting contacts (Keizer *et al.*, 2006).

As mentioned before, an interesting question is the origin of metallic ferromagnetism in CrO_2. This was explained in terms of the double-exchange (Zener) model by Korotin *et al.* (Korotin *et al.*, 1998; Schlottmann, 2003). The octahedral coordination in the rutile structure is slightly distorted. This leads to splitting of the degenerate t_{2g} state into a more localized d_{xy} state and more delocalized d_{xz} and d_{yz} states (or linear combinations of these). The localized filled d_{xy} state plays the same role as the filled t_{2g} majority-spin state in the Zener double-exchange model, while the partially occupied $d_{xy} \pm d_{yz}$ majority states in CrO_2 play the role of the partially occupied e_g states. The transport properties of CrO_2 have been investigated in detail (Watts *et al.*, 2000) and interpreted in terms of a two-band model, very much in line with the double-exchange model for CrO_2.

The importance of explicit electron-electron interactions in CrO_2 remains a subject of active research. On the one hand, Mazin, Singh, and Ambrosch-Draxl (1999) compared local spin-density approximation (LSDA) calculations with experimental optical conductivities and found no indications for strong-correlation-related exotic phenomena. On the other hand, Craco, Laad, and Müller-Hartman (Laad *et al.*, 2001; Craco *et al.*, 2003) considered photoemission results and conductivity (both dc and optical) and confirmed the importance of dynamical correlation effects. The ferromagnetic correlated state was also investigated in a combined local and nonlocal approach (Chioncel *et al.*, 2007), which demonstrates that the d_{xy} orbital is not completely filled and localized as described by the LDA+U or model calculations (Korotin *et al.*, 1998; Schlottmann, 2003; Toropova *et al.*, 2005). More recently, Toropova, Kotliar, Savrasov, and Oudovenko (Toropova *et al.*, 2005) concluded that the low-temperature experimental data are best fitted without taking into account the Hubbard U corrections. Chromium dioxide will clearly remain an area of active research.

2. The colossal-magnetoresistance materials

The interest in ternary oxides of manganese with divalent or trivalent main group metals goes back to Van Santen and Jonker (Jonker and Santen, 1950). The occurrence of ferromagnetism in transition-metal oxides, considered unusual at that time, was explained by Zener (1951) with the introduction of the "double-exchange" mechanism. In the 1970s and 1980s, these systems were investigated theoretically in connection with the problem of phase separation and "ferron" (magnetic polaron) formation in ferromagnetic semiconductors (Auslender and Katsnelson, 1982; Nagaev, 1983). The interest in spintronics developing 15 years ago revived the interest in the ternary manganese perovskites, generally referred to as colossal-magnetoresistance (CMR) materials. A wealth of interesting physics is combined in a single phase diagram of, for example, $La_{1-x}Sr_xMnO_3$. From a "traditional" antiferromagnetic insulator for $x=1$, the reduction of x results in a ferromagnetic metallic state, while finally at $x=0$ a Mott insulating antiferromagnet is found. Some of the transitions are accompanied by charge and/or orbital ordering. Finite temperatures and applied magnetic fields complicate the phase diagram substantially. The ferromagnetic metallic phase for intermediate values of x is presumably half metallic (Pickett and Singh, 1996). We concentrate on this phase here and refer to other reviews for a more complete overview of the manganites (Nagaev, 2001; Salamon and Jaime, 2001; Ziese, 2002; Dagotto, 2003).

Once the occurrence of ferromagnetic magnetic ordering is explained, the discussion of half-metallic magnetism is rather straightforward. Manganese possesses around 3.5 d electrons in the metallic high-spin state; its rather localized majority-spin t_{2g} state is filled, the majority, much more dispersive, e_g state is partially occupied, and the minority d states are positioned at higher energy, thus being empty. Hence, a rather large band gap exists for the minority spin at the Fermi energy, and the manganites are strong magnets. Correlation effects are expected to be much stronger here. Notice that no reference has been made to the actual crystal structure: subtleties such as those in the Heusler structure are absent here. The half-metallic properties basically stem from the valence of the manganese alone. Surface sensitivity of the HMF properties is not expected as long as the valence of the manganese is maintained: this is easily accomplished in the layered manganites (de Boer and Groot, 1999).

Experimental verification of half-metallic properties has not been without debate. The origin of the controversy is that the calculated position of the Fermi energy in the energy gap is invariably very close to the bottom of the conduction band. Experimental confirmation of the HMF behavior by photoemission (Park *et al.*, 1998) was contested on the basis of Andreev reflection measurements that showed minority-spin d states at the Fermi energy (Nadgorny *et al.*, 2001; Nadgorny, 2007). Also, tunneling experiments initially cast doubt on the half-metallic properties (Viret *et al.*, 1997; Jo, Mathur, Evetts, and Blamire, 2000; Jo, Mathur, Todd, and Blamire, 2000). Mazin subsequently introduced the concept of a transport half metal: the Fermi energy may straddle the bottom of the minority-spin t_{2g} band, but since these states are localized this does not influence the half-metallic properties as far as transport is concerned (Mazin *et al.*, 1999; Nadgorny, 2007). Recent magnetotransport measurements on better samples support the HMF picture of the CMR materials (Bowen *et al.*, 2003). Recent *GW* calculations by Kino *et al.* (2003) shed a different light on this matter. In these calculations, the half-metallic band gap is increased by as much as 2 eV with respect to the DFT value. This implies that the minority-spin d band is not even close to the Fermi energy, and the CMR materials should be considered as genuine HMFs.

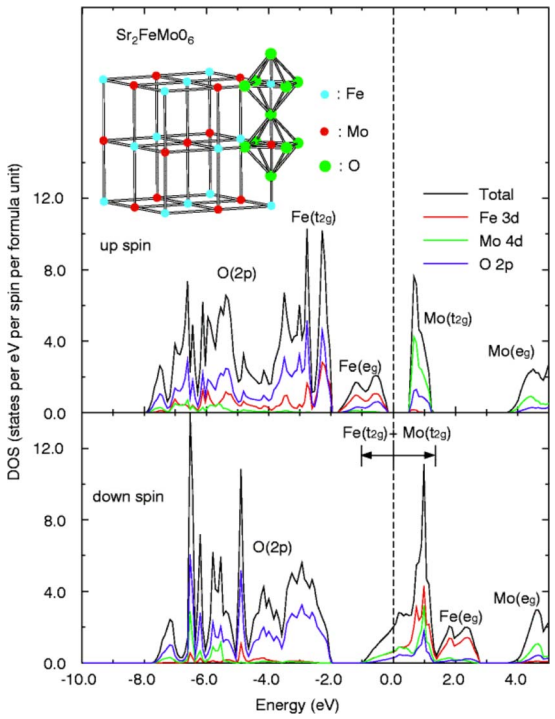

FIG. 3. (Color online) Density of states (DOS) of Sr_2FeMoO_6 (Kobayashi *et al.*, 1998).

C. Weakly magnetic half metals with majority-spin gap

1. The double perovskites

The double perovskites have a unit cell twice the size of the regular perovskite structure. The two transition-metal sites are occupied by different elements. Double perovskites are interesting for two reasons: first-, half-metallic antiferromagnetism has been predicted to occur for La_2VMnO_6 (Pickett, 1998) (we return to this in Sec. II.E.2); second, high Curie temperatures can be occur as compared with the regular perovskites. Sr_2FeMoO_6 was the first example to be studied in this respect by means of band-structure calculations (Kobayashi *et al.*, 1998). The density of states is shown in Fig. 3. In the majority-spin direction, the valence band consists of filled oxygen

2*s* and 2*p* states as well as a completely filled Fe 3*d* band, showing the usual crystal-field splitting. A band gap separates the conduction band, which is primarily formed by molybdenum *d* states. The minority-spin direction shows an occupied oxygen-derived valence band and a hybridized *d* band of mixed iron and molybdenum character. It intersects the Fermi energy.

The Curie temperature is in the range 410–450 K. More recently, a similar behavior was found for Sr_2FeReO_6 (Kobayashi *et al.*, 1999). Optical measurements did show excitations across the half-metallic band gap of 0.5 eV (Tomioka *et al.*, 2000). A substantially higher Curie temperature is found in Sr_2CrReO_5, $T_C = 635$ K (Kato *et al.*, 2002), but band-structure calculations showed that the band gap for the majority-spin direction is closed by the spin-orbit interaction (Vaitheeswaran *et al.*, 2005).

2. Magnetite

Magnetite Fe_3O_4 is one of the most widespread natural iron compounds and the most ancient magnetic material known. Surprisingly, we still have no complete explanation of its magnetic, electronic, and even structural properties; many issues about this substance remain controversial. At room temperature, magnetite has inverted cubic spinel structure with tetrahedral *A* sites occupied by Fe^{3+} ions, whereas octahedral *B* sites are randomly occupied by Fe^{2+} and Fe^{3+} ions with equal concentrations. Fe_3O_4 is a ferrimagnet with a high Curie temperature $T_C \simeq 860$ K. As discovered by Verwey (1939), at $T_V \simeq 120$ K magnetite undergoes a structural distortion and metal-insulator transition. Usually the Verwey transition is treated as a charge ordering of Fe^{2+} and Fe^{3+} states in octahedral sites [for a review, see Mott (1974, 1980)]. The nature of the Verwey transition and the low-temperature phase of Fe_3O_4 has been the subject of numerous investigations which are beyond the scope of our topic; see, e.g., recent reviews (Walz, 2002; Garsia and Sabias, 2004). As demonstrated by a band-structure calculation (Yanase and Siratori, 1984), magnetite in the cubic spinel structure is a rather rare example of a HMF with majority-spin gap. This means a saturated state of itinerant 3*d* electrons propagating over *B* sites, the magnetic moment being close to $4\mu_B$ per formula unit. Recently, this picture was questioned by x-ray magnetic circular dichroism (XMCD) data (Huang *et al.*, 2004), which were interpreted as evidence of a large orbital contribution to the magnetization and nonsaturated spin state. However, later XMCD experiments (Goering *et al.*, 2006) confirmed the purely spin-saturated magnetic state. Direct measurements of spin polarization by spin-polarized photoemission spectroscopy (Mortonx *et al.*, 2002) yield a value of about −40% (instead of −100% predicted by a naive band picture), which might be due to both surface effects and electron correlations in the bulk (see Sec. III.C). The transport properties of Fe_3O_4-based films have been intensively studied [see, e.g., Eerenstein *et al.* (2002) and Zhao *et al.* (2005)]. In particular, a large magnetoresistance was found, owing to electron propagation through antiphase boundaries (Eerenstein *et al.*, 2002).

Unlike the Heusler alloys, magnetite is a system with a narrow 3*d* band and therefore strong-correlation effects. The metal-insulator transition can already be considered as evidence of strong electron-electron interaction (Mott, 1974). The influence of these effects on the electronic structure of Fe_3O_4 was considered recently by Craco *et al.* (2006) and Leonov *et al.* (2006).

D. Strongly magnetic half metals with majority-spin gap

1. Anionogenic ferromagnets

Until recently, strongly magnetic HMFs with a majority-spin band gap were unknown. The chemical composition of the compounds calculated to be half metallic in this category was quite unexpected: heavy alkali-metal oxides (Attema *et al.*, 2005). The magnetic moment is carried by complex oxygen ions, hence the name. In addition to the oxygen molecule, which has two unpaired electrons, the O^{2-} ion occurs in the so-called hyperoxides such as RbO_2 and CsO_2. These are antiferromagnetic insulators with rather low Néel temperatures. Another molecular ion of interest is the nonmagnetic peroxide ion O_2^{2-}. In the series molecular oxygen–hyperoxide ion–peroxide ion, the antibonding π orbital is progressively filled, leading to vanishing of the magnetic moment for the peroxides. Sesquioxides also exist; these have a composition between peroxide and hyperoxide. They are rather stable thermally, but do react with atmospheric water and carbon dioxide. The analogy between the holes in the antibonding doubly degenerate π level and the electrons in the doubly degenerate antibonding e_g level of the colossal-magnetoresistance materials motivated a computational study. This yielded a HMF state with surprisingly high Curie temperatures (300 K). A partial explanation is the absence of superexchange in these oxides, since the mediators for it, the alkali-metal ions, do not possess the required electron states in the vicinity of the Fermi level. Direct experimental evidence is unfortunately lacking. Indirect evidence is the cubic crystal structure measured down to 5 K (unlike in peroxides and hyperoxides), the crystallographic equivalence of molecular oxygen ions, the occurrence of charge fluctuations down to 5 K (Jansen *et al.*, 1999), the opaque optical properties, and indications of unusual widths of the stability regions of the sequioxides in the oxygen-rubidium and oxygen-cesium phase diagrams (Rengade, 1907).

E. Sulfides

The spectacular developments in the area of high-temperature superconductivity followed by the interest in colossal-magnetoresistance materials have pushed the interest in sulfides and selenides somewhat into the background. These materials have some advantages over oxides, however. Two main differences, both due to the increased metal-anion covalence as compared with

oxides, are of importance here: the more correlated behavior of the oxides as well as their preference for a high-spin configuration. Sulfides often prefer a low-spin configuration, which makes their behavior less predictable without careful computation. So the sulfur analog of magnetite, the mineral greigite, has a magnetic moment of $2\mu_B$ only, compared with $4\mu_B$ of magnetite. Consequently, it is not half metallic. In the widespread mineral pyrite, FeS_2, iron has a nonmagnetic d^6 configuration, unimaginable in oxides. As mentioned before, magnetite shows half-metallic properties, but is at the brink of Mott localization: cooling below 120 K suffices to accomplish this. On the other hand, the much less correlated behavior of sulfospinels allows a broad range of transition metals to occupy the octahedral and tetrahedral cation sites without the risk of a Mott insulating state. This does not hold for all the pyrites, however. Thus FeS_2 is a nonmagnetic semiconductor. The excellent agreement between LDA calculations and the photoemission spectra indicates negligible correlation effects (Folkerts *et al.*, 1987). CoS_2 is a ferromagnetic metal with a Curie temperature of 122 K. The magnetic moments were calculated as a function of the Hubbard U, and comparison with experimental data indicated the importance of U (of less than1 eV). NiS_2 is a Mott insulator. $NiSe_2$ is metallic while in $NiSe_{2x}S_{2(1-x)}$ the strength of the correlation effects can be adjusted by variations in the composition.

Magnetic ordering temperatures, important for maintaining the polarization of charge carriers at finite temperature, of oxides are usually higher than those of sulfides and selenides.

1. Pyrites

Saturated itinerant ferromagnetism in the pyrite-structure system $Fe_{1-x}Co_xS_2$ was discovered experimentally by Jarrett *et al.* (1968) and discussed from the theoretical-model point of view by Auslender *et al.* (1988). Half-metallic ferromagnetism in pyrites was first considered in band calculations by Zhao, Callaway, and Hayashibaran (1993). Their results for CoS_2 near the Fermi energy show two completely filled t_{2g} bands for the two spin directions: a partial filled e_g majority band as well as a minority e_g band just overlapping the Fermi energy. At slightly higher energy, antibonding sulfur $3p$ states are found. Clearly, cobalt disulfide is an almost half-metallic ferromagnet. It has also been suggested that half-metallic magnetism can be obtained in the ternary system $Fe_xCo_{1-x}S_2$, an idea explored further by Mazin (2000). He calculated that the expected HMF region in the phase diagram extends from 0.2 to 0.9. A detailed study, both computational and experimental (Wang *et al.*, 2005), revealed a strong dependence of the spin polarization at the Fermi level on the composition. Theoretically, 100% spin polarization is obtained for $x=0.25$, whereas the maximal polarization (85%) determined with Andreev reflection at 4.2 K is obtained at $x=0.15$; the polarization drops for higher concentrations of iron. The Fermi level is located very close to the bottom of the conduction band. This can lead to thermal instabilities of the half metallicity as discussed for NiMnSb. Recently, half-metallic properties of pyrite-structure compounds have been reviewed by Leighton *et al.* (2007).

2. Spinels

For the spinels, there is less activity in the area of half metallicity. A complication in this class of compounds is that of cation ordering. The application of high temperatures leads to disproportionation, so long annealing at lower temperatures may be required. The type of cation ordering depends on the preparation conditions. On the other hand, once controlled, the cation occupancy can form a degree of freedom to achieve HMF materials.

$CuCr_2S_4$, one of the compounds considered in a study on chromium chalcogenides, is of interest here. It shows an almost HMF band structure: the Fermi level is positioned 50 meV below the top of the valence band (Antonov *et al.*, 1999).

Sulfospinels were also considered in detail in the quest for the elusive half-metallic antiferromagnet (Park *et al.*, 2001; Min *et al.*, 2004). $Mn(CrV)S_4$, with chromium and vanadium occupying the octahedral sites, is calculated to satisfy all the requirements. It shows a band gap of approximately 2 eV, while the Fermi level intersects a band of primarily vanadium character. The Mn moment is compensated by the moments of chromium and vanadium on the octahedral sites. Another sulfospinel with predicted half-metallic properties is $(Fe_{0.5}Cu_{0.5})(V_{0.5}Ti_{1.5})_2S_4$. In this case, the metallic behavior is attributed to the atoms at the tetrahedral site; their magnetic moments are exactly canceled by those at the octahedral site.

F. Miscellaneous

1. Ruthenates

The $3d$ transition elements and their compounds have been studied in much more detail than their $4d$ and $5d$ analog. Part of the reason for this is that magnetism is expected to be favored more in the $3d$ series where no d core is present. Ruthenium is a perfect example of the contrary. The binary and ternary oxides of this $4d$ transition metal show a rich variety of physical properties such as ferromagnetism in $SrRuO_3$ and unconventional superconductivity in Sr_2RuO_4 (Maeno *et al.*, 1994). Here we consider the case of $SrRuO_3$. Ruthenium is tetravalent in this compound, just as in RuO_2. The latter compound is a nonmagnetic metal with $4d$ electrons in the slightly split t_{2g} subband. In $SrRuO_3$, a magnetic, low-spin state occurs with a filled t_{2g} majority-spin band and a partially filled t_{2g} minority-spin band. Thus all ingredients seem to be present for a half metal. Calculations showed that the exchange and crystal-field splitting are not sufficient to create a band gap large enough to encompass the Fermi energy. Recently, it was shown that the application of the LDA+U method leads to a sub-

stantial increase in the band gap in conjunction with orbital ordering. Thus a half-metallic solution is obtained. Comparison with experiment does not lead to a definite conclusion. No experimental determination of U is available. The measured magnetic moment is more in line with the LDA results ($0.8\mu_B$–$1.6\mu_B$), but extrapolation to the high-field limit could lead to an integer magnetic moment. There is no experimental evidence for orbital ordering, however.

The research on ruthenates is relatively recent; in particular, ternary compounds have not yet been investigated exhaustively.

2. Organic half metals

Conducting organic materials have been an area of active research since the discovery of electrical conduction in doped polyacetylene (Shirakawa *et al.*, 1977). A surge of activities has resulted in applications generally referred to as plastic electronics. Recently, attempts have been made to develop HMFs suitable for these applications. Originally, the focus was on carbon nanotubes in which magnetism was achieved by the introduction of 3*d* metals. Calculations were performed for 3,3 single-wall carbon nanotubes with a linear iron nanowire inside (Rahman *et al.*, 2004). Structure optimization resulted in a slightly asymmetrical position of the iron wire in the nanotube. The results were somewhat disappointing: the iron loses its magnetic moment and the overall system is semiconducting. A subsequent investigation of the 3,3 single-wall carbon nanotube with a linear cobalt wire inside resulted in a HMF band structure with the band gap for the minority-spin direction of order 1 eV. This band structure is very much like that of the iron system. The metallic properties are caused by the extra electron of the cobalt system, which is completely absorbed by the majority-spin band structure.

Another series of materials investigated is inspired by the molecule ferrocene. This is a so-called sandwich complex with an Fe ion between two cyclopentadienyl anions. Ferrocene can be considered to be the first member of a series of so-called multiple-decker sandwich structures. They are formed by adding additional pairs of iron atoms and cyclopentadienyl molecules. Thus the chemical structure is fundamentally different from the nanotubes discussed above: The latter can be thought of as two interacting wires in parallel, one of organic and one of metal nature. The former is characterized by a parallel stacking of cyclopentadienyl (or benzene) rings coupled together by transition-metal atoms. The synthesis of these systems was shown to be possible for various vanadium-benzene clusters (Hoshino *et al.*, 1995). The most promising candidate at the moment is the one-dimensional manganese-benzene polymer (Xiang *et al.*, 2006). It is a genuine HMF with a moment of $1\mu_B$. The ferromagnetic ordering is much more stable than the antiferromagnetic. This large difference (0.25 eV) can be traced back to the coexistence of a rather narrow and rather dispersive band for the metallic spin direction, a scenario reminiscent of the double-exchange model.

III. MODEL THEORETICAL APPROACHES

A. Electron spectrum and strong itinerant ferromagnetism in the Hubbard model

To investigate the spectrum of single-particle and spin-wave excitations in metallic magnets, we use many-electron models that enable us to describe the effects of interelectron correlations. The simplest such model is the Hubbard model. In the case of a nondegenerate band, its Hamiltonian reads

$$\mathcal{H} = \sum_{\mathbf{k}\sigma} t_{\mathbf{k}} c^{\dagger}_{\mathbf{k}\sigma} c_{\mathbf{k}\sigma} + \mathcal{H}_{\mathrm{int}},$$

$$\mathcal{H}_{\mathrm{int}} = U \sum_i c^{\dagger}_{i\uparrow} c_{i\uparrow} c^{\dagger}_{i\downarrow} c_{i\downarrow} \tag{1}$$

with U being the on-site repulsion parameter and $t_{\mathbf{k}}$ the bare electron spectrum. The Hubbard model was widely used to consider itinerant electron ferromagnetism since it takes into account the largest term of the Coulomb interaction, namely, the intra-atomic one. Despite its apparent simplicity, this model contains very complex physics, and its rigorous investigation is a difficult problem.

The simplest Hartree-Fock (Stoner) approximation in the Hubbard model (1), which corresponds formally to first-order perturbation theory in U, yields an electron spectrum of the form

$$E_{\mathbf{k}\sigma} = t_{\mathbf{k}} + U n_{-\sigma} = t_{\mathbf{k}} + U\left(\frac{n}{2} - \sigma\langle S^z\rangle\right) \equiv t_{\mathbf{k}\sigma} \tag{2}$$

($n_\sigma = \langle c^{\dagger}_{i\sigma} c_{i\sigma}\rangle$), so that we have for the spin splitting $\Delta = U(n_\uparrow - n_\downarrow) = 2U\langle S^z\rangle$, and U plays the role ofthe Stoner parameter.

Consider more strictly the case of a half-metallic (saturated) ferromagnet in which $n_\uparrow = n = 1 - n_0$, $n_\downarrow = 0$ (note that, for realistic HMFs, the saturated ferromagnetic behavior is described by the generalized Slater-Pauling rule; see Sec. III.F). Then the spin-up electrons behave at $T = 0$ K as if free,

$$G_{\mathbf{k}\uparrow}(E) = (E - t_{\mathbf{k}})^{-1}. \tag{3}$$

For spin-down states, the situation is nontrivial. Writing down the sequence of equations of motion for $G_{\mathbf{k}\downarrow}(E)$ and for the Green's function

$$\Phi_{\mathbf{kp}}(E) = \langle\langle S^{+}_{\mathbf{p}} c_{\mathbf{k}-\mathbf{p}\uparrow} | c^{\dagger}_{\mathbf{k}\downarrow}\rangle\rangle_E, \quad S^{+}_{\mathbf{q}} = \sum_{\mathbf{k}} c^{\dagger}_{\mathbf{k}\uparrow} c_{\mathbf{k}+\mathbf{q}\downarrow} \tag{4}$$

and performing decoupling in the spirit of a ladder approximation, we obtain for the self-energy

$$\Sigma_{\mathbf{k}\downarrow} = \frac{U n_\uparrow}{1 - U R_{\mathbf{k}}(E)}, \tag{5}$$

where

$$R_{\mathbf{k}}(E) = \sum_{\mathbf{q}} \frac{1 - n_{\mathbf{k}-\mathbf{q}}}{E - t_{\mathbf{k}-\mathbf{q}} - \omega_{\mathbf{q}}} \tag{6}$$

describes the electron-magnon scattering, $n_{\mathbf{k}} = f(t_{\mathbf{k}})$ is the Fermi function. This result corresponds to the Edwards-Hertz approximation (Edwards and Hertz, 1973).

In a more general nonsaturated situation, one obtains for the self-energy to second order in U (Irkhin and Katsnelson, 1990)

$$\Sigma_{\mathbf{k}\sigma}(E) = -U^2 \sum_{\mathbf{q}} \int_{-\infty}^{\infty} \frac{d\omega}{\pi} \mathrm{Im}\langle\langle S_{\mathbf{q}}^{\sigma} | S_{-\mathbf{q}}^{-\sigma} \rangle\rangle_{\omega} \frac{N_B(\omega) + n_{\mathbf{k}+\mathbf{q},-\sigma}}{E - t_{\mathbf{k}+\mathbf{q},-\sigma} + \omega}, \tag{7}$$

where $N_B(\omega)$ is the Bose function. Retaining only the magnon pole contribution to the spin spectral density (i.e., neglecting the spin-wave damping), we have

$$\Sigma_{\mathbf{k}\uparrow}(E) = U\Delta \sum_{\mathbf{q}} \frac{N_{\mathbf{q}} + n_{\mathbf{k}+\mathbf{q}\downarrow}}{E - t_{\mathbf{k}+\mathbf{q}\downarrow} + \omega_{\mathbf{q}}}, \tag{8}$$

$$\Sigma_{\mathbf{k}\downarrow}(E) = U\Delta \sum_{\mathbf{q}} \frac{1 + N_{\mathbf{q}} - n_{\mathbf{k}-\mathbf{q}\uparrow}}{E - t_{\mathbf{k}-\mathbf{q}\uparrow} - \omega_{\mathbf{q}}}, \tag{9}$$

where $\omega_{\mathbf{q}}$ is the magnon energy, $N_{\mathbf{q}} = N_B(\omega_{\mathbf{q}})$. These results are valid in the s-d model ($U \to I$, see below) to first order in the small parameter $1/2S$. Taking into account the relation

$$\langle S^z \rangle = S_0 - \sum_{\mathbf{p}} N_{\mathbf{p}}, \tag{10}$$

where S_0 is the saturation magnetization, one obtains for the spin-wave correction to the electron energy

$$\delta E_{\mathbf{k}\sigma}(T) = \sum_{\mathbf{q}} A_{\mathbf{k}\mathbf{q}}^{\sigma} N_{\mathbf{q}} = \frac{v_0}{2\langle S^z \rangle} \frac{\zeta(5/2)}{32\pi^{3/2}} \left(\frac{T}{D}\right)^{5/2} \left[\frac{\partial^2 t_{\mathbf{k}}}{\partial k_x^2} - \frac{\sigma}{U\langle S^z \rangle} \left(\frac{\partial t_{\mathbf{k}}}{\partial \mathbf{k}}\right)^2\right], \tag{11}$$

where $\zeta(x)$ is the Riemann function, v_0 is the lattice cell volume,

$$\mathcal{A}_{\mathbf{k}\mathbf{q}}^{\sigma} = \sigma U \frac{t_{\mathbf{k}+\mathbf{q}} - t_{\mathbf{k}}}{t_{\mathbf{k}+\mathbf{q}} - t_{\mathbf{k}} + \sigma\Delta}. \tag{12}$$

The $T^{5/2}$ dependence of the electron spectrum owing to magnons is weaker than the $T^{3/2}$ dependence of the magnetization. This is the because the electron-magnon interaction amplitude $\mathcal{A}$ vanishes at zero magnon wave vector, as a result of the symmetry of the exchange interaction. Such a weakening of the temperature dependence of spin splitting was observed in iron (Springford, 1980). The one-electron damping in the half-metallic situation was calculated by Auslender and Irkhin (1984a); they obtained a Fermi-liquid-type behavior (small damping near the Fermi level containing high powers of temperature).

The problem of ferromagnetic ordering in narrow energy bands has been discussed extensively. To stabilize the ferromagnetic solution within the Hubbard model is another difficult problem. It was proved recently that the necessary conditions for ferromagnetism are a density of state with large spectral weight near the band edges (Ulmke, 1998) and Hund's rule coupling for the degenerate case (Vollhardt *et al.*, 1999). Real examples of saturated ferromagnetic ordering are provided by pyrite-structure systems $Fe_{1-x}Co_xS_2$ with itinerant-electron ferromagnetism in a doubly degenerate narrow e_g band (Jarrett *et al.*, 1968; Auslender *et al.*, 1988; Ramesha *et al.*, 2004). CMR manganites, the magnetite Fe_3O_4 above the Verwey transition temperature, and "anionic" half-metallic ferromagnets are other examples (see Sec. V). Recently, a model of sp-electron magnetism in narrow impurity bands was proposed (Edwards and Katsnelson, 2006) that may be applicable to some carbon- or boron-based systems such as doped CaB_6. In this model, the magnon excitations turn out to have higher energy than the Stoner ones. Also, T-matrix renormalization of the Stoner exchange parameter, which decreases its value considerably in a typical itinerant-electron magnet, is much less relevant. For these reasons, narrowband sp systems can provide an example of real Stoner magnets that can have rather high Curie temperatures at a small enough magnetization value (Edwards and Katsnelson, 2006). According to that model, these ferromagnets should also be saturated.

Systems with strong interelectron correlations are the most difficult for standard approaches in itinerant-electron magnetism theory (band calculations, spin-fluctuation theories). Physically, the magnetism picture in this case differs substantially from the Stoner picture of weak itinerant magnetism (Moriya, 1985), since correlations lead to a radical reconstruction of the electron spectrum, namely, the formation of Hubbard subbands (Hubbard, 1963), which are intimately connected with the local magnetic moments (Auslender *et al.*, 1988).

In the limit $U \to \infty$, considering the case in which the number of electrons $n = 1 - \delta < 1$ (δ is the hole concentration), the Hubbard Hamiltonian reads

$$\mathcal{H} = \sum_{\mathbf{k}\sigma} \varepsilon_{\mathbf{k}} X_{-\mathbf{k}}^{0\sigma} X_{\mathbf{k}}^{\sigma 0}, \tag{13}$$

where $X_{\mathbf{k}}^{\alpha\beta}$ is the Fourier transform of the Hubbard operators $X_i^{\alpha\beta} = |i\alpha\rangle\langle i\beta|$, and $\varepsilon_{\mathbf{k}} = -t_{\mathbf{k}}$. According to Nagaoka (1966), the ground state for simple lattices is a saturated ferromagnetic state for a low density δ of current carriers ("doubles" or "holes" in an almost half-filled band). Roth (1969a, 1969b) applied a variational principle to this problem and obtained two critical concentrations. The first one, δ_c, corresponds to the instability of a saturated ferromagnetic state, and the second one, δ_c', to the transition from a nonsaturated ferromagnetic to a paramagnetic state. For the simple cubic (sc) lattice, the values $\delta_c = 0.37$ and $\delta_c' = 0.64$ were obtained. Next, the stability of ferromagnetism was investigated within various approximations and methods. Most calculations for a number of lattices yield a value of δ_c that is close to 0.3.

In particular, the Gutzwiller method (Fazekas *et al.*, 1990), the t/U expansion (Zhao *et al.*, 1987), the density-matrix renormalization-group approach, and the quantum Monte Carlo (QMC) method (Liang and Pang, 1995) yielded $\delta_c=0.2-0.35$.

At the same time, for the critical concentrations δ_c', the interval of values is broader and varies from 0.38 to 0.64. Irkhin and Zarubin (2004, 2006) obtained the distribution of the density of states (DOS) in a Hubbard ferromagnet, taking into account the Kondo scattering and spin-polaron contributions, and they calculated the values of the critical concentrations of current carriers. This approach yields a rather simple interpolational description of saturated and nonsaturated ferromagnetism.

The simplest "Hubbard-I" approximation for the electron spectrum (Hubbard, 1963) corresponds to the zeroth order in the inverse nearest-neighbor number $1/z$ ("mean-field" approximation in the electron hopping). This approximation is quite unsatisfactory for describing ferromagnetism (in particular, ferromagnetic solutions are absent, except for peculiar models with bare density of states). Therefore, to treat the problems connected with ferromagnetism formation in narrow bands, the one-particle Green's functions were calculated to first order in $1/z$ and in the corresponding self-consistent approximations.

The retarded anticommutator Green's functions $G_{\mathbf{k}\sigma}(E)=\langle\langle X_{\mathbf{k}}^{\sigma 0}|X_{-\mathbf{k}}^{0\sigma}\rangle\rangle_E$ can be calculated using the equation-of motion approach of Irkhin and Katsnelson (1988) and Irkhin and Zarubin (2004, 2006) taking into account spin fluctuations. In the locator representation, one obtains (Irkhin and Zarubin, 2004)

$$G_{\mathbf{k}\sigma}(E)=[F_{\mathbf{k}\sigma}(E)-\varepsilon_{\mathbf{k}}]^{-1},\quad F_{\mathbf{k}\sigma}(E)=\frac{b_{\mathbf{k}\sigma}(E)}{a_{\mathbf{k}\sigma}(E)},\tag{14}$$

with

$$a_{\mathbf{k}\sigma}(E)=n_0+n_\sigma+\sum_{\mathbf{q}}\varepsilon_{\mathbf{k}-\mathbf{q}}\frac{\chi_{\mathbf{q}}^{\sigma-\sigma}+n_{\mathbf{k}-\mathbf{q}-\sigma}}{n_0+n_{-\sigma}}\times G_{\mathbf{k}-\mathbf{q}-\sigma}^0(E-\sigma\omega_{\mathbf{q}})+\sum_{\mathbf{q}}\varepsilon_{\mathbf{k}-\mathbf{q}}\frac{\chi_{\mathbf{q}}^{-\sigma-\sigma}}{n_0+n_\sigma}G_{\mathbf{k}-\mathbf{q}\sigma}^0(E),$$

$$b_{\mathbf{k}\sigma}(E)=E+\sum_{\mathbf{q}}\varepsilon_{\mathbf{k}-\mathbf{q}}^2\frac{n_{\mathbf{k}-\mathbf{q}-\sigma}}{n_0+n_{-\sigma}}G_{\mathbf{k}-\mathbf{q}-\sigma}^0(E-\sigma\omega_{\mathbf{q}}),\tag{15}$$

where $\chi_{\mathbf{q}}^{\sigma-\sigma}=\langle S_{\mathbf{q}}^{\sigma}S_{-\mathbf{q}}^{-\sigma}\rangle=\langle X_{\mathbf{q}}^{\sigma-\sigma}X_{-\mathbf{q}}^{-\sigma\sigma}\rangle$ and $\chi_{\mathbf{q}}^{-\sigma-\sigma}=\langle\delta X_{\mathbf{q}}^{-\sigma-\sigma}\delta X_{-\mathbf{q}}^{-\sigma-\sigma}\rangle$ are the correlation functions for spin and charge densities, and $n_{\mathbf{k}\sigma}=\langle X_{-\mathbf{k}}^{0\sigma}X_{\mathbf{k}}^{\sigma 0}\rangle$. To simplify numerical calculations, the long-wavelength dispersion law $\omega_{\mathbf{q}}=\mathcal{D}q^2$ ($\mathcal{D}$ is the spin-wave stiffness constant) was used, with the magnon spectral function $K_{\mathbf{q}}(\omega)$ being the average of this in $\mathbf{q}$. Following Nagaoka (1966), the value $\mathcal{D}=0.66\delta|t|$ was taken for the cubic lattice and the same $\bar{K}(\omega)$ was adopted for other lattices (the choice of $\mathcal{D}$ weakly influences the critical concentration). Thus $a(E)$ and $b(E)$ do not depend on $\mathbf{k}$ and can be expressed in terms of the bare electron density of states. In the case of saturated ferromagnetism, expressions (14) reduce approximately to the result (6) for $U\to\infty$,

$$\Sigma_{\mathbf{k}\downarrow}(E)=-(1-n_0)\left(\sum_{\mathbf{q}}\frac{n_{\mathbf{k}-\mathbf{q}}}{E-\varepsilon_{\mathbf{k}-\mathbf{q}}+\omega_{\mathbf{q}}}\right)^{-1}.\tag{16}$$

To write down the self-consistent approximation, one has to replace in Eqs. (15) $G_{\mathbf{k}\sigma}^0(E)\to G_{\mathbf{k}\sigma}(E)$ and calculate $n_{\mathbf{k}\sigma}$ via the spectral representation. In such an approach, large electron damping is present that smears the Kondo peak.

The $1/z$ corrections lead to a nontrivial structure of the one-particle density of states. In the non-self-consistent approach, the integral of the Fermi functions yields a logarithmic singularity, as in the Kondo problem (Irkhin and Zarubin, 2000). For very low δ, a significant logarithmic singularity exists only in the imaginary part of the Green's function, which corresponds to a finite jump in the density of states (Irkhin and Katsnelson, 1985a). However, when δ increases, it is necessary to take into account the resolvents in both the numerator and denominator of the Green's function, so that the real and imaginary parts are "mixed" and a logarithmic singularity appears in the DOS. The magnon frequencies in the denominators of Eqs. (15) result in the singularity being spread out over the interval $\omega_{\max}$ and the peak becoming smoothed. In the self-consistent approximation, the form of $N_\downarrow(E)$ approaches the bare density of states and the peak is smeared, even if spin dynamics is neglected.

There are no poles of the Green's function for $\sigma=\downarrow$ above the Fermi level at small δ, i.e., the saturated ferromagnetic state is preserved. Unlike most other analytical approaches, the results of Irkhin and Zarubin (2004, 2006) for the one-particle Green's function describe the formation of nonsaturated ferromagnetism as well, the account of longitudinal spin fluctuations $\chi_{\mathbf{q}}^{-\sigma-\sigma}$ being decisive for obtaining the nonsaturated solution and calculating the second critical concentration δ_c' where the magnetization vanishes. For $\delta>\delta_c$, this dependence deviates from the linear one, $\langle S^z\rangle=(1-\delta)/2$. The calculations of Irkhin and Zarubin (2004, 2006) yield δ_c' values that are considerably smaller than the results of the spin-wave approximation (Roth, 1969a, 1969b). In the nonsaturated state, a spin-polaron pole occurs, so that quasiparticle states with $\sigma=\downarrow$ occur above the Fermi level (Fig. 4).

The finite-U case can also be treated with the Green's function methods. The Edwards-Hertz approximation (5) enables one to investigate the stability of the saturated ferromagnetic state only, i.e., to calculate δ_c. The corresponding results are presented in Fig. 5. For comparison, the variational results of von der Linden and Edwards (1991) are shown, which yield a strict upper boundary for the saturated state. Agreement occurs for large U (far from antiferromagnetic and phase-separation instability, which are not taken into account in the calculations). It should be noted that DMFT

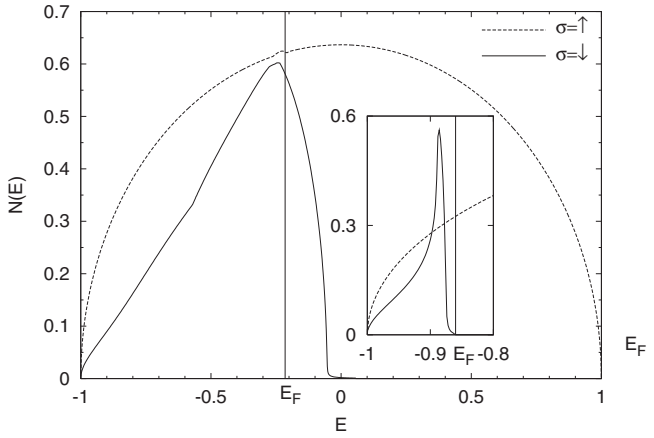

FIG. 4. Density of states for the semielliptic DOS at a concentration of current carriers $\delta=0.35$ ($\delta_c<\delta<\delta_c'$) and $\delta=0.02<\delta_c$ (inset) in the self-consistent approximation.

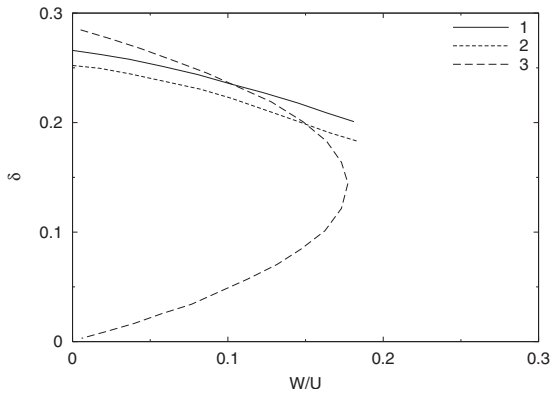

FIG. 5. Boundary of the saturated ferromagnetic region in the approximation (5) for the semielliptic band (solid line) and square lattice (short-dashed line), W the bandwidth. The results of von der Linden and Edwards (1991) for the square lattice are shown by a long-dashed line.

yields qualitatively similar results (Obermeier *et al.*, 1997). One can see that saturated ferromagnetism can occur for large $U/|t|$, and its existence at realistic U is, generally speaking, a not very simple problem.

Now we treat the orbital-degenerate case, which is more realistic for transition-metal compounds. Consider the many-electron system with two ground terms of d^n and d^{n+1} configurations, $\Gamma_n=\{SL\}$ and $\Gamma_{n+1}=\{S'L'\}$. The representation of the Fermi operators in terms of the many-body atomic quantum numbers is suitable (Irkhin and Irkhin, 1994, 2007),

$$c_{il\sigma m}^{\dagger}=(n+1)^{1/2}\sum G_{SL}^{S'L'}C_{L\mu,lm}^{L'\mu'}C_{SM,(1/2)\sigma}^{S'M'}\times X_i(S'L'M'\mu',SLM\mu), \tag{17}$$

where $G_{SL}^{S'L'}$ are the fractional parentage coefficients and $\hat{C}$ are the Clebsch-Gordan coefficients. We can introduce a further simplification by assuming that only one of the competing configurations has nonzero orbital moment $L=l$. This assumption holds for the d^5 and d^6 ground-state configurations of Fe^{3+} and Fe^{2+}, respectively, the first configuration having zero orbital moment. A similar situation occurs, for the CMR manganites (with d^3 and d^4 configurations for Mn^{4+} and Mn^{3+}; due to the relevance of t_{2g}-e_g crystal-field splitting, the former configuration corresponds to the completely filled t_{2g} band with $L=0$).

We treat the narrowband case, which should be described by a two-configuration Hubbard model where both conduction electrons and local moments belong to the same d band, the states with $n+1$ electrons playing the role of current-carrier states. After performing the procedure of mapping onto the corresponding state space, the one-electron Fermi operators for the strongly correlated states $c_{il\sigma m}^{\dagger}$ are replaced by many-electron operators according to Eq. (17). Taking into account the values of the Clebsch-Gordan coefficients that correspond to the coupling of momenta S and $1/2$, we obtain the double-exchange Hamiltonian

$$\mathcal{H}=\sum_{\mathbf{k}\sigma m}t_{\mathbf{k}m}g_{\mathbf{k}\sigma m}^{\dagger}g_{\mathbf{k}\sigma m}. \tag{18}$$

Here we have redefined the band energy by including the many-electron renormalization factor $t_{\mathbf{k}m}(n+1)(G_{SL}^{S'0})^2/(2l+1)\to t_{\mathbf{k}m}$, and

$$g_{i\sigma m}^{\dagger}=\begin{cases}\displaystyle\sum_{M=-S}^{S}\sqrt{\frac{S-\sigma M}{2S+1}}X_i\left(S-1/2,M+\frac{\sigma}{2};SMm\right), & S'=S-1/2\\ \displaystyle\sum_{M=-S}^{S}\sqrt{\frac{S+\sigma M+1}{2S+1}}X_i\left(S+1/2,M+\frac{\sigma}{2};SMm\right), & S'=S+1/2,\end{cases} \tag{19}$$

where $|SMm\rangle$ are the empty states with the orbital index m, and $|S'M'\rangle$ are the singly occupied states with the total on-site spin $S'=S\pm1/2$ and its projection M', $\sigma=\pm$. We see that the two-configuration Hamiltonian is a generalization of the narrowband s-d exchange model with $|I|\to\infty$ (double-exchange model) (Irkhin and Katsnelson, 1985a; Irkhin and Irkhin, 1994, 2007): in the case in which the configuration d^{n+1} has larger spin than

the configuration d^n, we have the effective *s-d* exchange model with ferromagnetic coupling, and in the opposite case with antiferromagnetic coupling. In the absence of orbital degeneracy, the model (18) is reduced to the narrowband Hubbard model.

For $S=1/2$, the narrowband *s-d* exchange model with $|I|\to-\infty$ is equivalent to the Hubbard model with the replacement $t_{\mathbf{k}}\to t_{\mathbf{k}}/2$, so that the ferromagnetism picture corresponds to the one already described. In a general case, the criteria for spin and orbital instabilities (Irkhin and Katsnelson, 2005b) are different. It turns out that the saturated spin ferromagnetism is more stable than the orbital one in the realistic case $S>1/2$ (e.g., for magnetite and for colossal-magnetoresistance manganites). This means that half-metallic ferromagnetic phases with both saturated and nonsaturated orbital moments can arise. The phase diagram at finite temperatures was discussed by Edwards (2002).

In contrast with the usual itinerant-electron ferromagnets, additional collective excitation branches (orbitons) occur in the model. Also, mixed excitations with simultaneous change of spin and orbital projections exist (optical magnons). These excitations can be well defined in the whole Brillouin zone, the damping due to the interaction with current carriers being small enough (Irkhin and Katsnelson, 2005b).

The XMCD data (Huang *et al.*, 2004) suggest large orbital contributions to magnetism in Fe_3O_4. However, more recent experimental XMCD data (Goering *et al.*, 2006) yield very small orbital moments in Fe_3O_4 and confirm the HMF behavior of magnetite. In any case, the model of orbital itinerant ferromagnetism (Irkhin and Katsnelson, 2005b) is of general physical interest and can be applied, e.g., to CMR manganites.

B. Electron spectrum in the *s-d* exchange model: The nonquasiparticle density of states

Besides the Hubbard model, it is often convenient to use the *s-d*(*f*) exchange model for a theoretical description of magnetic metals. The *s-d* exchange model was first proposed for transition *d* metals to consider the peculiarities of their electrical resistivity (Vonsovsky, 1974). This model postulates the existence of two electron subsystems: itinerant *s* electrons, which play the role of current carriers, and localized *d* electrons, which give the main contribution to the magnetic moments. This assumption can hardly be justified quantitatively for *d* metals, but is useful in the qualitative consideration of some physical properties, especially transport phenomena. At the same time, the *s-d* model provides a good description of magnetism in rare-earth metals and their compounds with well-localized 4*f* states. Now this model is widely used in the theory of anomalous *f* systems (intermediate-valence compounds, heavy fermions, etc.) as the Kondo-lattice model (Hewson, 1993).

The Hamiltonian of the *s-d* exchange model in the case of an arbitrary inhomogeneous potential reads

$$\mathcal{H}=\int d\mathbf{r}\Bigg(\sum_{\sigma}\Psi_{\sigma}^{\dagger}(\mathbf{r})\mathcal{H}_0^{\sigma}\Psi_{\sigma}(\mathbf{r}) - I\sum_{\sigma\sigma'}\delta\mathbf{S}(\mathbf{r})\cdot\Psi_{\sigma}^{\dagger}(\mathbf{r})\boldsymbol{\sigma}_{\sigma\sigma'}\Psi_{\sigma'}(\mathbf{r})\Bigg)+\mathcal{H}_d,$$

$$\mathcal{H}_0^{\sigma}=-\frac{\hbar^2}{2m}\nabla^2+V_{\sigma}(\mathbf{r}), \tag{20}$$

where $V_{\sigma}(\mathbf{r})$ is the potential energy (taking into account the electron-electron interaction in the mean-field approximation), which is supposed to be spin dependent, $\Psi_{\sigma}(\mathbf{r})$ is the field operator for the spin projection σ, $\boldsymbol{\sigma}_{\sigma\sigma'}$ are the Pauli matrices, $\mathbf{S}(\mathbf{r})$ is the spin density of the localized-moment system, and $\delta\mathbf{S}(\mathbf{r})=\mathbf{S}(\mathbf{r})-\langle\mathbf{S}(\mathbf{r})\rangle$ is its fluctuating part, the effect of the average spin polarization $\langle\mathbf{S}(\mathbf{r})\rangle$ included in $V_{\sigma}(\mathbf{r})$. We use the approximation of contact electron-magnon interaction described by the *s-d* exchange parameter *I*,

$$\mathcal{H}_d=-\sum_{\mathbf{q}}J_{\mathbf{q}}\mathbf{S}_{\mathbf{q}}\cdot\mathbf{S}_{-\mathbf{q}} \tag{21}$$

(for simplicity, we neglect the inhomogeneity effects for the magnon subsystem), where $\mathbf{S}_{\mathbf{q}}$ are operators for localized spins and $J_{\mathbf{q}}$ are the Fourier transforms of the exchange parameters between localized spins. In rare-earth metals, the latter interaction is usually the indirect Ruderman-Kittel-Kasuya-Yosida (RKKY) exchange via conduction electrons, which is due to the same *s-d* interaction. However, when constructing perturbation theory, it is convenient to include this interaction in the zero-order Hamiltonian.

Although more complicated in its form, the *s-d* model turns out to be simpler in some respects than the Hubbard model (1) since it enables us to construct the quasiclassical expansion in the small parameter $1/2S$. Within simple approximations, the results in the *s-d*(*f*) and Hubbard models differ as a rule by the replacement $I\to U$ only. To describe the effects of electron-magnon interaction, we use the formalism of the exact eigenfunctions (Irkhin and Katsnelson, 1984, 2006). In the representation of exact eigenfunctions for the Hamiltonian $\mathcal{H}_0^{\sigma}$,

$$\mathcal{H}_0^{\sigma}\psi_{\nu\sigma}=\varepsilon_{\nu\sigma}\psi_{\nu\sigma},$$

$$\Psi_{\sigma}(\mathbf{r})=\sum_{\nu}\psi_{\nu\sigma}(\mathbf{r})c_{\nu\sigma}, \tag{22}$$

one can rewrite the Hamiltonian (20) in the following form:

$$\mathcal{H}=\sum_{\nu\sigma}\varepsilon_{\nu\sigma}c_{\nu\sigma}^{\dagger}c_{\nu\sigma}-I\sum_{\mu\nu\alpha\beta\mathbf{q}}(\nu\alpha,\mu\beta|\mathbf{q})\delta\mathbf{S}_{\mathbf{q}}c_{\nu\alpha}^{\dagger}\boldsymbol{\sigma}_{\alpha\beta}c_{\mu\beta}+\mathcal{H}_d, \tag{23}$$

where

$$(\nu\sigma,\mu\sigma'|\mathbf{q}) = \langle\mu\sigma'|e^{i\mathbf{q}\cdot\mathbf{r}}|\nu\sigma\rangle. \tag{24}$$

We take into account again the electron-spectrum spin splitting in the mean-field approximation by keeping the dependence of the eigenfunctions on the spin projection.

In the spin-wave region, one can use for the spin operators the magnon (e.g., Dyson-Maleev) representation. Then we have for the one-electron Green's function

$$G_\nu^\sigma(E) = [E - \varepsilon_{\nu\sigma} - \Sigma_\nu^\sigma(E)]^{-1}, \tag{25}$$

with the self-energy $\Sigma_\nu^\sigma(E)$ describing correlation effects.

We start with the perturbation expansion in the electron-magnon interaction. To second order in I, one has

$$\Sigma_\nu^\uparrow(E) = 2I^2S\sum_{\mu\mathbf{q}} |(\nu\uparrow,\mu\downarrow|\mathbf{q})|^2 \frac{N_\mathbf{q} + n_\mu^\downarrow}{E - \varepsilon_{\mu\downarrow} + \omega_\mathbf{q}},$$

$$\Sigma_\nu^\downarrow(E) = 2I^2S\sum_{\mu\mathbf{q}} |(\nu\downarrow,\mu\uparrow|\mathbf{q})|^2 \frac{1 + N_\mathbf{q} - n_\mu^\uparrow}{E - \varepsilon_{\mu\uparrow} - \omega_\mathbf{q}}, \tag{26}$$

where $n_\mu^\sigma = f(\varepsilon_{\mu\sigma})$ (discussion of a more general ladder approximation is given below). Using the expansion of the Dyson equation (25), we obtain for the spectral density

$$\begin{aligned}\mathcal{A}_{\nu\sigma}(E) &= -\frac{1}{\pi}\,\mathrm{Im}\, G_\nu^\sigma(E) \\ &= \delta(E - \varepsilon_{\nu\sigma}) - \delta'(E - \varepsilon_{\nu\sigma})\mathrm{Re}\,\Sigma_\nu^\sigma(E) \\ &\quad - \frac{1}{\pi}\frac{\mathrm{Im}\,\Sigma_\nu^\sigma(E)}{(E - \varepsilon_{\nu\sigma})^2}.\end{aligned} \tag{27}$$

The second term on the right-hand side of Eq. (27) gives the shift of quasiparticle energies. The third term, which arises from the branch cut of the self-energy, describes the incoherent (nonquasiparticle) contribution owing to scattering by magnons. One can see that this does not vanish in the energy region corresponding to the "alien" spin subband with the opposite projection $-\sigma$.

Neglecting temporarily in Eq. (26) the magnon energy $\omega_\mathbf{q}$ in comparison with typical electron energies and using the identities

$$\sum_{\mu\mathbf{q}} \frac{|(\nu\mu|\mathbf{q})|^2}{E - \varepsilon_\mu} F(\varepsilon_\mu) = -\frac{1}{\pi}\int dE' \frac{F(E')}{E - E'} \times \mathrm{Im}\langle\nu|(E' - \mathcal{H}_0 + i0)^{-1}|\nu\rangle, \tag{28}$$

one derives at zero temperature

$$\Sigma_\nu^\uparrow(E) = 2I^2S\int dE' \frac{f(E')}{E - E'}\langle\nu\uparrow|\delta(E - E' - \mathcal{H}_0^\downarrow)|\nu\uparrow\rangle, \tag{29}$$

$$\Sigma_\nu^\downarrow(E) = 2I^2S\int dE' \frac{1 - f(E')}{E - E'}\langle\nu\downarrow|\delta(E - E' - \mathcal{H}_0^\uparrow)|\nu\downarrow\rangle. \tag{30}$$

Using the tight-binding model for the ideal-crystal Hamiltonian, one obtains in the real-space representation

$$\Sigma_{\mathbf{R},\mathbf{R}'}^\uparrow(E) = 2I^2S\int dE' f(E')\left(-\frac{1}{\pi}\,\mathrm{Im}\, G_{\mathbf{R},\mathbf{R}}^\downarrow(E - E')\right)\delta_{\mathbf{R},\mathbf{R}'}, \tag{31}$$

$$\Sigma_{\mathbf{R},\mathbf{R}'}^\downarrow(E) = 2I^2S\int dE'[1 - f(E')] \times\left(-\frac{1}{\pi}\,\mathrm{Im}\, G_{\mathbf{R},\mathbf{R}}^\uparrow(E - E')\right)\delta_{\mathbf{R},\mathbf{R}'}, \tag{32}$$

where $\mathbf{R},\mathbf{R}'$ are lattice site indices, and therefore

$$\Sigma_\nu^\sigma(E) = \sum_\mathbf{R} |\psi_{\nu\sigma}(\mathbf{R})|^2\Sigma_{\mathbf{R},\mathbf{R}}^\sigma(E). \tag{33}$$

One can generalize the above results to the case of arbitrary *s-d* exchange parameter. Simplifying the sequence of equations of motion (cf. Irkhin and Katsnelson, 1984), we have for the operator Green's function

$$G^\sigma(E) = \left(E - \mathcal{H}_0^\sigma + \sigma I(\mathcal{H}_0^\sigma - \mathcal{H}_0^{-\sigma}) \times\frac{1}{1 + \sigma IR^\sigma(E)}R^\sigma(E)\right)^{-1}. \tag{34}$$

If we consider the spin dependence of the electron spectrum in the simplest rigid-splitting approximation $\varepsilon_{\nu\sigma} = \varepsilon_\nu - \sigma I\langle S^z\rangle$ and thus neglect the spin dependence of the eigenfunctions $\psi_{\nu\sigma}(\mathbf{R})$, Eqs. (29) and (30) are drastically simplified. Then the self-energy does not depend on ν,

$$\Sigma^\sigma(E) = \frac{2I^2SR^\sigma(E)}{1 + \sigma IR^\sigma(E)}, \tag{35}$$

$$R^\uparrow(E) = \sum_\mu \frac{n_\mu^\downarrow}{E - \varepsilon_{\mu\downarrow}}, \quad R^\downarrow(E) = \sum_\mu \frac{1 - n_\mu^\uparrow}{E - \varepsilon_{\mu\uparrow}}. \tag{36}$$

If $\mathcal{H}_0^\sigma$ is the crystal Hamiltonian ($\mu = \mathbf{k}$, $\varepsilon_{\nu\sigma} = t_{\mathbf{k}\sigma}$, $t_{\mathbf{k}\sigma}$ is the band energy for spin projection σ), Eq. (34) coincides with the result for the Hubbard model after the replacement $I \to U$ (see Sec. III.A). The imaginary part of $\Sigma^\sigma(E)$ determines the NQP states. Description of such states in the Hubbard model with arbitrary U by the dynamical mean-field theory will be presented in Sec. IV.A

Equation (34) can be also represented in the form

$$G^\sigma(E) = \left(E - \mathcal{H}_0^{-\sigma} - (\mathcal{H}_0^\sigma - \mathcal{H}_0^{-\sigma})\frac{1}{1 + \sigma IR^\sigma(E)}\right)^{-1}. \tag{37}$$

Equation (37) is convenient in the narrowband case. In this limit where spin splitting is large in comparison with the bandwidth of the conduction electrons, we have $\mathcal{H}_0^\uparrow$

$-\mathcal{H}_0^{\uparrow}=-2IS$, and we obtain for the lower spin subband with $\sigma=-\mathrm{sgn}\, I$

$$G^{\sigma}(E)=\left(E-\mathcal{H}_0^{-\sigma}+\frac{2S}{R^{\sigma}(E)}\right)^{-1}. \tag{38}$$

For a periodic crystal, Eq. (38) takes the form

$$G_{\mathbf{k}}^{\sigma}(E)=\left(E-t_{\mathbf{k}-\sigma}+\frac{2S}{R^{\sigma}(E)}\right)^{-1}. \tag{39}$$

This expression yields the exact result in the limit $I\to+\infty$,

$$G_{\mathbf{k}}^{\downarrow}(E)=\left(\epsilon-t_{\mathbf{k}}+\frac{2S}{R(\epsilon)}\right)^{-1},\quad R(\epsilon)=\sum_{\mathbf{k}}\frac{1-f(t_{\mathbf{k}})}{\epsilon-t_{\mathbf{k}}} \tag{40}$$

with $\epsilon=E+IS$. In the limit $I\to-\infty$, Eq. (39) gives correctly the spectrum of spin-down quasiparticles,

$$G_{\mathbf{k}}^{\downarrow}(E)=\frac{2S}{2S+1}(\epsilon-t_{\mathbf{k}}^{*})^{-1}, \tag{41}$$

with $\epsilon=E-I(S+1)$ and $t_{\mathbf{k}}^{*}=[2S/(2S+1)]t_{\mathbf{k}}$. However, it does not describe the NQP states correctly; more accurate expressions can be obtained using the atomic-representation (Irkhin and Katsnelson, 2005b),

$$G_{\mathbf{k}}^{\uparrow}(E)=\frac{2S}{2S+1}\left(\epsilon-t_{\mathbf{k}}^{*}+\frac{2S}{R^{*}(\epsilon)}\right)^{-1},\quad R^{*}(\epsilon)=\sum_{\mathbf{k}}\frac{f(t_{\mathbf{k}}^{*})}{\epsilon-t_{\mathbf{k}}^{*}}. \tag{42}$$

The Green's functions (39), (40), and (42) have no poles, at least for small current carrier concentration, and the whole spectral weight of minority states is provided by the branch cut (nonquasiparticle states) (Irkhin and Katsnelson, 1983, 1985b, 1990). For surface states, this result was obtained by Katsnelson and Edwards (1992) in a narrowband Hubbard model. Now we see that this result can be derived in an arbitrary inhomogeneous case. For a HMF with the gap in the minority-spin subband, NQP states occur above the Fermi level, and for the gap in the majority-spin subband they occur below the Fermi level.

In the absence of spin dynamics (i.e., neglecting the magnon frequencies), the NQP density of states has a jump at the Fermi level. However, the magnon frequencies can be restored in the final result, in analogy with the case of the ideal crystal, which leads to a smearing of the jump on the energy scale of the characteristic magnon energy $\bar{\omega}$. It should be mentioned again that we restrict ourselves to the case of the three-dimensional magnon spectrum and we do not consider the influence of surface states on the spin-wave subsystem. The expressions obtained enable us to investigate the energy dependence of the spectral density.

An analysis of the electron-spin coupling yields different DOS pictures for two possible signs of the *s-d* exchange parameter I. For $I>0$, the spin-down NQP scattering states form a "tail" of the upper spin-down band, which starts from E_F (Fig. 6) since the Pauli principle prevents electron scattering into occupied states.

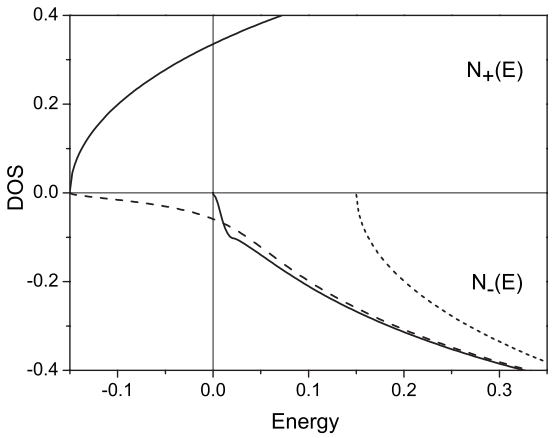

FIG. 6. Density of states in the *s-d* exchange model of a half-metallic ferromagnet with $S=1/2, I=0.3$ for the semielliptic bare band with width of $W=2$. The Fermi energy calculated from the band bottom is 0.15 (the energy is referred to E_F). The magnon band is also assumed semielliptic with width of $\omega_{\max}=0.02$. The nonquasiparticle tail of the spin-down subband (lower half of the figure) occurs above the Fermi level. The corresponding picture for the empty conduction band is shown by a dashed line; the short-dashed line corresponds to the mean-field approximation.

For $I<0$, spin-up NQP states are present below the Fermi level as an isolated region (Fig. 7): occupied states with the total spin $S-1$ are a superposition of the states $|S\rangle|\downarrow\rangle$ and $|S-1\rangle|\uparrow\rangle$. The entanglement of the states of electron and spin subsystems, which is necessary to form the NQP states, is a purely quantum effect formally disappearing at $S\to\infty$. To understand better why the NQP states are formed only below E_F, in this case we can treat the limit $I=-\infty$. Then the current carrier is really a many-body state of the occupied site as a whole with

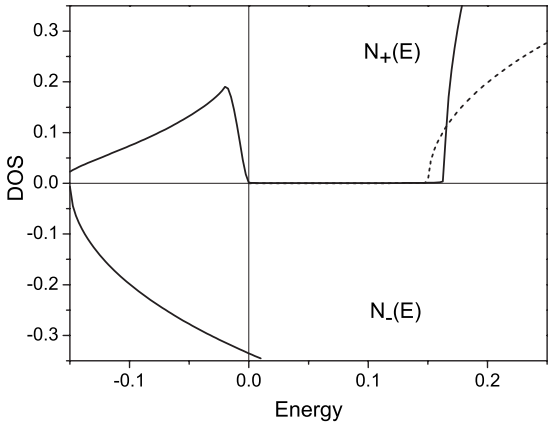

FIG. 7. Density of states in a half-metallic ferromagnet with $I=-0.3<0$, other parameters the same as in Fig. 1. The spin-down subband (lower half of the figure) nearly coincides with the bare band shifted by IS. Nonquasiparticle states in the spin-up subbands (upper half of the figure) occur below the Fermi level; the short-dashed line corresponds to the mean-field approximation.

total spin $S-1/2$, which propagates in the ferromagnetic medium with spin S at any site. The fractions of states $|S\rangle|\downarrow\rangle$ and $|S-1\rangle|\uparrow\rangle$ in the current carrier state are $1/(2S+1)$ and $2S/(2S+1)$, respectively, so that the first number is a spectral weight of occupied spin-up electron NQP states. At the same time, the density of empty states is measured by the number of electrons with a given spin projection that one can add to the system. It is obvious that one cannot put any spin-up electrons in the spin-up site at $I=-\infty$. Therefore, the density of NQP states should vanish above E_F.

It is worthwhile to note that in most of the known HMFs, the gap exists for minority-spin states (Irkhin and Katsnelson, 1994). This is similar to the case $I>0$, so that the NQP states should arise above the Fermi energy. For exceptional cases with the majority-spin gap such as the double perovskite Sr_2FeMoO_6 (Kobayashi *et al.*, 1998) and magnetite, one should expect the formation of NQP states below the Fermi energy.

The presence of space inhomogeneity (e.g., surfaces, interfaces, impurities) does not change the spectral density picture qualitatively, except for smoothing the matrix elements. Later in this section we consider, for simplicity, the case of a clean infinite crystal; all temperature and energy dependences of the spectral density will be basically the same, e.g., for the surface layer.

The second term on the right-hand side of Eq. (27) describes the renormalization of quasiparticle energies. The third term, which arises from the branch cut of the self-energy $\Sigma_\sigma(E)$, describes the incoherent (nonquasiparticle) contribution owing to scattering by magnons. One can see that this does not vanish in the energy region corresponding to the alien spin subband with the opposite projection $-\sigma$. Consider for definiteness the case $I>0$ (the case $I<0$ differs, roughly speaking, by a particle-hole transformation). On summing up Eq. (27) to find the total DOS $N_\sigma(E)$ and neglecting the quasiparticle shift, we get

$$N_\uparrow(E)=\sum_{\mathbf{kq}}\left[1-\frac{2I^2SN_\mathbf{q}}{(t_{\mathbf{k}+\mathbf{q}\downarrow}-t_{\mathbf{k}\uparrow})^2}\right]\delta(E-t_{\mathbf{k}\uparrow}),$$

$$N_\downarrow(E)=2I^2S\sum_{\mathbf{kq}}\frac{1+N_\mathbf{q}-n_{\mathbf{k}\uparrow}}{(t_{\mathbf{k}+\mathbf{q}\downarrow}-t_{\mathbf{k}\uparrow}-\omega_\mathbf{q})^2}\delta(E-t_{\mathbf{k}\uparrow}-\omega_\mathbf{q}). \tag{43}$$

The $T^{3/2}$ dependence of the magnon contribution to the residue of the Green's function, i.e., of the effective electron mass in the lower spin subband, and an increase with temperature of the incoherent tail from the upper spin subband, result in a strong temperature dependence on the partial densities of states $N_\sigma(E)$, the corrections being of opposite sign. At the same time, the temperature shift of the band edge for the quasiparticle states is proportional to $T^{5/2}$ rather than to the magnetization (Irkhin and Katsnelson, 1983, 1984, 1985b).

It is worth noting that there exists a purely single-particle mechanism of the gap filling in HMFs which is due to relativistic interactions. Specifically, one should take into account spin-orbit coupling effects that connect the spin-up and spin-down channels through the angular momentum $\boldsymbol{l}$. The strength of this interaction is proportional to the spatial derivatives of the crystal potential $V(\mathbf{r})$: $V_{\mathrm{SO}}\propto|\nabla V|(\boldsymbol{l}\cdot\mathbf{s})$, off-diagonal elements $V_{\mathrm{SO}}^{\sigma,\sigma'}$ being nonzero. For a HMF with a gap in the minority-spin (spin-down) channel, one could construct the wave function for spin-down electrons within perturbation theory, so that the DOS in the gap has a square dependence on the spin-orbit coupling strength, $\delta n_\downarrow^{\mathrm{SO}}(E)\propto(V_{\mathrm{SO}}^{\downarrow,\uparrow})^2$ (Mavropoulos *et al.*, 2004). There is an obvious qualitative distinction between the many-body and spin-orbit contributions in the minority-spin channel; besides that, the latter is orders of magnitude smaller and weakly temperature dependent. For further discussions of the spin-orbit effects in HMFs, see Pickett and Eschrig (2007).

The exact solution in the atomic limit (for one conduction electron), which is valid not only in the spin-wave region but also for arbitrary temperatures, reads (Auslender *et al.*, 1983)

$$G^\sigma(E)=\frac{S+1+\sigma\langle S^z\rangle}{2S+1}\frac{1}{E+IS}+\frac{S-\sigma\langle S^z\rangle}{2S+1}\frac{1}{E-I(S+1)}. \tag{44}$$

In this case, the energy levels are not temperature dependent, whereas the residues are strongly temperature dependent via the magnetization.

Now we consider the case $T=0$ K for finite band filling. The picture of $N(E)$ in HMFs (or degenerate ferromagnetic semiconductors) demonstrates a strong energy dependence near the Fermi level (Figs. 6 and 7). If we neglect magnon frequencies in the denominators of Eq. (43), the partial density of incoherent states should occur by a jump above or below the Fermi energy E_F for $I>0$ and $I<0$, respectively, owing to the Fermi distribution functions. Taking account of finite magnon frequencies $\omega_\mathbf{q}=\mathcal{D}q^2$ ($\mathcal{D}$ is the spin-wave stiffness constant) leads to smearing of these singularities, $N_{-\alpha}(E_F)$ being equal to zero. For $|E-E_F|\ll\bar{\omega}$, we obtain

$$\frac{N_{-\alpha}(E)}{N_\alpha(E)}=\frac{1}{2S}\left|\frac{E-E_F}{\bar{\omega}}\right|^{3/2}\theta(\alpha(E-E_F)),\quad \alpha=\operatorname{sgn} I \tag{45}$$

($\alpha=\pm$ corresponds to the spin projections $\uparrow,\downarrow$). With increasing $|E-E_F|$, $N_{-\alpha}/N_\alpha$ tends to a constant value that is of the order of I^2 within perturbation theory.

In the strong-coupling limit where $|I|\to\infty$, we have from Eq. (43)

$$\frac{N_{-\alpha}(E)}{N_\alpha(E)}=\frac{1}{2S}\theta(\alpha(E-E_F)),\quad |E-E_F|\gg\bar{\omega}. \tag{46}$$

In fact, this expression is valid only in the framework of the $1/2S$ expansion, and in the narrowband quantum case we have to use more exact expressions (40) and (42).

To investigate the details of the energy dependence of $N(E)$ in the broadband case, we assume the simplest isotropic approximation for the majority-spin electrons,

$$t_{\mathbf{k}\uparrow} - E_F \equiv \xi_{\mathbf{k}} = \frac{k^2 - k_F^2}{2m^*}. \tag{47}$$

Provided that we use the rigid-splitting approximation $t_{\mathbf{k}\downarrow} = t_{\mathbf{k}\uparrow} + \Delta (\Delta = 2IS, I > 0)$, the half-metallic situation (or, more precisely, the situation of a degenerate ferromagnetic semiconductor) takes place for $\Delta > E_F$. Then, qualitatively, Eq. (45) works to the accuracy of a prefactor. It is worth noting that the NQP contribution to the DOS occurs also for a usual metal where $\Delta < E_F$. In the case of small Δ, there is a crossover energy (or temperature) scale

$$T^* = \mathcal{D}(m^* \Delta / k_F)^2, \tag{48}$$

which is the magnon energy at the boundary of the Stoner continuum, $T^* \simeq \bar{\omega}(\Delta / E_F)^2 \ll \bar{\omega}$. At $|E - E_F| \ll \bar{\omega}$, Eq. (43) for the NQP contribution reads

$$\delta N_\downarrow(E) \propto \left(\frac{1}{2} \ln \left| \frac{1 + \sqrt{(E - E_F)/T^*}}{1 - \sqrt{(E - E_F)/T^*}} \right| - \sqrt{(E - E_F)/T^*} \right) \theta(E - E_F). \tag{49}$$

At $|E - E_F| \ll T^*$, this gives the same results as above. However, at $T^* \ll |E - E_F| \ll \bar{\omega}$, this contribution is proportional to $-\sqrt{(E - E_F)/T^*}$ and is negative (of course, the total DOS is always positive). This demonstrates that one should be careful when discussing the NQP states for systems that are not half metallic.

The model of rigid spin splitting used above is in fact not applicable for a real HMF, where the gap has a hybridization origin (de Groot, Mueller, v. Engen, *et al.*, 1983; Irkhin and Katsnelson, 1994). The simplest model for the HMF is as follows: a normal metallic spectrum for majority electrons (47) and a hybridization gap for minority ones,

$$t_{\mathbf{k}\downarrow} - E_F = \tfrac{1}{2}(\xi_{\mathbf{k}} + \mathrm{sgn}(\xi_{\mathbf{k}}) \sqrt{\xi_{\mathbf{k}}^2 + \Delta^2}). \tag{50}$$

Here we assume for simplicity that the Fermi energy lies exactly in the middle of the hybridization gap (otherwise one needs to shift $\xi_{\mathbf{k}} \to \xi_{\mathbf{k}} + E_0 - E_F$ in the last equation, E_0 being the middle of the gap). One can replace in Eq. (43) $\xi_{\mathbf{k}+\mathbf{q}}$ by $\mathbf{v}_{\mathbf{k}} \cdot \mathbf{q}$, $\mathbf{v}_{\mathbf{k}} = \mathbf{k}/m^*$. Integrating over the angle between the vectors $\mathbf{k}$ and $\mathbf{q}$, we derive

$$\left\langle \left(\frac{1}{t_{\mathbf{k}+\mathbf{q}\downarrow} - t_{\mathbf{k}\uparrow} - \omega_{\mathbf{q}}} \right)^2 \right\rangle = \frac{8}{v_F q \Delta} \left(\frac{2}{3}[X^3 - (X^2 + 1)^{3/2} + 1] + X \right), \tag{51}$$

where the angular brackets stand for the average over the angles of the vector $\mathbf{k}$, and $X = k_F q / m^* \Delta$. Here we do have a crossover with the energy scale T^*, which can be small for a small enough hybridization gap. For example, in NiMnSb the conduction-band width is about 5 eV and the distance from the Fermi level to the nearest gap edge (i.e., the indirect energy gap, which is proportional to Δ^2) is smaller than 0.5 eV, so that $(\Delta / E_F)^2 \leq 0.1$.

For the case $0 < E - E_F \ll \bar{\omega}$, one has

$$N_\downarrow(E) \propto b\left(\frac{E - E_F}{T^*} \right),$$

$$b(y) = \frac{2}{5}[y^{5/2} - (1 + y)^{5/2} + 1] + y + y^{3/2} \simeq \begin{cases} y^{3/2}, & y \ll 1 \\ y, & y \gg 1. \end{cases} \tag{52}$$

Thus the behavior $N_\downarrow(E) \propto (E - E_F)^{3/2}$ occurs only for very small excitation energies $E - E_F \ll T^*$, whereas in a broad interval $T^* \ll E - E_F \ll \bar{\omega}$ one has the linear dependence $N_\downarrow(E) \propto E - E_F$.

C. The problem of spin polarization

The functionality of devices that exploit charge as well as spin degrees of freedom depends in a crucial way on the behavior of the spin polarization of current carriers (Prinz, 1998). Unfortunately, many potentially promising half-metallic systems exhibit a dramatic decrease in spin polarization. Crystal imperfections (Ebert and Schutz, 1991), interfaces (de Wijs and de Groot, 2001), and surfaces (Galanakis, 2003) constitute important examples of static perturbations of the ideal periodic potential that affect the states in the half-metallic gap.

In addition, several other depolarization mechanisms have been suggested that are based on magnon and phonon excitations (Skomski and Dowben, 2002; Dowben and Skomski, 2003, 2004; Skomski, 2007). These papers extend the view of spin disorder as random interatomic exchange fields and claim that disorder rotates the spin direction locally and thus modifies the local magnetic moment and spin polarization (MacDonald *et al.*, 1998; Orgassa *et al.*, 1999, 2000; Itoh *et al.*, 2000). The coupling between atomic moments can be treated in terms of Heisenberg-type interactions (see Secs. VI.A and VI.B). The sign and magnitude of the exchange constants determine whether the spin structure is collinear (Sandratskii, 2001).

Simple qualitative considerations (Edwards, 1983), as well as direct Green's functions calculations (Auslender and Irkhin, 1984a, 1984b) for ferromagnetic semiconductors, demonstrate that the spin polarization of conduction electrons in the spin-wave region is proportional to the magnetization,

$$P \equiv \frac{N_\uparrow - N_\downarrow}{N_\uparrow + N_\downarrow} = P_0 \langle S^z \rangle / S. \tag{53}$$

A weak ground-state depolarization $1 - P_0$ occurs in the case of the empty conduction band where $I > 0$. As discussed in the preceding section, in the case of the Fermi statistics of charge carriers (degenerate ferromagnetic semiconductors and HMFs), the NQP states at $T = 0$ ex-

ist only below E_F for the majority-spin gap ($I<0$ for the case of semiconductors) and only above E_F for the minority-spin gap ($I>0$ for the case of semiconductors).

Spin-resolved photoelectron spectra for magnetite slightly above the Verwey transition point have been measured by Mortonx *et al.* (2002), a negative polarization about −40% being found near the Fermi energy. The strong deviation from −100% polarization may be, at least partially, related to NQP states. Since according to the electronic-structure calculations (Yanase and Siratori, 1984) magnetite is a HMF with a majority-spin gap, the NQP should exist below the Fermi energy and thus be relevant for photoelectron spectroscopy. Since electron correlations in Fe_3O_4 are quite strong, the spectral weight of the NQP states should be considerable. Of course, photoemission is a surface-sensitive method, and it is not quite clear to what degree these data characterize the electronic structure of bulk Fe_3O_4.

An instructive limit is the Hubbard ferromagnet with infinitely strong correlations $U=\infty$ (13) and electron concentration $n<1$. The DOS calculations yield (Irkhin and Katsnelson, 1983, 1985b)

$$N_{\downarrow}(E)=\sum_{\mathbf{k}\sigma} f(t_{\mathbf{k}+\mathbf{q}})\delta(E-t_{\mathbf{k}+\mathbf{q}}+\omega_{\mathbf{q}}) = \begin{cases} N_{\uparrow}(E), & E-E_F \gg \omega_{\max} \\ 0, & E<E_F. \end{cases} \tag{54}$$

A schematic density of states is shown in Fig. 29(a) [a more realistic picture is presented in Fig. 4; see also Irkhin and Katsnelson (2005b)]. The result (54) has a simple physical meaning. Since the current carriers are spinless doubles (doubly occupied sites), electrons with spins up and down may be selected with an equal probability from the states below the Fermi level of doubles, so that these states are fully depolarized. On the other hand, according to the Pauli principle, only the spin-down electrons may be added in the singly occupied states in the saturated ferromagnet.

The behavior $P(T)\sim\langle S^z\rangle$ is qualitatively confirmed by experimental data on field emission from ferromagnetic semiconductors (Kisker *et al.*, 1978) and transport properties of half-metallic Heusler alloys (Otto *et al.*, 1989). An attempt was made (Skomski and Dowben, 2002; Dowben and Skomski, 2003) to generalize the result (53) in the HMF case [in fact, using qualitative arguments that are valid only in the atomic limit, see Eq. (44)]. However, the situation for HMFs is more complicated. We focus on the magnon contribution to the DOS (43) and calculate the function

$$\Lambda=\sum_{\mathbf{k},\mathbf{q}} \frac{2I^2SN_{\mathbf{q}}}{(t_{\mathbf{k}+\mathbf{q}\downarrow}-t_{\mathbf{k}\uparrow}-\omega_{\mathbf{q}})^2}\delta(E_F-t_{\mathbf{k}\uparrow}). \tag{55}$$

Using the parabolic electron spectrum $t_{\mathbf{k}\uparrow}=k^2/2m^*$ and averaging over the angles of the vector $\mathbf{k}$, we obtain

$$\Lambda=\frac{2I^2Sm^2}{k_F^2}\rho\sum_{\mathbf{q}}\frac{N_{\mathbf{q}}}{(q^*)^2-q^2}, \tag{56}$$

where $\rho=N_{\uparrow}(E_F,T=0)$; we have used the condition $q\ll k_F, q^*=m^*\Delta/k_F=\Delta/v_F$, where $\Delta=2|I|S$ is the spin splitting. In a ferromagnetic semiconductor, we have, in agreement with the qualitative considerations presented above,

$$\Lambda=\frac{S-\langle S^z\rangle}{2S}\rho\propto\left(\frac{T}{T_C}\right)^{3/2}\rho. \tag{57}$$

Now we consider the spectrum model (47) and (50) where the gap has a hybridization origin. At $T\ll T^*$, we reproduce the result (57), which is actually universal for this temperature region. At $T^*\ll T\ll\tilde{\omega}$, we derive

$$\Lambda=\sum_{\mathbf{k},\mathbf{q}} 2I^2SN_{\mathbf{q}}\delta(\xi_{\mathbf{k}})\frac{16}{3v_Fq\Delta}\propto q^*\sum_{\mathbf{q}}\frac{N_{\mathbf{q}}}{q}\propto\frac{T^{*1/2}}{T_C^{1/2}}T\ln\frac{T}{T^*}. \tag{58}$$

This result distinguishes HMFs such as the Heusler alloys from ferromagnetic semiconductors and narrowband saturated ferromagnets. In the narrowband case, the spin polarization follows the magnetization up to the Curie temperature T_C.

For finite temperatures, the density of NQP states at the Fermi energy is given by

$$N(E_F)\propto\int_0^{\infty}d\omega\frac{K(\omega)}{\sinh(\omega/T)}. \tag{59}$$

The filling of the energy gap is important for possible applications of HMFs in spintronics: in fact, HMFs have clear advantages only if $T\ll T_C$. Since a single-particle Stoner-like theory leads to the much less restrictive inequality $T\ll\Delta$, the many-body treatment of the spin-polarization problem (inclusion of collective spin-wave excitations) is crucial. Generally, for temperatures comparable with the Curie temperature T_C, there are no essential differences between half-metallic and ordinary ferromagnets since the gap is filled.

The corresponding symmetry analysis was performed by Irkhin *et al.* (1989, 1994) for a model of conduction electrons interacting with pseudospin excitations in ferroelectric semiconductors. The symmetric (with respect to E_F) part of $N(E)$ in the gap can be attributed to the smearing of electron states by electron-magnon scattering; the asymmetric (Kondo-like) part is the density of NQP states owing to the Fermi distribution function.

Skomski and Dowben (Skomski and Dowben, 2002; Dowben and Skomski, 2003, 2004; Skomski, 2007) investigated spin-mixing effects for NiMnSb by using a simple tight-binding approximation. Figure 8 shows a schematic comparison between this approximation and many-body results. In the tight-binding approach, the distortion of the spin-up and spin-down DOSs is presented by the dark regions. The spin mixing gives a nonzero symmetric $N_{\downarrow}(E)$, the DOS being weakly modified by thermal fluctuations.

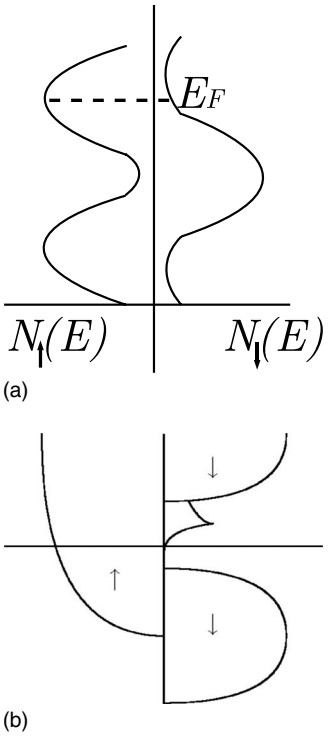

FIG. 8. Schematic half-metallic DOS with and without the spin mixing. (a) Classical picture (Dowben and Skomski, 2004). (b) Schematic half-metallic DOS, and the presence of NQP states, a genuine many-body effect.

Itoh *et al.* (2000) calculated the polarization for a ferromagnet-insulator magnetic tunnel junction with and without spin fluctuations in a thermally randomized atomic potential. The results indicate that the effect of spin fluctuations is significant. The idea of spin fluctuations was further developed by Lezaic *et al.* (2006) by considering the competition between hybridization and thermal spin fluctuation in the prototype HMF NiMnSb.

Figure 9 shows the sublattice susceptibilities computed within a generalized Heisenberg-type Hamiltonian. These results demonstrate that the Ni-sublattice magnetic order is lost already at 50 K (this effect is a consequence of the weakness of the coupling between the Ni moments and neighboring atoms); however, neutron-diffraction data (Hordequin, Lelivre-Bernab, and Pierre, 1997; Hordequin, Pierre, and Currat, 1997) do not support this scenario. The right-hand side of Fig. 9 presents the polarization $P(T)$ calculated in a disordered local moment (DLM) approach (Gyorffy *et al.*, 1985), representing the system at finite temperatures in a mean-field way. It was concluded that the thermal collapse of the polarization is connected with a change in hybridization due to the moment fluctuation, the effect of noncollinearity being much milder.

The issue of finite-temperature spin polarization in half metals remains an open question. Magnons play a crucial role, independent of the theoretical approach. In addition, the role of phonon modes in many-sublattice half metals is not excluded. Nevertheless, a nontrivial

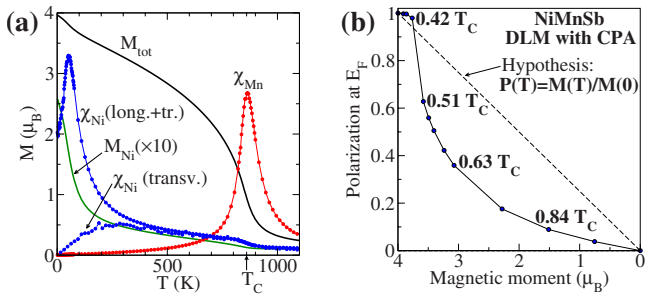

FIG. 9. (Color online) Monte Carlo results for finite-temperature magnetic properties. (a) Magnetization as a function of temperature. (b) Polarization at E_F as a function of total spin moment in the DLM picture for $NiMn^{\uparrow}_{1-x}Mn^{\downarrow}_{x}Sb$ calculated with CPA (Lezaic *et al.*, 2006).

contribution to the physics of half-metallic ferromagnets comes from genuine many-body effects. The corresponding first-principles calculations will be presented in Sec. V.

D. Tunneling conductance and spin-polarized STM

A useful tool to probe the spin polarization and nonquasiparticle states in HMFs is provided by tunneling phenomena (Auslender and Irkhin, 1985b; Bratkovsky, 1998; Auth *et al.*, 2003; Gercsi *et al.*, 2006; Sakuraba, Hattori, Oogane, *et al.*, 2006; Sakuraba, Miyakoshi, Oogane, *et al.*, 2006; Sakuraba *et al.*, 2007), and particularly by Andreev reflection spectroscopy for a HMF-superconductor tunnel junction (Tkachov *et al.*, 2001). The most direct way is the measurement of a tunnel current between two pieces of the HMF with opposite magnetization directions.

Here we explain in a simple qualitative way why the NQP states are important for tunneling transport. With this aim, we consider the above-discussed narrowband saturated Hubbard ferromagnet where the current carriers are the holes in the lowest Hubbard band, and the NQP states provide all of the spectral weight for the minority-spin projection. Suppose we have a tunnel junction with two pieces of this ferromagnet with either parallel [Fig.29(b)] or antiparallel [Fig. 29(c)] magnetization directions. From the one-particle point of view, spin-conserving tunneling is forbidden in the latter case. However, in the framework of a many-particle picture, the charge current is a transfer process between an empty site and a singly occupied site rather than the motion of an electron irrespective of the site, as in band theory, and therefore the distinction between these two cases (see Fig. 29) is due only to the difference in the densities of states. This means that the estimations of the tunneling magnetoresistance based on a simple one-electron picture are too optimistic; even for antiparallel spin orientation of two pieces of the half-metallic ferromagnets in the junction for zero temperature, the current is not zero, due to nonquasiparticle states. More exactly, it vanishes for zero bias since the density of NQP states at the Fermi energy is equal to zero. How-

ever, it grows sharply with the bias, having the scale of typical *magnon* energies, i.e., millivolts.

Formally, we consider a standard tunneling Hamiltonian [see, e.g., Mahan (1990)],

$$\mathcal{H} = \mathcal{H}_L + \mathcal{H}_R + \sum_{\mathbf{k},\mathbf{p}} (T_{\mathbf{kp}} c^\dagger_{\mathbf{k}\uparrow} c_{\mathbf{p}\downarrow} + \text{H.c.}), \tag{60}$$

where $\mathcal{H}_{L,R}$ are the Hamiltonians of the left (right) half spaces, respectively, $\mathbf{k}$ and $\mathbf{p}$ are the corresponding quasimomenta, and spin projections are defined with respect to the magnetization direction of a given half space (spin is conserved in the global coordinate system). Carrying out standard calculations of the tunneling current $\mathcal{I}$ in second order in $T_{\mathbf{k},\mathbf{p}}$, one has [cf. Mahan (1990)]

$$\mathcal{I} \propto \sum_{\mathbf{k},\mathbf{q},\mathbf{p}} |T_{\mathbf{k},\mathbf{p}}|^2 [1 + N_{\mathbf{q}} - f(t_{\mathbf{p}-\mathbf{q}})][f(t_{\mathbf{k}}) - f(t_{\mathbf{k}} + eV)] \times \delta(eV + t_{\mathbf{k}} - t_{\mathbf{p}-\mathbf{q}} + \omega_{\mathbf{q}}), \tag{61}$$

where V is the bias voltage.

A new experimental method is spin-polarized scanning-tunneling microscopy (STM) (Wiesendanger *et al.*, 1990; Heinze *et al.*, 2000; Kleiber *et al.*, 2000), which enables one to directly probe the spectral density with spin resolution in magnetic systems. The spin-polarized STM should be able to probe the NQP states via their contribution to the differential tunneling conductivity $d\mathcal{I}_\sigma/dV \propto N_\sigma(eV)$ (Irkhin and Katsnelson, 2006). Note that the value $N_\sigma(eV)$ vanishes for $|eV| < \hbar\omega_0$, where $\hbar\omega_0$ is the anisotropy gap in the magnon spectrum (Irkhin and Katsnelson, 2002), which is small, but could be changed by suitable substitution (Attema *et al.*, 2004). Keeping in mind that ferromagnetic semiconductors can be considered as a particlular case of HFMs (Irkhin and Katsnelson, 1983), taking account of NQP states can be important for a proper description of spin diodes and transistors (Flatte and Vignale, 2001; Tkachov *et al.*, 2001).

The above formulas are derived for the usual one-electron density of states at E_F, which is observed, say, in photoemission measurements. However, the factors that are present in the expression for the tunneling current do not influence the temperature dependence, and therefore these results are valid for spin polarization from tunneling conductance at zero bias in STM (Ukraintsev, 1996; Irkhin and Katsnelson, 2006). Unlike photoemission spectroscopy, which probes only occupied electron states, STM detects the states both above and below E_F, depending on the sign of the bias.

One should keep in mind that sometimes the surface of the HMF is not half metallic; in particular, this is the case of a prototype HMF, NiMnSb (de Wijs and de Groot, 2001). In such a situation, the tunneling current for minority electrons is due to surface states only. However, the NQP states can still be visible in the tunneling current via hybridization of the bulk states with the surface one. This leads to the Fano antiresonance picture, which is usually observed in STM investigations of the Kondo effect at metallic surfaces. In such cases, the tunneling conductance will be proportional to a mixture of N_σ and the real part of the on-site Green's function L_σ. Surprisingly, in this case the effect of NQP states on the tunneling current can be even more pronounced than in the ideal crystal. The reason is that the analytical continuation of the jump in $N_\sigma(E)$ is logarithmic; both singularities are cut at the energy $\bar{\omega}$. Nevertheless, the energy dependence of $L_\sigma(E)$ can be pronounced (Irkhin and Katsnelson, 2006).

STM measurements of the electron DOS also give the opportunity to probe *bosonic* excitations interacting with conduction electrons. Due to electron-phonon coupling, the derivative $dN_\sigma(E)/dE$ and thus $d^2\mathcal{I}_\sigma(V)/dV^2$ at $eV = E$ have peaks at energies $E = \pm\omega_i$ corresponding to the peaks in the phonon DOS. According to the above treatment [see, e.g., Eq. (43)], the same effect should be observable for the case of the electron-magnon interaction. However, in the latter case these peaks are essentially asymmetric with respect to the Fermi energy (zero bias) due to asymmetry of nonquasiparticle contributions. This asymmetry can be used to distinguish phonon and magnon peaks.

Thermoelectric power in the tunnel situation was theoretically investigated by McCann and Fal'ko (2002, 2003). The relative polarizations of ferromagnetic layers can be manipulated by an external magnetic field, and a large difference occurs for a junction between two ferromagnets with antiparallel and parallel polarizations. This magnetothermopower effect becomes very large in the extreme case of a junction between two half-metallic ferromagnets, since the thermopower is inversely proportional to the area of the maximal cross section of the Fermi surface of minority electrons in the plane parallel to the interface. One has a strong polarization dependence of the thermopower

$$\mathcal{Q}_{AP} = 0.64 k_B/e, \quad \mathcal{Q}_P \propto k_B^2 T/eE_F. \tag{62}$$

This result is independent of temperature and of the specific half-metallic material, and it represents a very large magnetothermopower effect, $\Delta\mathcal{Q} \simeq \mathcal{Q}_{AP} = -55\ \mu\text{V/K}$.

E. Spin waves

Unlike the Stoner theory, the Hubbard model and other models with electron correlations enable one to describe spin-wave excitations in an itinerant ferromagnet. This was already done in the old approaches based on the random-phase approximation (RPA) (Herring, 1966). To discuss related approaches, we present the interaction Hamiltonian in terms of the spin density operators,

$$\mathcal{H}_{\text{int}} = \frac{U}{2} \sum_{\mathbf{k}\sigma} c^\dagger_{\mathbf{k}\sigma} c_{\mathbf{k}\sigma} - \frac{U}{2} \sum_{\mathbf{q}} (S^-_{-\mathbf{q}} S^+_{\mathbf{q}} + S^+_{\mathbf{q}} S^-_{-\mathbf{q}}), \tag{63}$$

where $S^\alpha_{\mathbf{q}}$ are the Fourier components of the spin-density operators. The first term in Eq. (63) yields a renormalization of the chemical potential and may be omitted. Writing down the sequence of equations of motion for the spin Green's function

$$G_{\mathbf{q}}(\omega) = \langle\langle S_{\mathbf{q}}^{+} | S_{-\mathbf{q}}^{-} \rangle\rangle_{\omega}, \tag{64}$$

one derives (Irkhin and Katsnelson, 1990)

$$G_{\mathbf{q}}(\omega) = \frac{\langle S^{z} \rangle - \Omega_{\mathbf{q}}(\omega)/U}{\omega - \Omega_{\mathbf{q}}(\omega) - \pi_{\mathbf{q}}(\omega)}, \tag{65}$$

where

$$\Omega_{\mathbf{q}}(\omega) = U \sum_{\mathbf{k}} \frac{t_{\mathbf{k}+\mathbf{q}} - t_{\mathbf{k}}}{t_{\mathbf{k}+\mathbf{q}} - t_{\mathbf{k}} + \Delta - \omega} (n_{\mathbf{k}\uparrow} - n_{\mathbf{k}+\mathbf{q}\downarrow}), \tag{66}$$

where Δ is the spin splitting defined after Eq. (2) and the self-energy π describes corrections to the RPA. Unlike the standard form of the RPA,

$$G_{\mathbf{q}}(\omega) = \frac{\Pi_{\mathbf{q}}(\omega)}{1 - U\Pi_{\mathbf{q}}(\omega)}, \tag{67}$$

$$\Pi_{\mathbf{q}}(\omega) = -\sum_{\mathbf{k}} \frac{n_{\mathbf{k}\uparrow} - n_{\mathbf{k}+\mathbf{q}\downarrow}}{\omega + t_{\mathbf{k}\uparrow} - t_{\mathbf{k}+\mathbf{q}\downarrow}}, \tag{68}$$

the equivalent representation (65) yields explicitly the magnon (spin-wave) pole

$$\omega_{\mathbf{q}} \simeq \Omega_{\mathbf{q}}(0) = \sum_{\mathbf{k}\sigma} \mathcal{A}_{\mathbf{k}\mathbf{q}}^{\sigma} n_{\mathbf{k}\sigma}, \tag{69}$$

where $\mathcal{A}_{\mathbf{k}\mathbf{q}}^{\sigma}$ is given by Eq. (12). Expanding in q, we get $\omega_{\mathbf{q}} = \mathcal{D}_{\alpha\beta} q_{\alpha} q_{\beta}$, where

$$\mathcal{D}_{\alpha\beta} = \frac{U}{\Delta} \sum_{\mathbf{k}} \left(\frac{\partial^2 t_{\mathbf{k}}}{\partial k_{\alpha} \partial k_{\beta}} (n_{\mathbf{k}\uparrow} + n_{\mathbf{k}\downarrow}) - \frac{1}{\Delta} \frac{\partial t_{\mathbf{k}}}{\partial k_{\alpha}} \frac{\partial t_{\mathbf{k}}}{\partial k_{\beta}} (n_{\mathbf{k}\uparrow} - n_{\mathbf{k}\downarrow}) \right). \tag{70}$$

Equation (70) is the spin-wave stiffness tensor component. For a weak ferromagnet ($\Delta \ll E_F, U$), we have $\mathcal{D} \propto \Delta$. The magnon damping in the RPA is given by

$$\gamma_{\mathbf{q}}^{(1)}(\omega) = -\operatorname{Im} \Omega_{\mathbf{q}}(\omega) = \pi U \Delta \omega \sum_{\mathbf{k}} \left(-\frac{\partial n_{\mathbf{k}\uparrow}}{\partial t_{\mathbf{k}\uparrow}} \right) \delta(\omega - t_{\mathbf{k}+\mathbf{q}\downarrow} + t_{\mathbf{k}\uparrow}), \tag{71}$$

$$\gamma_{\mathbf{q}}^{(1)} \equiv \gamma_{\mathbf{q}}^{(1)}(\omega_{\mathbf{q}}) \simeq \pi U \Delta \omega_{\mathbf{q}} N_{\uparrow}(E_F) N_{\downarrow}(E_F) \theta(\omega_{\mathbf{q}} - \omega_{-}) \tag{72}$$

with $\theta(x)$ being the step function. Here $\omega_{-} = \omega(q^{*})$ is the threshold energy, which is determined by the condition of entering into the Stoner continuum (decay into the Stoner excitations, i.e., electron-hole pairs), q^{*} being the minimal (in $\mathbf{k}$) solution to

$$t_{\mathbf{k}+\mathbf{q}^{*}\downarrow} = t_{\mathbf{k}\uparrow} = E_F. \tag{73}$$

The quantity ω_{-} determines a characteristic energy scale separating two temperature regions, namely, the contributions of spin waves [poles of the Green's function (65) dominate at $T < \omega_{-}$ and those of Stoner excitations (its branch cut) at $T > \omega_{-}$].

Although the formal expressions in the *s-d* exchange model are similar, the presence of two electron subsystems leads to some new effects, in particular to the possible occurrence of the "optical mode" pole $\omega \simeq 2|I|S$. The problem of the optical mode formation and its damping was investigated in degenerate ferromagnetic semiconductors (Auslender and Irkhin, 1984a, 1985a; Irkhin and Katsnelson, 1985a; Irkhin, 1987). Kaplan *et al.* (2001) performed exact diagonalization studies of the double-exchange model which indicate the existence of continuum states in the single-spin-flip channel that overlap the magnons at very low energies (of order 10^{-2} eV) and extend to high energies. This picture differs dramatically from the prevalent view, in which there are magnons plus the Stoner continuum at the high-energy scale, with nothing in between. The peculiarities of magnons in HMFs, especially in the collossal-magnetoresistance materials have recently been reviewed by Zhang *et al.* (2007).

In the case of weak ferromagnets, the contribution of the branch cut from the spin Green's function may be treated approximately as that of a paramagnon pole at imaginary ω, and we obtain

$$q^{*} = k_{F\uparrow} - k_{F\downarrow}, \quad \omega_{-} = \mathcal{D}(k_{F\uparrow} - k_{F\downarrow})^2 \sim \Delta^3 \sim T_C^2 / E_F. \tag{74}$$

Since q^{*} is small, we have at small $q > q^{*}$, instead of Eq. (72),

$$\gamma_{\mathbf{q}}^{(1)}(\omega_{\mathbf{q}}) \simeq \frac{U\Delta\omega}{q} \frac{\Omega_0}{4\pi} (m^{*})^2 \equiv A/q, \tag{75}$$

with Ω_0 the lattice cell volume. The estimation (74) holds also for the *s-d*(*f*) exchange model with the indirect RKKY interaction, where $\mathcal{D} \sim T_C/S \sim I^2 S / E_F$.

The damping at very small $q < q^{*}$ [where Eq. (71) vanishes] is due to two-magnon scattering processes. To consider these, we have to calculate the function π to leading order in the fluctuating part of the Coulomb interaction. Writing down the equation of motion for the Green's function (64), we obtain

$$\pi_{\mathbf{q}}(\omega) = \sum_{\mathbf{p}\mathbf{k}} (A_{\mathbf{k}\mathbf{q}}^{\uparrow})^2 [B(\mathbf{k}\uparrow, \mathbf{k}+\mathbf{q}-\mathbf{p}\uparrow, \omega_{\mathbf{p}} - \omega) + B(\mathbf{k} + \mathbf{p}\downarrow, \mathbf{k}+\mathbf{q}\downarrow, \omega_{\mathbf{p}} - \omega) - B(\mathbf{k}+\mathbf{p}\downarrow, \mathbf{k}\uparrow, \omega_{\mathbf{p}}) - B(\mathbf{k}+\mathbf{q}\downarrow, \mathbf{k}+\mathbf{q}-\mathbf{p}\uparrow, \mathbf{p}, \omega_{\mathbf{p}})], \tag{76}$$

where

$$B(\mathbf{k}'\boldsymbol{\sigma}', \mathbf{k}\boldsymbol{\sigma}, \omega) = \frac{N_{\mathbf{p}}(n_{\mathbf{k}'\boldsymbol{\sigma}'} - n_{\mathbf{k}\boldsymbol{\sigma}}) + n_{\mathbf{k}'\boldsymbol{\sigma}'}(1 - n_{\mathbf{k}\boldsymbol{\sigma}})}{\omega - t_{\mathbf{k}'\boldsymbol{\sigma}'} + t_{\mathbf{k}\boldsymbol{\sigma}}}. \tag{77}$$

The magnon damping needed is given by the imaginary part of Eq. (76),

$$\gamma_{\mathbf{q}}^{(2)}(\omega) = \pi \sum_{\mathbf{k}\mathbf{p}\boldsymbol{\sigma}} (A_{\mathbf{k}\mathbf{q}}^{\uparrow})^2 (n_{\mathbf{k}\boldsymbol{\sigma}} - n_{\mathbf{k}+\mathbf{q}-\mathbf{p}\boldsymbol{\sigma}}) [N_{\mathbf{p}} - N_B(\omega_{\mathbf{p}} - \omega)] \times \delta(\omega + t_{\mathbf{k}} - t_{\mathbf{k}+\mathbf{q}-\mathbf{p}} - \omega_{\mathbf{p}}). \tag{78}$$

Integration for the isotropic electron spectrum gives (Irkhin and Katsnelson, 1990)

$$\gamma_{\mathbf{q}}^{(2)}(\omega)=\frac{\Omega_0^2}{12\pi^3}\frac{q^4}{4\langle S^z\rangle^2}\sum_{\sigma}k_{F\sigma}^2 \times\begin{cases}\omega_{\mathbf{q}}/35, & T\ll\omega_{\mathbf{q}}\\ (T/4)\left[\ln(T/\omega_{\mathbf{q}})+\frac{5}{3}\right], & T\gg\omega_{\mathbf{q}}.\end{cases} \tag{79}$$

These results were obtained by Silin and Solontsov (1984) within the phenomenological Fermi-liquid theory and Auslender and Irkhin (1984a, 1985a) within the *s-d* exchange model. Golosov (2000) reproduced the results of Auslender and Irkhin (1984a, 1985a) and Irkhin and Katsnelson (1985a) within the $1/2S$ expansion and performed numerical investigations of the magnon spectrum and damping in the limit of large $|I|$ (double-exchange situation) in application to colossal-magnetoresistance compounds.

The real part of Eq. (76) describes the temperature dependence of the spin stiffness owing to two-magnon processes [in addition to the simplest T^2 contribution, which occurs from the temperature dependence of the Fermi distribution functions in Eq. (65)]. The spin-wave contribution connected with the magnon distribution functions is proportional to T. More interesting is the nonanalytical many-electron contribution owing to the Fermi functions,

$$\delta\mathcal{D}_{\alpha\beta}=\frac{1}{4\langle S^z\rangle^2}\sum_{\mathbf{pk}}\frac{\partial t_{\mathbf{k}}}{\partial k_\alpha}\frac{\partial t_{\mathbf{k}}}{\partial k_\beta}\left(\frac{n_{\mathbf{k}\downarrow}(1-n_{\mathbf{k}-\mathbf{p}\uparrow})}{t_{\mathbf{k}}-t_{\mathbf{k}-\mathbf{p}}-\omega_{\mathbf{p}}}+\frac{n_{\mathbf{k}+\mathbf{p}\downarrow}(1-n_{\mathbf{k}\downarrow})}{t_{\mathbf{k}+\mathbf{p}}-t_{\mathbf{k}}-\omega_{\mathbf{p}}}-\frac{n_{\mathbf{k}+\mathbf{p}\downarrow}(1-n_{\mathbf{k}\uparrow})}{t_{\mathbf{k}+\mathbf{p}\downarrow}-t_{\mathbf{k}\uparrow}-\omega_{\mathbf{p}}}-\frac{n_{\mathbf{k}\downarrow}(1-n_{\mathbf{k}-\mathbf{p}\downarrow})}{t_{\mathbf{k}\downarrow}-t_{\mathbf{k}-\mathbf{p}\uparrow}-\omega_{\mathbf{p}}}\right). \tag{80}$$

Performing integration for parabolic spectra of electrons and magnons yields

$$\delta\mathcal{D}(T)=\left(\frac{\pi\Omega_0 T}{12\langle S^z\rangle m^*}\right)^2\frac{1}{D}\left(\sum_{\sigma}N_\sigma^2(E_F)\ln\frac{T}{\omega_+}-2N_\uparrow(E_F)N_\downarrow(E_F)\ln\frac{\max(\omega_-,T)}{\omega_+}\right) \tag{81}$$

with

$$\omega_\pm=\mathcal{D}(k_{F\uparrow}\pm k_{F\downarrow})^2,\quad N_\sigma(E_F)=m^*\Omega_0 k_F/2\pi^2. \tag{82}$$

It should be noted that the correction (81) dominates at low temperatures over the above-mentioned T^2 correction, which demonstrates an important role of corrections to the RPA. Unfortunately, the $T^2\ln T$ term has not yet been considered when analyzing magnon spectra of ferromagnetic metals. We see that the temperature dependences of spin-wave characteristics in conducting magnets differ considerably from those in the Heisenberg model.

F. Magnetization and local moments

To treat the problem of magnetic moments in the Hubbard model, we consider corrections to the magnetization $\langle S^z\rangle$. We have

$$\langle S^z\rangle=\frac{n}{2}-\sum_{\mathbf{q}}\langle S_{\mathbf{q}}^- S_{\mathbf{q}}^+\rangle-\langle\hat{n}_{i\uparrow}\hat{n}_{i\downarrow}\rangle. \tag{83}$$

The first average involved in Eq. (83) is calculated from the spectral representation of the RPA Green's function (65),

$$\langle S_{-\mathbf{q}}^- S_{\mathbf{q}}^+\rangle=\begin{cases}2S_0 N_{\mathbf{q}} & (q<q^*) \quad (84)\\ \frac{1}{\pi}\int_{-\infty}^{\infty}d\omega\frac{N_B(\omega)\gamma_{\mathbf{q}}^{(1)}(\omega)(\Delta-\omega)/U}{[\omega-\mathrm{Re}\,\Omega_{\mathbf{q}}(\omega)]^2+[\gamma_{\mathbf{q}}^{(1)}(\omega)]^2} & (q>q^*). \quad (85)\end{cases}$$

In contradiction with Eqs. (83) and (84), in the true Bloch spin-wave contribution to magnetization every magnon should decrease $\langle S^z\rangle$ by unity. Agreement may be restored by allowing not only the magnon pole but also branch cut contributions (Irkhin and Katsnelson, 1990). In the semiphenomenological manner, it is convenient to introduce magnon operators that satisfy on average the Bose commutation relations,

$$b_{\mathbf{q}}=(2S_0)^{-1/2}S_{\mathbf{q}}^+,\quad b_{\mathbf{q}}^\dagger=(2S_0)^{-1/2}S_{-\mathbf{q}}^-. \tag{86}$$

Then we have

$$\delta\langle S^z\rangle=-\sum_{\mathbf{q}}\langle b_{\mathbf{q}}^\dagger b_{\mathbf{q}}\rangle=\frac{1}{(2S_0)}\sum_{\mathbf{q}}\langle S_{-\mathbf{q}}^- S_{\mathbf{q}}^+\rangle. \tag{87}$$

Performing integration over ω in Eq. (84) at $T=0$ K, we obtain

$$\delta\langle S^z\rangle=-\frac{1}{\pi}\sum_{\mathbf{q}}\frac{\gamma_{\mathbf{q}}^{(1)}}{\omega_{\mathbf{q}}}\ln\frac{W}{\omega_{\mathbf{q}}}, \tag{88}$$

with W the bandwidth. This contribution of the order of $U^2\ln(W/\omega_+)$ describes a zero-point decrease of the magnetization due to the ground-state magnon damping, which is caused by the Stoner excitations. For parabolic electron and magnon spectra, neglecting the damping in

the denominator of Eq. (85), we obtain at low temperatures $T<\omega_-$ the dependence $\delta\langle S^z\rangle_{\rm cl}\propto U^2(T/\omega_+)^2$. For a weak ferromagnet, the temperature correction is proportional to $(T/T_C)^2$, in agreement with the self-consistent renormalization theory (Moriya, 1985). It should be noted that the T^2 correction obtained is much larger than the Stoner contribution of the order of $(T/E_F)^2$. The spin-wave corrections to the local magnetic moment at a site $\langle \mathbf{S}^2\rangle=(3/4)(n-2\langle \hat{n}_{i\uparrow}\hat{n}_{i\downarrow}\rangle)$ at low $T\ll\omega_-$ have a weak dependence $-(T/T_C)^{5/2}$ (Irkhin and Katsnelson, 1990). This justifies their omission in the above discussion of the magnetization (83).

At high $T>\omega_-$, the damping in the denominator dominates at small q in the case of a weak ferromagnet. Taking into account Eq. (75), we obtain from Eq. (84)

$$\delta\langle S^-_{\mathbf{q}}S^+_{\mathbf{q}}\rangle=\frac{\Delta}{\pi U}\int_{-\infty}^{\infty}d\omega\, N_B(\omega)\int_0^{\infty}\frac{\omega A q\, dq}{(\mathcal{D}q^2)^2+A^2\omega^2/q^2}$$
$$\propto\left(\frac{T}{E_F}\right)^{4/3}. \tag{89}$$

Thus we get from Eq. (83) the $T^{4/3}$ contribution to the magnetization, which agrees with the result of the phase-transition scaling theory near $T=T_C$. For a ferromagnet with well-localized magnetic moments, damping may be neglected and we derive a small correction $\delta\langle S^z\rangle_{\rm el}\propto -I^2\omega_-\ln(T/\omega_-)$ (Irkhin and Katsnelson, 1996).

Now we discuss a more realistic situation in HMFs, in particular in the Heusler alloys. These compounds demonstrate high values of the saturation magnetization and Curie temperature [see Irkhin and Katsnelson (1994), Galanakis and Dederichs (2005), Fecher *et al.* (2006), Ozdogan *et al.* (2006)]. The strong ferromagnetism is due mainly to local moments of well-separated Mn atoms. On the other hand, the highest magnetic moment ($6\mu_B$) and Curie temperature (1100 K) in the classes of Heusler compounds as well as half-metallic ferromagnets were revealed for Co_2FeSi (Wurmehl *et al.*, 2005). It was found empirically that the Curie temperature of Co_2-based Heusler compounds can be estimated from a nearly linear dependence on the magnetic moment (Fecher *et al.*, 2006).

The high spin polarization and magnetic moment of half-metallic ferromagnets can be treated within the generalized Slater-Pauling rule (Galanakis *et al.*, 2002b; Fecher *et al.*, 2006). According to the original formulation by Slater and Pauling, the magnetic moments m of $3d$ elements and their binary compounds can be described by the mean number of valence electrons n_V per atom. A plot of m versus magnetic valence $m(n_M)$ is called the generalized Slater-Pauling rule, as described by Kübler (1984). According to Hund's rule, it is often favorable for the majority d states to be fully occupied ($n_{d\uparrow}=5$). Starting from $m=2n_\uparrow-n_V$, this leads to the definition of the magnetic valence as $n_M=10-n_V$, so that the magnetic moment per atom is given by $m=n_M+2n_{sp\uparrow}$.

In the case of localized moments, the Fermi energy is pinned in a deep valley of the minority electron density. This constrains $n_{d\downarrow}$ to be approximately 3, and $m=n_V-6-2n_{sp\uparrow}$. HMFs are supposed to exhibit a real gap in the minority density of states where the Fermi energy is pinned. Then the number of occupied minority states has to be an integer. Thus, the Slater-Pauling rule will be strictly satisfied with the spin magnetic moment per atom $m=n_V-6$. The situation for the HMF and non-HMF full Heusler alloys is shown in Fig. 10.

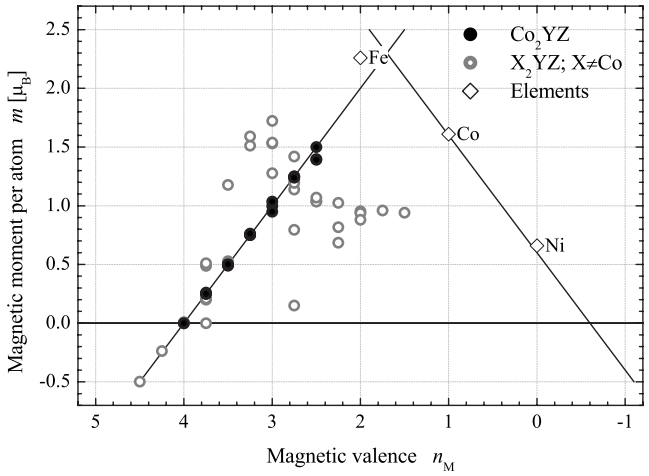

FIG. 10. Slater-Pauling graph for Heusler compounds (Fecher *et al.*, 2006).

For ordered compounds with different kinds of atoms, it may be more convenient to consider the total spin magnetic moment M_t of all unit cell atoms. This quantity scales with the valence electron number Z_t: $M_t=Z_t-18$ for the half Heusler and $M_t=Z_t-24$ for the full Heusler alloys. Thus, in both types of compound, the spin magnetic moment per unit cell is strictly integer for the HMF situation. On the other hand, for alloys with non-integer site occupancies like the quaternaries $X_2Y_{1-x}Y_xZ$, the moment may become noninteger depending on the composition, even for the HMF state. First-principles calculations of the quaternary Heusler alloys $Co_2(Cr_{1-x}Mn_x)Al$, $Co_2Mn(Al_{1-x}Sn_x)$, and $[Fe_{1-x}Co_x]_2MnAl$ (Galanakis, 2004) demonstrated the Slater-Pauling behavior and half-metallic properties. Moreover, this behavior was investigated theoretically in V-based Heusler alloys Mn_2VZ (Z=Al, Ga, In, Si, Ge, Sn), which are predicted to demonstrate half-metallic ferrimagnetism (Weht and Pickett, 1999; Sasioglu, Galanakis, Sandratskii, *et al.*, 2005; Ozdogan *et al.*, 2006).

An interesting feature of the half-metallic Heusler alloys is that the Rhodes-Wolfarth ratio p_C/p_s (p_C are the effective moments, p_s the saturation moments) can be considerably smaller than unity (Irkhin and Katsnelson, 1994). Moreover, the effective moment in the paramagnetic state, determined from the paramagnetic susceptibility, decreases appreciably with temperature. We recall that for Heisenberg magnets (atomiclike magnetic states) we have $p_C/p_s=1$, and for weak itinerant ferromagnets such as $ZrZn_2$, $p_C/p_s\gg 1$, in accordance with the concept of thermally induced local magnetic mo-

ments (Moriya, 1985). In the case of conventional strong itinerant ferromagnets (for example, Fe and Ni), this ratio is also greater than unity [for a detailed discussion, see Lichtenstein *et al.* (2001)]. It follows, therefore, that the inequality $p_C/p_s<1$ is a striking property of HMFs that could be used in their preliminary experimental identification.

This behavior may be explained by a change of electronic structure. The temperature dependence of the magnetic moment in the paramagnetic state may be due to short-range magnetic order (local densities of states are similar to those in the ferromagnetic state). Numerical calculations demonstrate that the reduction in the moments is a consequence of a change in the electron structure as a result of rotation of the magnetic moments, as demonstrated for Fe and Ni by Turzhevskii *et al.* (1990). One would expect such changes to be particularly large in the case of HMFs, and they should be of a qualitative nature [smearing out of the hybridization gap because of spin disorder; for a review, see Irkhin and Katsnelson (1994)]. From the many-electron model point of view, the decrease of the local moment with increasing temperature is connected with the absence of corrections to ground-state magnetization of the type (88). However, such corrections do occur at high temperatures.

G. Nuclear magnetic relaxation

Nuclear magnetic resonance (NMR), which is one of most powerful tools for investigating various physical properties, has a number of peculiarities for magnetically ordered materials, and especially for HMFs. The localized-spin Heisenberg model is inadequate to describe the systems mentioned above, where the role of conduction electrons is essential for the magnetic properties. Usually the data on the longitudinal nuclear magnetic relaxation rate $1/T_1$ are discussed within itinerant-electron models such as the Hubbard model or phenomenological spin-fluctuation theories (Ueda and Moriya, 1975; Moriya, 1985, 1994; Millis *et al.*, 1990; Ishigaki and Moriya, 1996). On the other hand, in the *s*-*d*(*f*) exchange model (well-separated localized and itinerant subsystems), magnetic properties differ essentially from those in the paramagnon regime. We discuss the contributions to $1/T_1(T)$ owing to electron-magnon interactions for three- and two-dimensional (3D and 2D) metallic ferromagnets with well-defined local magnetic moments, with special attention to the HMF case (Irkhin and Katsnelson, 2001).

The standard Hamiltonian of the hyperfine interaction $\mathcal{H}_{hf}=\mathbf{hI}$ ($h_\alpha=A_{\alpha\beta}S_\beta$, $\hat{A}$ is the hyperfine interaction matrix) contains the Fermi (contact) and dipole-dipole contributions, $A_{\alpha\beta}=A^F\delta_{\alpha\beta}+A^{\mathrm{dip}}_{\alpha\beta}$. According to Abragam (1961), we have

$$h^- = (A^F + \tfrac{1}{3}aF^{(0)})S^- + aF^{(2)}S^+ + 2aF^{(1)}S^z, \tag{90}$$

$$h^z = (A^F - \tfrac{2}{3}aF^{(0)})S^z + a(F^{(1)}S^+ + F^{(1)*}S^-), \tag{91}$$

where

$$F^{(0)} = \langle (1-3\cos^2\theta)/r^3\rangle,$$

$$F^{(1)} = \langle \sin\theta\cos\theta\exp(-i\phi)/r^3\rangle,$$

$$F^{(2)} = \langle \sin^2\theta\exp(-2i\phi)/r^3\rangle, \quad a = -\tfrac{3}{2}\gamma_e\gamma_n, \tag{92}$$

$\langle\cdots\rangle$ is the average over the electron subsystem states, and γ_e and γ_n are the gyromagnetic ratios for electron and nuclear moments, respectively. In the case of local cubic symmetry, we have $F^{(a)}=0$. The Fermi hyperfine interaction is proportional to the electron density at the nucleus and therefore only *s* states participate in it, the contribution of core *s* states (which are polarized due to local magnetic moments) being much larger than that of conduction electrons. This is a consequence of the considerably smaller localization area (and therefore higher density on nuclei) for the core states. It is obvious that magnetic *f* or *d* electrons dominate also in dipole interactions because of their large spin polarization. Hence the direct interaction of nuclear spins with those of conduction electrons can be neglected in magnets with well-defined local magnetic moments. Nevertheless, conduction electrons do affect nuclear relaxation via their influence on the local-moment system; besides that, as we show below, such contributions possess large exchange enhancement factors.

Using the expressions for $1/T_1$ and linewidth $1/T_2$ in terms of the Green's functions (Moriya, 1963),

$$\frac{1}{T_1} = -\frac{T}{2\pi}\,\mathrm{Im}\sum_{\mathbf{q}}\langle\langle h^+_{\mathbf{q}}|h^-_{-\mathbf{q}}\rangle\rangle_{\omega_n}/\omega_n, \tag{93}$$

$$\frac{1}{T_2} = \frac{1}{2T_1} - \frac{T}{2\pi}\lim_{\omega\to 0}\mathrm{Im}\sum_{\mathbf{q}}\langle\langle h^z_{\mathbf{q}}|h^z_{-\mathbf{q}}\rangle\rangle_{\omega}/\omega \tag{94}$$

($\omega_n=\langle h^z\rangle \ll T$ is the NMR frequency), we derive

$$\frac{1}{T_1} = \frac{T}{2}\{[(A^F+\tfrac{1}{3}aF^{(0)})^2 + a^2|F^{(2)}|^2]K^{+-} + 4a^2|F^{(1)}|^2K^{zz}\}, \tag{95}$$

$$\frac{1}{T_2} = \frac{1}{2T_1} + \frac{T}{2}\{(A^F - \tfrac{2}{3}aF^{(0)})^2K^{zz} + a^2[2|F^{(1)}|^2K^{+-}]\}, \tag{96}$$

$$K^{\alpha\beta} = -(1/\pi)\lim_{\omega\to 0}\mathrm{Im}\sum_{\mathbf{q}}\langle\langle S^+_{\mathbf{q}}|S^-_{-\mathbf{q}}\rangle\rangle_{\omega}/\omega. \tag{97}$$

Passing to the magnon representation, we obtain

$$\langle\langle S^+_{\mathbf{q}}|S^-_{-\mathbf{q}}\rangle\rangle_{\omega} = 2S/[\omega - \omega_{\mathbf{q}} + i\gamma_{\mathbf{q}}(\omega)], \tag{98}$$

where $\omega_{\mathbf{q}}=2S(J_{\mathbf{q}}-J_0)+\omega_0$ is the magnon frequency and $\gamma_{\mathbf{q}}(\omega)\propto\omega$ is the magnon damping. Thus we have

$$K^{+-} = \frac{2S}{\pi\omega_n}\sum_{\mathbf{q}} \frac{\gamma_{\mathbf{q}}(\omega_n)}{\omega_{\mathbf{q}}^2}. \tag{99}$$

The damping owing to the one-magnon decay processes can be represented as

$$\gamma_{\mathbf{q}}^{(1)}(\omega) = 2\pi I^2 S\omega \sum_{\mathbf{k}} \delta(t_{\mathbf{k}\uparrow})\delta(t_{\mathbf{k}-\mathbf{q}\downarrow}), \tag{100}$$

where the energy is referred to the Fermi level. The linearity of spin-fluctuation damping in ω is a characteristic property of metals. According to Eq. (95), this leads to T-linear contributions to $1/T_1$, which is the Korringa law. It is important that the simplest expression for the Korringa relaxation

$$1/T_1 \simeq 1/T_2 \simeq A^2 N_\uparrow(E_F) N_\downarrow(E_F) T \tag{101}$$

(A is the effective hyperfine interaction constant) is almost never applicable for magnetic metals: exchange enhancement factors can change even the order of magnitude of $1/T_1$ (Moriya, 1985; Irkhin and Katsnelson, 1994). An accurate expression for the Korringa contribution in the case under consideration can be derived by the substitution of Eqs. (99) and (100) into Eq. (95).

Apart from the three-dimensional case, we can also consider two-dimensional HMFs, keeping in mind, for example, layered CMR compounds like $LaSr_2Mn_2O_7$ (de Boer and Groot, 1999; Nagaev, 2001). According to Eq. (72), the damping (100) has a threshold value of q, which is determined by the spin splitting $\Delta = 2|I|S$, $q^* = \Delta/v_F$ (v_F is the electron velocity at the Fermi level), the corresponding characteristic temperature and energy scale being $\omega_- \sim (\Delta/v_F)^2 T_C$. After integration for the parabolic electron spectrum, the one-magnon damping contribution to Eq. (99) takes the form

$$\delta^{(1)}K^{+-} = \frac{N_\uparrow(E_F)N_\downarrow(E_F)}{\mathcal{D}^2 m^2} \times \begin{cases} 1/4, & D=3 \\ 1/(\pi q^*), & D=2, \end{cases} \tag{102}$$

with m the electron effective mass. Thus in the 3D case the factor of I^2 is canceled, and the factor of I^{-1} occurs in the 2D case, so that we obtain a strongly enhanced T-linear Korringa-type term (remember that $\mathcal{D} \sim J \sim I^2/W$ for the RKKY interaction). This means that the contribution of conduction electrons to the T-linear relaxation rate via their interaction with localized spins is indeed much more important than the "direct" contribution: perturbation theory in the s-d exchange coupling parameter I turns out to be singular.

In HMFs, the one-magnon decay processes are absent and electron-magnon (two-magnon) scattering processes should be considered (Sec. III.E). Substituting the corresponding damping into Eq. (99) yields for $D=3$

$$\delta^{(2)}K^{+-} = \frac{\Omega_0 T^{1/2}}{128\pi^2 S m^2 \mathcal{D}^{7/2}} \sum_\sigma N_\sigma^2(E_F) \times \begin{cases} 3\pi^{1/2}\zeta\left(\frac{3}{2}\right)T, & T \ll \omega_- \\ 5.2\omega_-, & T \gg \omega_-, \end{cases}$$

where $\zeta(z)$ is the Riemann function and Ω_0 is the lattice cell volume. This contribution can also considerably modify the temperature dependence of $1/T_1$ in usual ferromagnets, a crossover from $T^{5/2}$ to $T^{3/2}$ dependence of the correction taking place.

For $D=2$ and $T, \omega_- \gg \omega_0$, small magnon momenta of order of $(\omega_0/\mathcal{D})^{1/2}$ make the main contribution to Eq. (99). Using the high-temperature expression $N_{\mathbf{p}} = T/\omega_{\mathbf{p}}$, one gets

$$\delta^{(2)}K^{+-} = 1.23\frac{\Omega_0^3 k_F}{8\pi^4 S \mathcal{D}^{5/2}\omega_0^{1/2}} T. \tag{103}$$

Thus in the 2D FM case, in contrast with the 3D one, the relaxation rate $1/T_1$ is strongly dependent on the anisotropy gap. It is worth noting an important difference between relaxation processes via phonons and via magnons, due to the gap in the magnon spectrum. Usually $\omega_0 > \omega_n$ and therefore one-magnon processes contribute to the relaxation rate due to magnon damping only [cf. the discussion of the phonon-induced relaxation processes by Abragam (1961)]. However, the mechanisms of magnon damping in magnetic dielectrics (magnon-magnon interactions) are different from those in magnetic metals and degenerate semiconductors (Auslender and Irkhin, 1984a, 1985a).

H. Thermodynamic properties

Consider the renormalization of electronic specific heat in an itinerant ferromagnet due to interaction with spin fluctuations. Integration in Eqs. (8) and (9) at $T=0$ gives

$$\mathrm{Re}\,\Sigma_\sigma(k_{F\sigma}, E) = -\frac{U\Delta}{\omega_+ - \omega_-} N_{-\sigma}(E_F) \times \sum_{\alpha=\pm} \alpha(E-\omega_\alpha)\ln\frac{|E-\omega_\alpha|}{W}.$$

Then the inverse residue of the electron Green's function $1/Z_{\mathbf{k}\sigma}(E) = 1 - (\partial/\partial E)\mathrm{Re}\,\Sigma_{\mathbf{k}\sigma}(E)$, which determines the renormalization of the electron effective mass owing to the electron-magnon interaction, contains a logarithmic factor. We obtain for the coefficient at the linear term in the electronic specific heat at $T \ll \omega_-$

$$\gamma_\sigma = \gamma_\sigma^{(0)}/Z_\sigma(k_{F\sigma}, E_F) = \frac{\pi^2}{3}N_\sigma(E_F)\left(1 + \frac{U\Delta}{\omega_+ - \omega_-}N_{-\sigma}(E_F)\ln\frac{\omega_+}{\omega_-}\right). \tag{104}$$

For weak itinerant ferromagnets, we have

$$\ln \frac{\omega_+}{\omega_-} \simeq -2\ln[UN(E_F)-1] \tag{105}$$

so that a paramagnon enhancement of the specific heat is obtained, the numerical factor in Eq. (104) being inexact in this limit because of the neglect of longitudinal spin fluctuations [see Moriya (1985)]. On the other hand, we have a considerable enhancement of specific heat owing to spin fluctuations in strong ferromagnets, which is actually observed in a number of systems.

Other thermodynamic properties may be treated by calculating the free energy of the system. The spin-wave contribution to the free energy has the usual form for Bose excitations with a square dispersion law, and is proportional to $(T/T_C)^{5/2}$. At low $T<\omega_-$, the many-electron (branch cut) contribution reads

$$F_{\mathrm{el}} = \frac{1}{2S_0}\sum_{\mathbf{q}>\mathbf{q}^*} \omega_{\mathbf{q}}\langle S^-_{-\mathbf{q}} S^+_{\mathbf{q}}\rangle \simeq U\Delta \sum_{\mathbf{k}\mathbf{k}'} \frac{n_{\mathbf{k}'\downarrow}(1-n_{\mathbf{k}\uparrow})}{t_{\mathbf{k}\uparrow}-t_{\mathbf{k}'\downarrow}+\omega_{\mathbf{k}-\mathbf{k}'}}. \tag{106}$$

Differentiating Eq. (106) over T, one obtains

$$\delta C_{\mathrm{el}} = -\frac{\partial}{\partial T}\delta F_{\mathrm{el}}(T) = U^2 \frac{2\langle S^z\rangle}{\omega_+-\omega_-} N_\uparrow(E_F) N_\downarrow(E_F) \frac{2\pi^2}{3} T \ln \frac{\omega_+}{\max(\omega_-, T)}. \tag{107}$$

Thus at $T \gg \omega_-$ we have the $T\ln T$ dependence of specific heat instead of Eq. (104).

As one can see from Eq. (104), the enhancement of the effective mass and electronic specific heat owing to spin fluctuations is absent in the half-metallic state. We demonstrate that the specific heat of a conducting ferromagnet may contain spin-fluctuation contributions of another nature. A general expression for the specific heat in the *s-d* exchange model in terms of the total energy is

$$C(T) = \frac{\partial\langle\mathcal{H}\rangle}{\partial T} = \frac{\partial}{\partial T}\int dE\, Ef(E)N_t(E) = \frac{\pi^2}{3}N_t(E)T + \int dE\, Ef(E)\frac{\partial}{\partial T}N_t(E,T), \tag{108}$$

where

$$N_t(E) = -\frac{1}{\pi}\sum_{\mathbf{k}\sigma} \mathrm{Im}\, G_{\mathbf{k}\sigma}(E).$$

The first term on the right-hand side of Eq. (108) yields the standard result of the Fermi-liquid theory. The second term is due to the energy dependence of the density of states. Such a dependence occurs in the conducting ferromagnet owing to nonquasiparticle (incoherent) status. Using again the expressions for the self-energies (8) and (9), we derive (Irkhin and Katsnelson, 1990)

$$\delta C_\sigma(T) = 2\sigma I^2\langle S^z\rangle \sum_{\mathbf{k}\mathbf{q}} \frac{f(t_{\mathbf{k}+\mathbf{q},-\sigma}-\sigma\omega_{\mathbf{q}})}{(t_{\mathbf{k}+\mathbf{q},-\sigma}-t_{\mathbf{k},\sigma})^2}\frac{\partial}{\partial T} n_{\mathbf{k}+\mathbf{q},-\sigma}. \tag{109}$$

Since at low temperatures $f(t_{\mathbf{k}+\mathbf{q},\downarrow}-\omega_{\mathbf{q}})=1$, $f(t_{\mathbf{k}+\mathbf{q},\uparrow}-\omega_{\mathbf{q}})=0$, the nonquasiparticle states with $\sigma=\downarrow$ do not contribute to the linear specific heat since they are empty at $T=0$ K. In the half-metallic state, nonquasiparticle contributions (108) with $\sigma=\uparrow$ are present for $I<0$ only, and we obtain

$$\delta C_\uparrow(T) = \frac{2\pi^2}{3} I^2\langle S^z\rangle N_\downarrow(E_F) T \sum_{\mathbf{k}} \frac{1}{(t_{\mathbf{k}\uparrow}-E_F)^2}. \tag{110}$$

To avoid misunderstanding, it should be noted that the presence of such contributions to specific heat indicates the inapplicability of the Fermi-liquid description in terms of dynamical quasiparticles only, which are determined by poles of Green's functions. It may be shown that the entropy of interacting Fermi systems at low T is expressed in terms of Landau quasiparticles with the energies determined as variational derivatives of the total energy with respect to occupation numbers (Carneiro and Pethick, 1975). Thus, even in the presence of nonpole contributions to the Green's functions, the description of thermodynamics in terms of statistical quasiparticles (Carneiro and Pethick, 1975) holds. (However, the quasiparticle description is insufficient for spectral characteristics, e.g., optical and emission data.) The anomalous γT term is determined by the difference of the spectra between statistical and dynamical quasiparticles.

Similar contributions to the specific heat in the Hubbard model with strong correlations were also discussed by Irkhin and Katsnelson (1990). They dominate in the enhancement of specific heat for half-metallic ferromagnets and may be important, besides the effective-mass enhancement (104), for the usual magnets with well-defined local moments.

I. Transport properties

Transport properties of HMFs have been the subject of numerous experimental investigations [see, e.g., recent works for CrO_2 (Rabe *et al.*, 2002) and NiMnSb (Borca *et al.*, 2001), and the reviews (Irkhin and Katsnelson, 1994; Nagaev, 2001; Ziese, 2002)]. At the same time, the theoretical interpretation of these results is still a problem. As for electronic scattering mechanisms, the most important difference between HMFs and standard itinerant electron ferromagnets such as iron or nickel is the absence of one-magnon scattering processes in the former case (Irkhin and Katsnelson, 1994).

Since states with one spin projection exist only at the Fermi level and one-magnon scattering processes are forbidden in the whole spin-wave region, the corresponding T^2 term in resistivity is absent in the case of half-metallic ferromagnets. This seems to be confirmed by comparing experimental data on resistivity of Heusler alloys *T*MnSb (T=Ni, Co, Pt, Cu, Au) and PtMnSn (Otto *et al.*, 1989) (see also the discussion in Sec. V.A.1).

The T^2 contribution from one-magnon processes to the resistivity for half-metallic systems (T=Ni, Co, Pt) was not observed out, whereas the dependences $\rho(T)$ for the usual ferromagnets were considerably steeper.

Two-magnon scattering processes were considered many years ago, the temperature dependence of resistivity obtained being $T^{7/2}$ (Hartman-Boutron, 1965; Roesler, 1965). The temperature dependence of the resistivity obtained has the form $T^{7/2}$. At low enough temperatures, the first result fails and should be replaced by $T^{9/2}$ (Lutovinov and Reizer, 1979); the reason is the compensation of the transverse and longitudinal contributions in the long-wavelength limit, which is a consequence of the rotational symmetry of the *s-d* exchange Hamiltonian (Grigin and Nagaev, 1974; Auslender *et al.*, 1983; Nagaev, 1983). We discuss the effects of interaction of current carriers with local moments in the standard *s-d* exchange model in the spin-wave region,

$$\mathcal{H} = \mathcal{H}_0 - I(2S)^{1/2}\sum_{\mathbf{kq}} (c^\dagger_{\mathbf{k}\uparrow}c_{\mathbf{k+q}\downarrow}b^\dagger_{\mathbf{q}} + \text{H.c.}) + I\sum_{\mathbf{kqp}\sigma} \sigma c^\dagger_{\mathbf{k}\sigma}c_{\mathbf{k+q-p}\sigma}b^\dagger_{\mathbf{q}}b_{\mathbf{p}}. \tag{111}$$

The zero-order Hamiltonian includes noninteracting electrons and magnons,

$$\mathcal{H}_0 = \sum_{\mathbf{k}\sigma} E_{\mathbf{k}\sigma}c^\dagger_{\mathbf{k}\sigma}c_{\mathbf{k}\sigma} + \sum_{\mathbf{q}} \omega_{\mathbf{q}}b^\dagger_{\mathbf{q}}b_{\mathbf{q}},$$

$$E_{\mathbf{k}\sigma} = t_{\mathbf{k}} - \sigma\Delta/2, \quad \omega_{\mathbf{q}} = 2S(J_0 - J_{\mathbf{q}}), \tag{112}$$

with $\Delta = 2IS$ the spin splitting that is included in $\mathcal{H}_0$. In the half-metallic case, the spin-flip processes do not work in the second order in I since states with one spin projection only are present at the Fermi level. At the same time, we have to consider the renormalization of longitudinal processes in higher orders in I (formally, we have to include terms up to second order in the quasiclassical small parameter $1/S$). To this end, we can eliminate from the Hamiltonian the terms that are linear in the magnon operators using the canonical transformation (Grigin and Nagaev, 1974; Nagaev, 1983). Then we obtain the effective Hamiltonian

$$\tilde{\mathcal{H}} = \mathcal{H}_0 + \frac{1}{2}\sum_{\mathbf{kqp}\sigma} (\mathcal{A}^\sigma_{\mathbf{kq}} + \mathcal{A}^\sigma_{\mathbf{k+q-p,q}})c^\dagger_{\mathbf{k}\sigma}c_{\mathbf{k+q-p}\sigma}b^\dagger_{\mathbf{q}}b_{\mathbf{p}}. \tag{113}$$

Here $\mathcal{A}^\sigma_{\mathbf{kq}}$ is the *s-d* scattering amplitude, which is defined by Eq. (12) ($U \to I$). A more general interpolation expression for the effective amplitude, which does not assume the smallness of $|I|$ or $1/2S$, was obtained by Auslender *et al.* (1983) using a variational approach.

The most general and rigorous method for calculating the transport relaxation time is the use of the Kubo formula for the conductivity σ_{xx} (Kubo, 1957) [see details in Irkhin and Katsnelson (2002)],

$$\sigma_{xx} = \beta\int_0^\beta d\lambda \int_0^\infty dt \exp(-\varepsilon t)\langle j_x(t + i\lambda)j_x\rangle, \tag{114}$$

where $\beta = 1/T$, $\varepsilon \to 0$,

$$\mathbf{j} = -e\sum_{\mathbf{k}\sigma} \mathbf{v}_{\mathbf{k}\sigma}c^\dagger_{\mathbf{k}\sigma}c_{\mathbf{k}\sigma} \tag{115}$$

is the current operator, and $\mathbf{v}_{\mathbf{k}\sigma} = \partial E_{\mathbf{k}\sigma}/\partial\mathbf{k}$ is the electron velocity. Representing the total Hamiltonian in the form $\mathcal{H} = \mathcal{H}_0 + \mathcal{H}'$, the correlator in Eq. (114) may be expanded in the perturbation $\mathcal{H}'$ (Nakano, 1957; Mori, 1965). In the second order, we obtain for the electrical resistivity

$$\rho_{xx} = \sigma^{-1}_{xx} = \frac{T}{\langle j_x^2\rangle^2}\int_0^\infty dt\langle[j_x, \mathcal{H}'(t)][\mathcal{H}', j_x]\rangle, \tag{116}$$

where $\mathcal{H}'(t)$ is calculated with the Hamiltonian $\mathcal{H}_0$.

In the HMF situation, band states with one spin projection only, $\sigma = \operatorname{sgn} I$, are present at the Fermi level (Irkhin and Katsnelson, 1994). We consider the case $I > 0$, $\sigma = +$ and omit the spin indices in the electron spectrum to obtain for the transport relaxation time τ defined by $\sigma_{xx} = e^2\langle(v^x)^2\rangle\tau$

$$\frac{1}{\tau} = \frac{\pi}{4T}\sum_{\mathbf{kk'q}} (v^x_{\mathbf{k}} - v^x_{\mathbf{k'}})^2(\mathcal{A}^\uparrow_{\mathbf{kq}} + \mathcal{A}^\uparrow_{\mathbf{k',q-k'+k}})^2 \times N_{\mathbf{q}}(1 + N_{\mathbf{q-k'+k}})n_{\mathbf{k}}(1 - n_{\mathbf{k'}}) \times \delta(t_{\mathbf{k'}} - t_{\mathbf{k}} - \omega_{\mathbf{q}} + \omega_{\mathbf{q-k'+k}}) \Big/ \sum_{\mathbf{k}} (v^x_{\mathbf{k}})^2\delta(t_{\mathbf{k}}). \tag{117}$$

Averaging over the angles of the vector $\mathbf{k}$ leads to the result $1/\tau \propto I^2\Phi$ with

$$\Phi = \sum_{\mathbf{pq}} f_{\mathbf{pq}}\frac{\beta(\omega_{\mathbf{p}} - \omega_{\mathbf{q}})|\mathbf{p} - \mathbf{q}|}{\exp(\beta\omega_{\mathbf{p}}) - \exp(\beta\omega_{\mathbf{q}})}(1 + N_{\mathbf{q}})(1 + N_{\mathbf{p}}), \tag{118}$$

where $f_{\mathbf{pq}} = 1$ for $p, q \gg q^*$ and

$$f_{\mathbf{pq}} = \frac{[\mathbf{p}\times\mathbf{q}]^2}{(\mathbf{p} - \mathbf{q})^2(q^*)^2} \quad (p, q \ll q^*). \tag{119}$$

As discussed earlier, the wave vector q^* determines the boundary of the region where the $\mathbf{q}$ dependence of the amplitude become important, so that $t(\mathbf{k}+\mathbf{q}) - t(\mathbf{k}) \simeq \Delta$ at $q \simeq q^*$. In the case $q < q^*$, simple perturbation theory fails and we have to take into account the spin splitting by collecting terms of higher order in I. In the simple one-band model of HMF where $E_F < \Delta$, one has $q^* \sim \sqrt{\Delta/W}$ (W is the conduction bandwidth) (Grigin and Nagaev, 1974; Nagaev, 1983). The quantity q^* determines a characteristic temperature and energy scale $T^* = \mathcal{D}(q^*)^2 \propto \mathcal{D}(\Delta/W)$.

When estimating the temperature dependences of resistivity, one has to remember that each power of p or q gives $T^{1/2}$. At very low temperatures $T < T^*$, small quasimomenta $p, q < q^*$ yield main contribution to the integrals and

$$\rho(T) \propto (T/T_C)^{9/2}. \tag{120}$$

Such a dependence was obtained in the narrowband case (double-exchange model with large $|I|$), where the scale T^* is absent (Kubo and Ohata, 1972), and by the diagram approach in the broadband case (Lutovinov and Reizer, 1979). At the same time, at $T > T^*$ the function $f_{\mathbf{pq}}$ in Eq. (118) can be replaced by unity to obtain

$$\rho(T) \propto (T/T_C)^{7/2}. \tag{121}$$

Generally speaking, q^* may be sufficiently small provided that the energy gap is much smaller than W, which is the case for real HMF systems. We consider the model of the HMF spectrum (50) where the majority-spin band is metallic and the minority spin is semiconducting. For temperatures $T \ll T_C$, both the characteristic q and p are small in comparison with the inverse lattice constant and we can set

$$\mathcal{A}^{\sigma}_{\mathbf{kq}} = \frac{1}{2S}(t_{\mathbf{k}\downarrow} - t_{\mathbf{k}\uparrow})\frac{t_{\mathbf{k}+\mathbf{q}\uparrow} - t_{\mathbf{k}\uparrow}}{t_{\mathbf{k}+\mathbf{q}\uparrow} - t_{\mathbf{k}\downarrow}}. \tag{122}$$

The wave vector q^* determines the boundary of the region where the $\mathbf{q}$ dependence of the amplitude become important, so that $q^* = \Delta/v_F$ (the same value as for the spin polarization problem). The corresponding characteristic temperature and energy scale is

$$T^* = \mathcal{D}(q^*)^2 \propto \mathcal{D}(\Delta/W)^2, \tag{123}$$

which coincides with the case of a usual ferromagnetic metal. The above temperature dependences of resistivity are not changed (Irkhin and Katsnelson, 2002).

Now we treat the two-dimensional situation which may be appropriate for layered manganites (de Boer and Groot, 1999; Nagaev, 2001). At low temperatures, we obtain

$$\rho(T < T^*) \propto (T/T_C)^{7/2}. \tag{124}$$

At the same time, for $T > T^*$ we obtain, after replacing the scattering amplitude by unity, a logarithmically divergent integral that should be cut at T^*. Thus we get

$$\rho(T > T^*) \propto (T/T_C)^{5/2}\ln(T/T^*). \tag{125}$$

To discuss the magnetoresistivity, we have to introduce the gap in the magnon spectrum, $\omega_{\mathbf{q}\to 0} = \mathcal{D}q^2 + \omega_0$. Provided that the external magnetic field H is large in comparison with the anisotropy gap, ω_0 is proportional to H. In the 3D case, the resistivity at $T < T^*$ is linear in the magnetic field,

$$\rho(T,H) - \rho(T,0) \propto -\omega_0 T^{7/2}/T_C^{9/2}. \tag{126}$$

The situation at $T > T^*$ is more interesting since the quantity $\partial\Phi/\partial\omega_0$ contains a divergence that is cut at ω_0 or T^*. We have at $T > \omega_0, T^*$

$$\delta\rho(T,H) \propto -\frac{T^3\omega_0}{[\max(\omega_0, T^*)]^{1/2}} \tag{127}$$

(of course, at $T < \omega_0$ the resistivity is exponentially small). A negative H-linear magnetoresistance was observed in CrO_2 (Rabe *et al.*, 2002).

The discovery of giant magnetoresistance (GMR) led to tremendous effort to understand and develop technology based on high-density magnetic recording (Zutic *et al.*, 2004). Giant magnetoresistance for metallic multilayers (superlattices) containing HMFs was first predicted by Irkhin and Katsnelson (1994). NiMnSb-based spin-valve structures using Mo spacer layers NiMnSb/Mo/NiMnSb/$SmCo_2$ were successfully produced (Hordequin *et al.*, 1998). The associated GMR exhibits a clear spin-valve contribution of about $\Delta R/R \approx 1\%$ (Hordequin *et al.*, 1998). One limiting factor for such a small value is the large resistivity of the Mo layer, which determines the limited flow of active electrons exchanged between the two ferromagnetic layers without being scattered. The giant *tunneling* magnetoresistance differs in the use of a dielectric spacer instead of a metallic one. The GMR in tunnel junctions based on HMFs was considered theoretically by de Groot, Janner, and Mueller (1983) and Tkachov *et al.* (2001), and recently this issue became a subject of intensive experimental investigations (Gercsi *et al.*, 2006; Rybchenko *et al.*, 2006; Sakuraba, Hattori, Oogane, *et al.*, 2006; Sakuraba, Miyakoshi, Oogane, *et al.*, 2006; Sakuraba *et al.*, 2007).

It is important that NQP states do not contribute to the temperature dependence of the resistivity for pure HMFs. The opposite conclusion was drawn by Furukawa (2000). He attempted to calculate low-temperature resistivity of half-metals taking into account the non-rigid-band behavior of the minority band due to spin fluctuations at finite temperatures, and he derived that the unconventional one-magnon scattering process gives T^3 dependence in resistivity. However, this calculation was not based on a consistent use of the Kubo formula and, in our opinion, can be hardly justified.

In contrast, *impurity* contributions to transport properties in the presence of potential scattering are determined mainly by the NQP states (Irkhin and Katsnelson, 1994; Irkhin *et al.*, 1989, 1994). To second order in the impurity potential $\mathcal{U}$ that derived after neglecting vertex corrections and averaging over impurities, we obtain for the transport relaxation time

$$\delta\tau^{-1}_{\mathrm{imp}}(E) = -2\mathcal{U}^2\,\mathrm{Im}\sum_{\mathbf{p}} G^{(0)}_{\mathbf{p}\sigma}(E), \tag{128}$$

where $G^{(0)}_{\mathbf{p}\sigma}(E)$ is the exact Green's function for the ideal crystal. Thus the contributions under consideration are determined by the energy dependence of the density of states $N(E)$ for the interacting system near the Fermi level. The most nontrivial dependence comes from the nonquasiparticle (incoherent) states with the spin projection $\sigma = -\mathrm{sgn}\, I$, which are present near E_F. Near the Fermi level, the NQP contribution is determined by the magnon density of states $g(\omega)$ and follows a power law,

$$\delta N_{\mathrm{incoh}}(E) \propto \int_0^{\sigma E} d\omega g(\omega) \propto |E|^{\alpha}\theta(\sigma E) \quad (|E| \ll \bar{\omega}). \tag{129}$$

Here $\theta(x)$ is the step function, and E refers to E_F; we have $\alpha=\frac{3}{2}$ and $d=1$ for the 3D and 2D cases, respectively. The corresponding correction to resistivity reads

$$\frac{\delta\rho_{\mathrm{imp}}(T)}{\rho^2} = -\delta\sigma_{\mathrm{imp}}(T) \propto -\mathcal{U}^2 \int dE\left(-\frac{\partial f(E)}{\partial E}\right)\delta N_{\mathrm{incoh}}(E) \propto T^{\alpha}. \tag{130}$$

A contribution of the order of T^{α} with $\alpha \simeq 1.65$ (which is not too far from 3/2) was observed in the temperature dependence of the resistivity for NiMnSb (Borca *et al.*, 2001) above 100 K. The half-metallic properties above 100 K are being challenged, however. The incoherent contribution to magnetoresistivity is given by

$$\delta\rho_{\mathrm{imp}}(T,H) \propto \omega_0\, \partial\, \delta N_{\mathrm{incoh}}(\sigma T)/\partial T \propto \omega_0 T^{\alpha-1}, \tag{131}$$

so that we obtain a temperature-independent term in the 2D case.

The correction to thermoelectric power, which is similar to Eq. (130), reads [cf. Irkhin *et al.* (1989, 1994)]

$$\delta\mathcal{Q}(T) \propto \frac{1}{T}\int dE[-\partial f(E)/\partial E]E\,\delta N(E). \tag{132}$$

In addition, taking account of higher orders in impurity scattering leads to the replacement of the impurity potential V by the T matrix. For pointlike scattering, the latter quantity is given by

$$T(E) = \frac{\mathcal{U}}{1-\mathcal{U}\mathcal{R}(E)}, \quad \mathcal{R}(E) = \sum_{\mathbf{k}} G_{\mathbf{k}\sigma}(E). \tag{133}$$

Expanding Eq. (133) yields the term

$$\delta\mathcal{Q}(T) \propto \frac{1}{T}\int dE[-\partial f(E)/\partial E]E\ \mathrm{Re}\ \delta\mathcal{R}(E), \tag{134}$$

with $\delta\mathcal{R}(E)$ being obtained by analytical continuation from $\delta N(E)$. Thus we have $\delta\mathcal{Q}(T) \propto T^{3/2}$.

J. X-ray absorption and emission spectra. Resonant x-ray scattering

The NQP contributions in the presence of the potential U, which is induced by the impurity at a lattice site, can be treated in the *s-d* exchange model in the representation (23). The impurity potential results in the NQP contribution to this quantity being enhanced for $\mathcal{U}<0$ and suppressed for $\mathcal{U}>0$. These results can be used to consider the manifestations of NQP states in the core-level spectroscopy (Irkhin and Katsnelson, 2005a).

Various spectroscopy techniques such as x-ray absorption, x-ray emission, and photoelectron spectroscopies (XAS, XES, and XPS) give important information about the electronic structure of HMFs and related compounds, i.e., ferromagnetic semiconductors and colossal magnetoresistance materials [see, e.g., Yarmoshenko *et al.* (1998), Yablonskikh *et al.* (2001), Kurmaev *et al.* (2003) and Wessely *et al.* (2003)]. It is well known (Mahan, 1990) that many-body effects (e.g., dynamical core hole screening) can be important for core-level spectroscopy even when the system is not strongly correlated in the initial state. Therefore, it is interesting to study the interplay of these effects and NQP states, which are of essentially many-body origin themselves.

To consider the core-level problem in HMFs, we use the Hamiltonian of the *s-d* exchange model in the presence of the external potential $\mathcal{U}$ induced by the core hole,

$$\mathcal{H}' = \varepsilon_0 f^{\dagger} f + \mathcal{U}\sum_{\mathbf{k}\mathbf{k}'\sigma} c^{\dagger}_{\mathbf{k}\sigma} c_{\mathbf{k}'\sigma} f^{\dagger} f, \tag{135}$$

where $f^{\dagger}, f$ are core-hole operators and $\mathcal{U}<0$. X-ray absorption and emission spectra are determined by the Green's function (Mahan, 1990)

$$G^{\sigma}_{\mathbf{k}\mathbf{k}'}(E) = \langle\langle c_{\mathbf{k}\sigma} f | f^{\dagger}\, c^{\dagger}_{\mathbf{k}'\sigma}\rangle\rangle_E. \tag{136}$$

It follows from the investigation of the sequence of equations of motion (Irkhin and Katsnelson, 2005a) that, in the ladder approximation, the spectral density for the two-particle Green's function $G^{\sigma}_{\mathbf{k}\mathbf{k}'}(E)$ is equivalent to the one-particle spectral density in the presence of the core-hole potential $\mathcal{U}$ [note that the ladder approximation is inadequate to describe the XAS edge singularity in a vicinity close to the Fermi level (Mahan, 1990)]. Thus the core-hole problem is intimately connected with the impurity problem.

Since XAS probes empty states and XES occupied states, the local DOS

$$N^{\sigma}_{\mathrm{loc}}(E) = -\frac{1}{\pi}\,\mathrm{Im}\, G^{\sigma}_{00}(E) \tag{137}$$

describes the absorption spectrum for $E>E_F$ and the emission spectrum for $E<E_F$. To take into account the core-level broadening, a finite damping δ should be introduced (Irkhin and Katsnelson, 2005a). For small band filling, exciton effects (strong interaction with the core hole) result in a considerable enhancement of NQP contributions to the spectra in comparison with those to DOS. The results for the semielliptic bare band are shown in Figs. 11 and 12.

To probe the spin-polaron nature of the NQP states more explicitly, it would be desirable to use spin-resolved spectroscopic methods such as x-ray magnetic circular dichroism [XMCD; for a review, see Ebert (1996)]. Owing to the interference of electron-magnon scattering and exciton effects (interaction of electrons with the core hole), the NQP contributions to x-ray spectra can be considerably enhanced in comparison with those to the DOS of the ideal crystal. Thus the core-level (x-ray absorption, emission, and photoelectron) spectroscopy might be an efficient tool to investigate the NQP states in the electron energy spectrum.

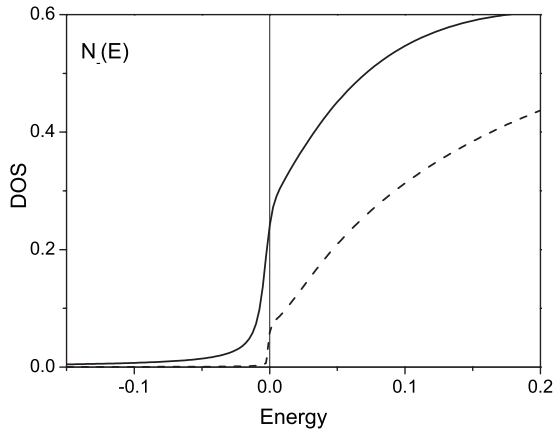

FIG. 11. Local density of states $N_{\mathrm{loc}}^{\downarrow}(E)$ (solid line) for a half-metallic ferromagnet with $S=1/2$, $I=0.3$, $\delta=0.01$ in the presence of the core-hole potential $\mathcal{U}=-0.2$. Dashed line shows the DOS $N_{\downarrow}(E)$ for the ideal crystal. The value of E_F calculated from the band bottom is 0.15.

Now we consider the NQP effects in resonant x-ray scattering processes. It was observed (Kurmaev *et al.*, 2003) that the elastic peak of the x-ray scattering in CrO_2 is more pronounced than in usual Cr compounds, e.g., in elemental chromium. These authors have put forward some qualitative arguments that the NQP states may give larger contributions to resonant x-ray scattering than usual itinerant electron states. Here we treat this question quantitatively and estimate explicitly the corresponding enhancement. The intensity of resonant x-ray emission induced by the photon with the energy ω and polarization q is given by the Kramers-Heisenberg formula

$$I_{q'q}(\omega',\omega) \propto \sum_n \left| \sum_l \frac{\langle n|C_{q'}|l\rangle\langle l|C_q|0\rangle}{E_0+\omega'-E_l-i\Gamma_l} \right|^2 \times \delta(E_n+\omega'-E_0-\omega). \tag{138}$$

Here q' and ω' are the polarization and energy of the emitted photon; $|n\rangle, |0\rangle$, and $|l\rangle$ are the final, initial, and intermediate states of the scattering system, respectively; E_i are the corresponding energies; and C_q is the operator of the dipole moment for the transition, which is proportional to $fc+c^{\dagger}f^{\dagger}$. Assuming for simplicity that Γ_l does not depend on the intermediate state, $\Gamma_l=\Gamma$, and taking into account only the main x-ray scattering channel (where the hole is filled from the conduction band), one obtains (Sokolov *et al.*, 1977)

$$I_{\omega'} \propto \left| \sum_{\sigma} G_{00}^{\sigma}(z) \right|^2, \tag{139}$$

where $z=\omega'-E_0+i\Gamma$. Owing to a jump in the DOS at the Fermi level, the NQP part of the Green's function contains a large $\ln(W/z)$ term at small z. This means that the corresponding contribution to the elastic x-ray scattering intensity ($\omega'=E_0$) is enhanced by a factor of $\ln^2(W/\Gamma)$, which makes a quantitative estimation for the qualitative effect as discussed by Kurmaev *et al.* (2003). Of course, the smearing of the jump in the density of NQP states by spin dynamics is irrelevant provided that $\Gamma \gg \bar{\omega}$ ($\bar{\omega}$ is a characteristic magnon frequency).

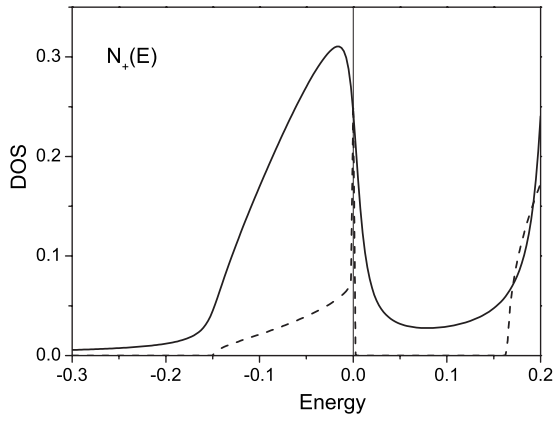

FIG. 12. Local density of states $N_{\mathrm{loc}}^{\uparrow}(E)$ (solid line) for a half-metallic ferromagnet with $S=1/2$, $I=-0.3$, $\delta=0.01$ in the presence of the core-hole potential $\mathcal{U}=-0.3$. Dashed line shows the DOS $N_{\uparrow}(E)$ for the ideal crystal. The value of E_F calculated from the band bottom is 0.15.

IV. MODERN FIRST-PRINCIPLES CALCULATIONS

A. Different functional schemes

In this section, we review contemporary approaches to the electronic-structure calculations, taking into account correlation effects. Model considerations discussed above demonstrate the relevance of the correlation effects (such as electron-magnon interactions) for the physics of half-metallic ferromagnets. In order to calculate the electronic structure of real materials, we have to solve a complicated many-body problem for a crystal, corresponding to inhomogeneous gas of interacting electrons in an external periodic potential,

$$\mathcal{H}=\mathcal{H}_0+\mathcal{H}_{\mathrm{int}},$$

$$\mathcal{H}_0=\sum_{\sigma}\int d\mathbf{r}\,\psi_{\sigma}^{+}(\mathbf{r})[-\tfrac{1}{2}\nabla^2+V_{\mathrm{ext}}(\mathbf{r})]\psi_{\sigma}(\mathbf{r}),$$

$$\mathcal{H}_{\mathrm{int}}=\frac{1}{2}\sum_{\sigma\sigma'}\int\int d\mathbf{r}\,d\mathbf{r}'\,\psi_{\sigma}^{+}(\mathbf{r})\psi_{\sigma'}^{+}(\mathbf{r}') \times V(\mathbf{r}-\mathbf{r}')\psi_{\sigma'}(\mathbf{r}')\psi_{\sigma}(\mathbf{r}). \tag{140}$$

In this section, we use atomic units ($\hbar=m=e=1$), $\psi_{\sigma}(\mathbf{r})$ is a field operator for electrons, $V_{\mathrm{ext}}(\mathbf{r})$ describes the interaction of electrons with static nuclei which are supposed to form the periodic crystal lattice and also may include other external potentials (defects, electric fields, etc.), and $V(\mathbf{r}-\mathbf{r}')=1/|\mathbf{r}-\mathbf{r}'|$ is the Coulomb interaction between electrons.

The modern view on various practical schemes for solution of this general many-electron problem is based on its functional formulation in the framework of the so-called effective action approach (Fukuda *et al.*, 1994; Georges *et al.*, 1996; Kotliar *et al.*, 2006). The partition

function of an electronic system within an imaginary-time functional integral formalism can be expressed as an integral over electronic Grassmann variables,

$$\mathcal{Z} = \sum_{\sigma} \int D[\psi_{\sigma}^{+}\psi_{\sigma}]e^{-S},$$

$$S = \sum_{\sigma} \int d\mathbf{r} \int_{0}^{\beta} d\tau \psi_{\sigma}^{+}(\mathbf{r},\tau)\frac{\partial}{\partial\tau}\psi_{\sigma}(\mathbf{r},\tau) + \int_{0}^{\beta} d\tau \mathcal{H}(\tau). \tag{141}$$

The free energy of the many-electron system $F = -T \ln \mathcal{Z}$ can be expressed as a function of optimally chosen physical variables for a given problem. The most accurate scheme corresponds to the Baym-Kadanoff or Luttinger-Ward functional (Luttinger and Ward, 1960; Baym and Kadanoff, 1961) of the one-electron Green's function,

$$G_{\sigma}(\mathbf{r}-\mathbf{r}',\tau-\tau') = -\langle T_{\tau}\psi_{\sigma}(\mathbf{r},\tau)\psi_{\sigma}^{+}(\mathbf{r}',\tau')\rangle, \tag{142}$$

T_{τ} is the time-ordering operator. In this formulation, one has to add constraint fields of dual variable Σ to the action,

$$S[\Sigma] = S + \sum_{\sigma} \int d\mathbf{r} \int d\mathbf{r}' \int_{0}^{\beta} d\tau \int_{0}^{\beta} d\tau' \times \Sigma_{\sigma}(\mathbf{r},\mathbf{r}',\tau,\tau')G_{\sigma}(\mathbf{r}',\mathbf{r},\tau',\tau), \tag{143}$$

and find the partition function in the presence of the auxiliary source field,

$$\mathcal{Z}[\Sigma] = e^{-F[\Sigma]} = \int D[\psi^{+}\psi]e^{-S[\Sigma]}. \tag{144}$$

The corresponding Baym-Kadanoff functional is defined as the Legendre transformation of $F[\Sigma]$ to the Green's function variable,

$$F[G] = F[\Sigma] - \mathrm{Tr}(\Sigma G), \tag{145}$$

with further use of the functional derivative $G = \delta F/\delta\Sigma$ to eliminate the constraint fields. Using the free-electron Green's function corresponding to the $\mathcal{H}_0$ part of the Hamiltonian, the final form of the functional with Kohn-Sham decomposition can be written in the following form:

$$F[G] = -\mathrm{Tr}\ln(G_0^{-1} - \Sigma) - \mathrm{Tr}(\Sigma G) + \Phi[G]; \tag{146}$$

here $\Phi[G]$ is the Luttinger generating functional, which can be represented as a sum of all irreducible diagrams without legs constructed from the exact Green's function G and the bare electron-electron interaction line (bare four-leg vertex) V. The Baym-Kadanoff functional is stationary in both G and Σ and its variation with respect to Σ leads to the Dyson equation

$$G^{-1} = G_0^{-1} - \Sigma, \tag{147}$$

and the G extremum gives the variational identity $\Sigma = \delta\Phi/\delta G$.

The Baym-Kadanoff functional allows us in principle to calculate not only free energy and thus thermodynamic properties of the system, but also the Green's function and thus the corresponding excitation spectrum. The main point that makes this scheme rather useful for model many-body analysis and preserves its broad practical use in electronic-structure calculations is related to the difficulties in finding an exact representation of $F[G]$ even for simple systems.

In this situation, the density-functional scheme of Kohn, Hohenberg, and Sham (Hohenberg and Kohn, 1964; Kohn and Sham, 1965) turns out to be the most successful scheme for electronic-structure calculations of an electronic systems with not too strong correlations. For this purpose, the functional of the static electronic density

$$\rho_{\sigma}(\mathbf{r}) = -\frac{1}{\pi}\,\mathrm{Im}\,G_{\sigma}(\mathbf{r},\tau=0^{-}) \tag{148}$$

is constructed. The corresponding constraint fields in the effective action are related to the Kohn-Sham interaction potential, which is represented as a sum of Hartree and exchange-correlation (xc) parts,

$$V_{\mathrm{int}} = V_H + V_{\mathrm{xc}}. \tag{149}$$

Finally, the Kohn-Sham free-energy functional can be written in the following form:

$$F[\rho] = -\mathrm{Tr}\ln(G_0^{-1} - V_{\mathrm{ext}} - V_{\mathrm{int}}) - \mathrm{Tr}(V_{\mathrm{int}}\rho) + F_H[\rho] + F_{\mathrm{xc}}[\rho], \tag{150}$$

where V_{ext} is an external potential and F_H is the Hartree potential. Again, there is a similar problem: an exact form of the exchange-correlation functional $F_{\mathrm{xc}}[\rho]$ is, generally speaking, unknown, and only a formal expression in terms of the integral over the coupling constant exists (Harris and Jones, 1974). The practical use of the density-functional theory (DFT) is related with the local-density approximation (LDA),

$$F_{\mathrm{xc}}[\rho] \approx \int d\mathbf{r}\rho(\mathbf{r})\epsilon_{\mathrm{xc}}[\rho(\mathbf{r})], \tag{151}$$

where $\epsilon_{\mathrm{xc}}[\rho]$ is the exchange-correlation energy per particle of homogeneous electron gas with a given density. It can be parametrized from numerically exact Monte Carlo calculations (Ceperley and Alder, 1980). Taking into account the spin dependence of the DFT through $\rho_{\sigma}(\mathbf{r})$, one can study the magnetic properties of complex materials. This was the method used in most of the electronic-structure calculations referred to above; in particular, the concept itself of half-metallic ferromagnetism was introduced based on this kind of calculation (de Groot, Mueller, v. Engen, *et al.*, 1983). In practice, the LDA scheme results sometimes in well-known difficulties; in particular, it usually underestimates energy gaps in semiconductors. For this reason, it can fail to describe properly the half-metallic state, e.g., in the case of colossal magnetoresistance manganites (Pickett and Singh, 1996). The DFT scheme is formally exact (assum-

ing that an exact E_{xc} is known) to find the energy and electronic density of the many-body systems by minimization of the density functional. However, the excitation spectrum, rigorously speaking, cannot be expressed in terms of the Kohn-Sham eigenenergies ε_i defined by

$$(-\tfrac{1}{2}\nabla^2 + V_{\text{ext}} + V_{\text{int}})\psi_i = \varepsilon_i \psi_i \tag{152}$$

(see, e.g., the discussion of NQP contributions to thermodynamic properties in Sec. III.H).

A reasonable scheme that can overcome the difficulties of the DFT scheme for the gap problem uses the so-called *GW* approximation proposed by Hedin (1965). The functional approach to the *GW* scheme was developed (Almbladh *et al.*, 1999; Chitra and Kotliar, 2000, 2001) and is related with the free-energy functional of both the total Green's function G and screened Coulomb interactions $W=(V^{-1}-\Pi)^{-1}$,

$$\begin{aligned} F[G,W] = &- \operatorname{Tr}\ln(G_0^{-1}-\Sigma) - Tr(\Sigma G) \\ &+ \tfrac{1}{2}\operatorname{Tr}\ln(V^{-1}-\Pi) + \tfrac{1}{2}\operatorname{Tr}(\Pi W) + F_H[\rho] \\ &+ \Phi[G,W], \end{aligned} \tag{153}$$

where Π is the polarization operator. Earlier a similar approach was used in the theory of phonon-induced superconductivity of disordered systems (Anokhin and Katsnelson, 1996). In the *GW* approximation, only the lowest-order diagram in the screened interactions is included in the generating functional,

$$\Phi[G,W] = \tfrac{1}{2}\operatorname{Tr}(GWG). \tag{154}$$

In this case, the polarization operator Π, which serves as a constraint field for the screened Coulomb interactions W, has the simplest form

$$\Pi = -2\frac{\delta\Phi[G,W]}{\delta W} = -GG, \tag{155}$$

and the corresponding electron self-energy reads

$$\Sigma = \frac{\delta\Phi[G,W]}{\delta G} = GW. \tag{156}$$

The *GW* scheme gives an accurate estimation of the screened Coulomb interactions in solids and can be used to define the first-principles values of local Hubbard-like multiorbital energy-dependent interactions for correlated local orbitals $\phi_i(\mathbf{r})$, which describe d states of transition-metal ions (Aryasetiawan *et al.*, 2004),

$$U_{ijkl}(\omega) = \langle \phi_i \phi_j | \tilde{W}(\omega) | \phi_k \phi_l \rangle, \tag{157}$$

where $\tilde{W}$ does not take into account the effects of d-d screening, the latter being explicitly taken into account further within an effective low-energy Hubbard-like model. The numerical estimation of U for metallic nickel (Aryasetiawan *et al.*, 2004) shows a relatively weak energy dependence within the d-band energy width and the static values of the order of 2–4 eV, in good agreement with the experimental values of the Hubbard parameters (van der Marel and Sawatzky, 1988).

The success of the *GW* approximation is closely related to the fact that the bare Coulomb interaction V is strongly screened in solids, thus one can use the lowest-order approximation for $\Phi[G,W]$. On the other hand, the spin dependence of self-energy in the *GW* scheme comes only from the spin dependence of the Green's function $G_\sigma(\mathbf{r},\tau)$ and not from the effective interactions W. In the Baym-Kadanoff formalism, this means that only the density-density channel was taken into account in the screening of the Coulomb interactions. It is well known that Hund's intra-atomic exchange interactions are weakly screened in crystals (van der Marel and Sawatzky, 1988), and strong spin-flip excitation processes will modify electronic self-energy in itinerant electron magnets. In particular, these processes are responsible for electron-magnon interaction and lead to the appearance of the NQP states in the gap region for half-metallic ferromagnets.

An accurate treatment of the effects of local screened Coulomb U and exchange J interactions beyond the *GW* or DFT methods can be carried out within the dynamical mean-field theory (DMFT) combined with the *GW* or LDA-GGA functionals. The DMFT scheme defines the best local approximation for the self-energy, which uses the mapping of the original many-body system with Hubbard-like interactions onto the multi-orbital quantum impurity model in the effective electronic bath under the self-consistency condition (Georges *et al.*, 1996). The corresponding *GW*+DMFT scheme (Biermann *et al.*, 2003) or spectral-density functional theory (Savrasov and Kotliar, 2004) is probably the best known way to treat correlation effects in the electronic structure of real materials. However, it is still very cumbersome and computationally expensive; also, methods of work with the frequency-dependent effective interaction (157) have not been developed enough yet [for examples of first attempts, see Rubtsov *et al.* (2005) and Savkin *et al.* (2005)]. The only way to consider the effects of spin-flip processes on the electronic structure of real materials is a simplified version of a general spectral-density functional known as the LDA+DMFT approach (Anisimov, Poteryaev, Korotin, *et al.*, 1997; Lichtenstein and Katsnelson, 1998). In a sense, one can consider the LDA+DMFT and the LDA as complementary approaches. In both cases, we split a complicated many-body problem for a crystal into a one-body problem for the crystal and a many-body problem for some appropriate auxiliary system where we calculate the correlation effects more or less accurately. For the LDA, we choose the homogeneous electron gas as this auxiliary system. For the LDA+DMFT, it is an atom in some effective medium. The latter choice is optimal to consider atomiclike features of d or f electrons in solids. The local Green's function in magnetic solids is obtained from the effective impurity action with the static (frequency-independent) Hubbard-like multiorbital interactions,

$$S_{\rm imp} = -\sum_{ij}\int_0^\beta d\tau\int_0^\beta d\tau' c_i^+(\tau)\mathcal{G}_{ij}^{-1}(\tau-\tau')c_j(\tau') + \frac{1}{2}\sum_{ijkl}\int_0^\beta d\tau c_i^+(\tau)c_j^+(\tau)U_{ijkl}c_l(\tau)c_k(\tau), \quad (158)$$

where $c_i(\tau)$ are the fermionic Grassmann variables for localized correlated d orbitals $\phi_i(\mathbf{r})$, and $\mathcal{G}_{ij}$ is the so-called bath Green's function, which is defined self-consistently within the single-particle lattice model. The corresponding interacting local Green's function

$$G_{ij}(\tau-\tau') = -\langle T_\tau c_i(\tau)c_j^+(\tau')\rangle_{S_{\rm imp}} \quad (159)$$

can be found, within the numerically exact quantum Monte Carlo scheme (Hirsch, 1983), or some perturbative approach that treats accurately spin-flip excitation processes in the particle-hole channel (Katsnelson and Lichtenstein, 1999). The corresponding self-energy matrix of the impurity model

$$\Sigma = \mathcal{G}^{-1} - G^{-1} \quad (160)$$

can be used in the spectral-density functional,

$$F[\mathcal{G}] = -\,\mathrm{Tr}\,\ln(G_0^{-1}-\Sigma) - \mathrm{Tr}(\Sigma\mathcal{G}) + \Phi[\mathcal{G}], \quad (161)$$

and satisfies the self-consistent equation for the bath Green's function,

$$\mathcal{G}(\omega) = \sum_{\mathbf{k}}[G_0^{-1}(\mathbf{k},\omega) - \Sigma(\omega)]^{-1} + \Sigma(\omega). \quad (162)$$

B. LDA+DMFT: The quantum Monte Carlo solution of the impurity problem

Now we describe the most rigorous way to solve an effective impurity problem using the multiband quantum Monte Carlo (QMC) method (Rozenberg, 1997). In the framework of LDA+DMFT, this approach was used first by Katsnelson and Lichtenstein (2000) for the case of ferromagnetic iron.

We start from the many-body Hamiltonian in the LDA+U form (Anisimov, Aryasetiawan, and Lichtenstein, 1997),

$$\mathcal{H} = \mathcal{H}_{\rm LDA}^{\rm dc} + \frac{1}{2}\sum_{i\{\sigma m\}} U^i_{m_1m_2m_1'm_2'}c^+_{im_1\sigma}c^+_{im_2\sigma'}c_{im_2'\sigma'}c_{im_1'\sigma},$$

$$\mathcal{H}_{\rm LDA}^{\rm dc} = \sum_{ij\sigma\{m\}} t^{ij}_{m_1m_2}c^+_{im_1\sigma}c_{jm_2\sigma} - E^{\rm dc}, \quad (163)$$

where (ij) represents different crystal sites, $\{m\}$ label different orbitals, $\{\sigma\}$ are spin indices, and $t^{ij}_{m_1m_2}$ are the hopping parameters. The Coulomb matrix elements are defined by

$$U^i_{m_1m_2m_1'm_2'} = \int\int d\mathbf{r}\,d\mathbf{r}'\Psi^*_{im_1}(\mathbf{r})\Psi^*_{im_2}(\mathbf{r}') \times V_{ee}(\mathbf{r}-\mathbf{r}')\Psi_{im_1'}(\mathbf{r})\Psi_{im_2'}(\mathbf{r}'), \quad (164)$$

where $V_{ee}(\mathbf{r}-\mathbf{r}')$ is the screened Coulomb interaction, which remains to be determined. We follow again the spirit of the LDA+U approach by assuming that within the atomic spheres, these interactions retain to a large measure their atomic nature. Moreover, the values of screened Coulomb (U) and exchange (J) interactions can be calculated within the supercell LSDA approach (Anisimov and Gunnarsson, 1991): the elements of the density matrix $n^\sigma_{mm'}$ are to be constrained locally, and the second derivative of the LSDA energy with respect to the variation of the density matrix yields the interactions required. In a spherical approximation, the matrix elements of V_{ee} can be expressed in terms of the effective Slater integrals $F^{(k)}$ (Judd, 1963) as

$$\langle m,m''|V_{ee}|m',m'''\rangle = \sum_k a_k(m,m',m'',m''')F^{(k)}, \quad (165)$$

where $0\le k\le 2l$ and

$$a_k(m,m',m'',m''') = \frac{4\pi}{2k+1}\sum_{q=-k}^{k}\langle lm|Y_{kq}|lm'\rangle \times\langle lm''|Y^*_{kq}|lm'''\rangle.$$

For d electrons, one needs $F^{(0)}$, $F^{(2)}$, and $F^{(4)}$; they are connected with the Coulomb and Stoner parameters U and J by $U=F^{(0)}$ and $J=(F^{(2)}+F^{(4)})/14$, while the ratio $F^{(2)}/F^{(4)}$ is to a good accuracy a constant, about 0.625 for the $3d$ elements (de Groot *et al.*, 1990; Anisimov *et al.*, 1993). $\mathcal{H}_{\rm LDA}^{\rm dc}$ represents the LDA Hamiltonian corrected by double counting of average static Coulomb interaction that is already presented in the LDA (Anisimov, Aryasetiawan, and Lichtenstein, 1997). The index i for U^i represents only the same correlated sites as the orbital indices $\{m\}$, unlike the LDA term $t^{ij}_{m_1m_2}$ (one-particle Hamiltonian parameters), where we have the contribution of all sites and orbitals in the unit cell.

The one-particle spin-polarized LDA+DMFT Green's function $G_\sigma(\mathbf{k},\omega)$ is related to the LDA Green's function and the local self-energy $\Sigma_\sigma(\omega)$ via the Dyson equation

$$G_\sigma^{-1}(\mathbf{k},\omega) = \omega+\mu-\mathcal{H}^{\rm dc}_{{\rm LDA},\sigma}(\mathbf{k}) - \Sigma_\sigma(\omega), \quad (166)$$

where $\mathcal{H}^{\rm dc}_{{\rm LDA},\sigma}(\mathbf{k})$ is the LDA Hamiltonian in a local orthogonal basis set depending on the Bloch vector $\mathbf{k}$, and μ is the chemical potential. In order to avoid "double counting," we can subtract the static part of the self-energy, $E^{\rm dc}=\mathrm{Tr}\,\Sigma_\sigma(0)$. It has been proven that this type of metallic double-counting is suitable for moderately correlated d-electron systems (Lichtenstein *et al.*, 2001).

The standard QMC scheme for local Coulomb interactions takes into account only density-density-like interactions, although the new continuous-time QMC method (Rubtsov *et al.*, 2005; Savkin *et al.*, 2005) can overcome this problem and include all elements of the interaction vertex. We use the functional integral formalism and describe the discrete Hubbard-Stratonovich transformations to calculate the partition functions and corresponding Green's function. In this method, the local Green's function is calculated for the imaginary time

interval $[0,\beta]$ with the mesh $\tau_l = l\Delta\tau$, $l=0,\ldots,L-1$ ($\Delta\tau = \beta/L, \beta = 1/T$) using the path-integral formalism (Georges *et al.*, 1996). The multiorbital DMFT problem with density-density interactions is described by the following effective impurity action:

$$S = -\int_0^\beta d\tau \int_0^\beta d\tau' \sum_{i,j} c_i^+(\tau)\mathcal{G}_{ij}^{-1}(\tau-\tau')c_j(\tau') + \frac{1}{2}\int_0^\beta d\tau \sum_{i,j} n_i(\tau)U_{ij}n_j(\tau), \tag{167}$$

where $i=\{m,\sigma\}$ labels both orbital and spin indices (we remind the reader that we have no site indices since we are now solving the one-site effective impurity problem). Thus we truncate the original four-index rotationally invariant vertex and use only the two-index approximation for it. This is a price we should pay for a more exact way to solve the effective impurity problem. Without spin-orbital coupling, we have $\mathcal{G}_{ij} = \mathcal{G}^{\sigma}_{m,m'}\delta_{\sigma\sigma'}$.

In the auxiliary fields Green's-function QMC scheme, one can use the discrete Hubbard-Stratonovich transformation introduced by Hirsch (1983),

$$\exp\left[-\Delta\tau U_{ij}\left(n_i n_j - \frac{1}{2}(n_i+n_j)\right)\right] = \frac{1}{2}\sum_{s_{ij}=\pm 1} \exp[\lambda_{ij}s_{ij}(n_i-n_j)], \tag{168}$$

where $S_{ij}(\tau)$ are the auxiliary Ising fields for each pair of spins, orbitals, and time slices with strength

$$\lambda_{ij} = \operatorname{arccosh}\left[\exp\left(\frac{\Delta\tau}{2}U_{ij}\right)\right]. \tag{169}$$

Using Hirsch's transformation (168), (169), we can transform the nonlinear action to a normal Gaussian one (for a given configuration of the auxiliary Ising fields s_{ij}) and integrate out exactly fermionic fields in the functional integral (167). As a result, the partition function and Green's function matrix have the form (Georges *et al.*, 1996)

$$Z = \frac{1}{2^{N_f L}}\sum_{s_{ij}(\tau)} \det[\hat{G}^{-1}(s_{ij})],$$

$$\hat{G} = \frac{1}{Z}\frac{1}{2^{N_f L}}\sum_{s_{ij}(\tau)} \hat{G}(s_{ij})\det[\hat{G}^{-1}(s_{ij})], \tag{170}$$

where N_f is the number of Ising fields, L is the number of time slices, and $\hat{G}(s_{ij})$ is the Green's function of noninteracting fermions for a given configuration of the external Ising fields,

$$G_{ij}^{-1}(s) = \mathcal{G}_{ij}^{-1} + \Delta_i\delta_{ij}\delta_{\tau\tau'},$$

$$\Delta_i = (e^{V_i}-1),$$

$$V_i(\tau) = \sum_{j(\neq i)} \lambda_{ij}s_{ij}(\tau)\sigma_{ij}. \tag{171}$$

Here we introduce the generalized Pauli matrix

$$\sigma_{ij} = \begin{cases} +1, & i<j \\ -1, & i>j. \end{cases} \tag{172}$$

To calculate the Green's function $G_{ij}(s)$ for an arbitrary configuration of the Ising fields, one can use the Dyson equation (Hirsch, 1983),

$$G' = [1+(1-G)(e^{V'-V}-1)]^{-1}G, \tag{173}$$

where V and G are the potential and Green's function before the Ising spin flip, and V' and G' after the flip. The QMC important sampling scheme allows one to integrate over the Ising fields with $|\det[\hat{G}^{-1}(S_{ij})]|$ being a stochastic weight (Hirsch, 1983; Georges *et al.*, 1996). Using the output local Green's function from QMC and the input bath Green's functions, the new self-energy is obtained via Eq. (160), the self-consistent loop being closed through Eq. (162). The main problem of the multiband QMC formalism is the large number of auxiliary fields $S^l_{mm'}$. For each time slice l, it is equal to $M(2M-1)$, where M is the total number of the orbitals, which gives 45 Ising fields for d states and 91 fields for f states. Analytical continuation of the QMC Green's functions from the imaginary time to the real energy axis can be performed by the maximum entropy method (Jarrell and Gubernatis, 1996). It is important to stress that for the diagonal Green's function $G_{ij}=G_i\delta_{ij}$, the determinant ratio is always positive. This means that the sign problem, which is the main obstacle for the application of the QMC method to fermionic problems (Troyer and Wiese, 2005), does not arise in this case. Real computational experience shows that even for the generic multiband case, the sign problem for the effective impurity calculations is not serious.

It is worthwhile to illustrate the QMC scheme for correlation effects in the electronic structures of HMFs using a simple example. Since solving the full one-band Hubbard model

$$\mathcal{H} = -\sum_{i,j,\sigma} t_{ij}c_{i\sigma}^\dagger c_{j\sigma} + U\sum_i n_{i\uparrow}n_{i\downarrow} \tag{174}$$

is difficult (see the discussion in Sec. III.A), we treat the dynamical mean-field theory (DMFT) (Georges *et al.*, 1996), which is formally exact in the limit of infinite dimensionality. Following this approach, we consider the Bethe lattice with coordination $z\to\infty$ and nearest-neighbor hopping $t_{ij}=t/\sqrt{z}$. In this case, a semielliptic density of states is obtained as a function of the effective hopping t, $N(\epsilon)=(2\pi t^2)^{-1}\sqrt{4t^2-\epsilon^2}$. In order to stabilize the toy model in the HMF state, we add an external magnetic spin splitting term Δ that mimics the local Hund polarization. This HMF state corresponds to a mean-field (HF) solution denoted in Fig. 13 as a dashed line.

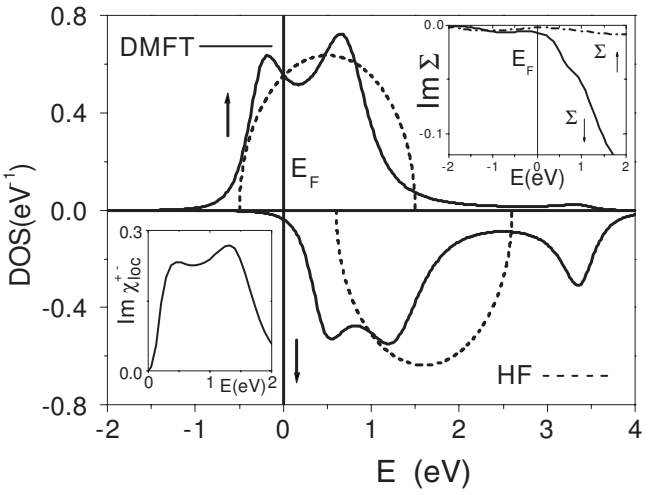

FIG. 13. Density of states for HMFs in the Hartree-Fock (HF) approximation (dashed line) and in QMC solution of the DMFT problem for the semicircular model (solid line) with bandwidth $W=2$ eV, Coulomb interaction $U=2$ eV, $\Delta=0.5$ eV, chemical potential $\mu=-1.5$ eV, and temperature $T=0.25$ eV. Insets: Imaginary part of the spin-flip susceptibility (left) and imaginary part of self-energy (right) (Chioncel, Katsnelson, de Groot, *et al.*, 2003).

The effective-medium Green's function $\mathcal{G}_\sigma$ is connected with the local Green's function G_σ on the Bethe lattice through the self-consistency condition (Georges *et al.*, 1996)

$$\mathcal{G}_\sigma^{-1} = i\omega_n + \mu - t^2 G_\sigma - 1/2\sigma\Delta, \tag{175}$$

where $\omega_n=(2n+1)\pi T$ $(n=0,\pm1,\pm2,\ldots)$ are the Matsubara frequencies. The Green's function corresponding to the DMFT effective action, Eq. (167), $G_\sigma(\tau-\tau')=-\langle T_\tau c_\sigma(\tau)c_\sigma^\dagger(\tau')\rangle_{S_{\text{eff}}}$, has been calculated using the quantum Monte Carlo scheme within the so-called exact enumeration technique (Georges *et al.*, 1996) using the time discretization parameter $L=25$ [for details, see Chioncel, Katsnelson, de Groot, *et al.* (2003)]. We emphasize that due to the symmetry of the ferromagnetic state, the local G_σ and the effective-medium Green's functions are diagonal in spin space, even in the presence of the interactions that enable the spin-flip scattering process. The magnon excitation can be studied through the two-particle correlation function

$$\chi_{\text{loc}}^{+-}(\tau-\tau') = \langle S^+(\tau)S^-(\tau')\rangle = \langle T_\tau c_\uparrow^\dagger(\tau)c_\downarrow(\tau)c_\downarrow^\dagger(\tau')c_\uparrow(\tau')\rangle_{S_{\text{eff}}}, \tag{176}$$

which is obtained by using the QMC procedure (Jarrell, 1992). Being local, this function is insufficient to find the **q** dependence of the magnon spectrum, but yields only a general shape of the magnon density of states.

The DMFT results are presented in Fig. 13. In comparison with a simple Hartree-Fock solution, one can see an additional well-pronounced feature appearing in the spin-down gap region, just above the Fermi level, namely the nonquasiparticle states that are visible in both spin channels of the DOS around 0.5 eV. In addition, a many-body satellite appears at 3.5 eV.

The left inset of Fig. 13 represents the imaginary part of the local spin-flip susceptibility. One can see a well pronounced shoulder ($\simeq$0.5 eV), which is related to a characteristic magnon excitation (Irkhin and Katsnelson, 1985b, 1990, 1994). There is a broad maximum at about 1 eV, which corresponds to the Stoner excitation energy. The right inset of Fig. 13 represents the imaginary part of self-energy. The spin-up channel can be described by a Fermi-liquid-type behavior with a parabolic energy dependence $-\text{Im}\,\Sigma^\uparrow \propto (E-E_F)^2$, whereas in the spin-down channel, the NQP shoulder at 0.5 eV is visible. Due to the relatively high temperature ($T=0.25$ eV) in the QMC calculation, the NQP tail extends below the Fermi level (remember that at zero temperature, the tail should vanish exactly at the Fermi level; see Sec. III.B).

C. Spin-polarized *T*-matrix fluctuating exchange approximation

Most HMF materials are moderately or weakly correlated systems. This means that one can use some perturbative approaches that make computations much less labor intensive and allow one to work with the complete four-index Coulomb interaction matrix. An efficient perturbative scheme was proposed by Bickers and Scalapino (1989) and was called the fluctuating exchange approximation (FLEX). This was generalized to the multiband case and used in the context of the DMFT by Lichtenstein and Katsnelson (1998) and Katsnelson and Lichtenstein (1999). The latter step means that this approach is not used directly for the whole crystal, but for the effective impurity problem, so that the momentum dependence of the Green's functions is neglected. On the other hand, the self-consistency of the DMFT procedure makes the description of the local effects in perturbative schemes more accurate. For example, in the case of the one-band half-filled Hubbard model, the second-order perturbation expression for the self-energy in the context of the DMFT provides the correct atomic limit and, actually, an accurate description of the metal-insulator transition (Kajueter and Kotliar, 1996). A starting point in the FLEX approximation is the separation of different interaction channels. The symmetrization of the bare U matrix is done over particle-hole and particle-particle channels,

$$U^d_{m_1m_1'm_2m_2'} = 2U^i_{m_1m_2m_1'm_2'} - U^i_{m_1m_2m_2'm_1'},$$

$$U^m_{m_1m_1'm_2m_2'} = -U^i_{m_1m_2m_2'm_1'},$$

$$U^s_{m_1m_1'm_2m_2'} = \tfrac{1}{2}(U^i_{m_1m_1'm_2m_2'} + U^i_{m_1m_1'm_2'm_2}),$$

$$U^t_{m_1m_1'm_2'm_2} = \tfrac{1}{2}(U^i_{m_1m_1'm_2'm_2} - U^i_{m_1m_1'm_2m_2'}). \tag{177}$$

The above expressions are the matrix elements of bare interaction, which can be obtained with pair operators corresponding to different channels:

- particle-hole density,

$$d_{12} = \frac{1}{\sqrt{2}}(c^+_{1\uparrow}c_{2\uparrow} + c^+_{1\downarrow}c_{2\downarrow}); \tag{178}$$

- particle-hole magnetic,

$$m^0_{12} = \frac{1}{\sqrt{2}}(c^+_{1\uparrow}c_{2\uparrow} - c^+_{1\downarrow}c_{2\downarrow}),$$

$$m^+_{12} = c^+_{1\uparrow}c_{2\downarrow},$$

$$m^-_{12} = c^+_{1\downarrow}c_{2\uparrow}; \tag{179}$$

- particle-particle singlet,

$$s_{12} = \frac{1}{\sqrt{2}}(c_{1\downarrow}c_{2\uparrow} - c_{1\uparrow}c_{2\downarrow}),$$

$$s^+_{12} = \frac{1}{\sqrt{2}}(c^+_{1\downarrow}c^+_{2\uparrow} - c^+_{1\uparrow}c^+_{2\downarrow}); \tag{180}$$

- particle-particle triplet,

$$t^0_{12} = \frac{1}{\sqrt{2}}(c_{1\downarrow}c_{2\uparrow} - c_{1\uparrow}c_{2\downarrow}),$$

$$t^{+0}_{12} = \frac{1}{\sqrt{2}}(c^+_{1\downarrow}c^+_{2\uparrow} - c^+_{1\uparrow}c^+_{2\downarrow}),$$

$$t^{\pm}_{12} = c_{1\uparrow,\downarrow}c_{2\downarrow,\uparrow},$$

$$t^{\pm}_{12} = c^+_{1\uparrow,\downarrow}c^+_{2\downarrow,\uparrow}. \tag{181}$$

These operators describe the correlated movements of the electrons and holes below and above the Fermi level and therefore play an important role in defining the spin-dependent effective potentials $W^{\sigma\sigma'}_{m_1m_2m_3m_4}$.

In the spin-polarized T-matrix fluctuating exchange approximation (SPTF) scheme (Katsnelson and Lichtenstein, 2002) the particle-particle interactions are described in the T-matrix approach (Galitski, 1958; Kanamori, 1963) where for the effective interaction the sum over the ladder graphs is carried out with the aid of the so-called T matrix, which obeys the Bethe-Salpether-like integral equation,

$$\langle 13|T^{\sigma\sigma'}(i\Omega)|24\rangle = \langle 13|v|24\rangle - \frac{1}{\beta}\sum_{\omega}\sum_{5678} G^{i\sigma}_{56}(i\omega) \times G^{i\sigma'}_{78}(i\omega)G(i\Omega - i\omega) \times \langle 68|T^{\sigma\sigma'}(i\Omega)|24\rangle. \tag{182}$$

The corresponding contributions to the self-energy are described by the Hartree and Fock diagrams with the formal replacement of the bare interaction by the T matrix,

$$\Sigma^{(TH)}_{12,\sigma}(i\omega) = \frac{1}{\beta}\sum_{\Omega}\sum_{34\sigma'}\langle 13|T^{\sigma\sigma'}(i\Omega)|24\rangle G^{\sigma'}_{43}(i\Omega - i\omega), \tag{183}$$

$$\Sigma^{(TF)}_{12,\sigma}(i\omega) = -\frac{1}{\beta}\sum_{\Omega}\sum_{34\sigma'}\langle 14|T^{\sigma\sigma}(i\Omega)|32\rangle G^{i\sigma}_{34}(i\Omega - i\omega). \tag{184}$$

The Hartree contribution dominates for small concentration of electrons and holes; these two contributions together contain all second-order-in-V terms in the self-energy.

Combining the density and magnetic parts of the particle-hole channel, we can write an expression for the interaction part of the Hamiltonian (Lichtenstein and Katsnelson, 1998; Katsnelson and Lichtenstein, 1999),

$$\mathcal{H}_U = D * H^U * D^+,$$

$$\mathcal{H}_U = \tfrac{1}{2}\,\mathrm{Tr}(D^+ * V^{\parallel} * D + m^+ * V^{\perp}_m * m^- + m^- * V^{\perp}_m * m^+), \tag{185}$$

where D is a row vector with elements (d, m^0), and D^+ is a column vector with elements $(d^+ m^+_0)$; * stands for the matrix multiplication with respect to the pairs of orbital indices. It follows from the model consideration presented above that for a proper description of the effects of electron-magnon interactions, it is important to replace the bare spin-flip potential by a static limit of the T matrix [see Eqs. (6) and (35)]. With this replacement, the expression of the effective potential is

$$V^{\parallel}(i\omega) = \frac{1}{2}\begin{pmatrix} V^{dd} & V^{dm} \\ V^{md} & V^{mm} \end{pmatrix},$$

$$(V^{\perp}_m)_{1234} = \langle 13|T^{\uparrow\downarrow}|42\rangle. \tag{186}$$

The matrix elements of the effective interaction for z (longitudinal) spin fluctuations are

$$V_{dd} = \frac{1}{2}\sum_{\sigma}\left(\sum_{\sigma'}\langle 13|T^{\sigma\sigma'}|42\rangle - \langle 13|T^{\sigma'\sigma'}|42\rangle\right),$$

$$V_{dm} = V_{md} = \frac{1}{2}\sum_{\sigma\sigma'}\sigma(\langle 13|T^{\sigma\sigma}|42\rangle - \langle 13|T^{\sigma\sigma}|24\rangle + \langle 13|T^{\sigma'\sigma}|42\rangle),$$

$$V_{mm} = \frac{1}{2}\sum_{\sigma}\left(\sum_{\sigma'}\sigma\sigma'\langle 13|T^{\sigma\sigma'}|42\rangle - \langle 13|T^{\sigma'\sigma'}|42\rangle\right). \tag{187}$$

Further, we introduce the expressions for the generalized longitudinal ($\chi^{\parallel}$) and transverse ($\chi^{\perp}$) susceptibilities,

$$\chi^{\perp}(i\omega) = [1 + V^{\perp}_m\Gamma^{\uparrow\downarrow}(i\omega)]^{-1} * \Gamma^{\uparrow\downarrow}(i\omega), \tag{188}$$

$$\chi^{\parallel}(i\omega) = [1 + V^{\parallel} * \chi_0^{\parallel}(i\omega)]^{-1} * \chi_0^{\parallel}(i\omega), \tag{189}$$

where $\Gamma(i\omega)$ is the Fourier transform of the empty loop,

$$\Gamma^{\sigma\sigma'}_{m_1m_2m_3m_4}(\tau) = -G^{i\sigma}_{m_2m_3}(\tau)G^{i\sigma'}_{m_4m_1}(-\tau), \tag{190}$$

and the bare matrix longitudinal susceptibility is

$$\chi_0^{\parallel}(i\omega) = \frac{1}{2}\begin{pmatrix} \Gamma^{\uparrow\uparrow} + \Gamma^{\downarrow\downarrow} & \Gamma^{\uparrow\uparrow} - \Gamma^{\downarrow\downarrow} \\ \Gamma^{\uparrow\uparrow} - \Gamma^{\downarrow\downarrow} & \Gamma^{\uparrow\uparrow} + \Gamma^{\downarrow\downarrow} \end{pmatrix}. \tag{191}$$

The four matrix elements correspond to the density-density (dd), density-magnetic (dm^0), magnetic-density (m^0d), and magnetic-magnetic channels (m^0m^0) and couple longitudinal magnetic fluctuation with density magnetic fluctuation. In this case, the particle-hole contribution to the self-energy is

$$\Sigma^{(ph)}_{12\sigma}(\tau) = \sum_{34\sigma'} W^{\sigma\sigma'}_{1342}(\tau)G^{\sigma'}_{34} \tag{192}$$

with the particle-hole fluctuation potential matrix

$$W^{\sigma\sigma'}(i\omega) = \begin{pmatrix} W_{\uparrow\uparrow} & W_{\uparrow\downarrow} \\ W_{\downarrow\uparrow} & W_{\downarrow\downarrow} \end{pmatrix}, \tag{193}$$

and the spin-dependent effective potentials are defined by

$$\begin{aligned} W_{\uparrow\uparrow} &= \tfrac{1}{2}V^{\parallel} * (\chi^{\parallel} - \chi_0^{\parallel}) * V^{\parallel}, \\ W_{\downarrow\downarrow} &= \tfrac{1}{2}V^{\parallel} * (\tilde{\chi}^{\parallel} - \tilde{\chi}_0^{\parallel}) * V^{\parallel}, \\ W_{\uparrow\downarrow} &= \tfrac{1}{2}V_m^{\perp} * (\chi^{+-} - \chi_0^{+-}) * V_m^{\perp}, \\ W_{\downarrow\uparrow} &= \tfrac{1}{2}V_m^{\perp} * (\chi^{-+} - \chi_0^{-+}) * V_m^{\perp}, \end{aligned} \tag{194}$$

where $\tilde{\chi}^{\parallel}, \tilde{\chi}_0^{\parallel}$ differ from the values of $\chi^{\parallel}, \chi_0^{\parallel}$ by the replacement $\Gamma^{\uparrow\uparrow} \leftrightarrow \Gamma^{\downarrow\downarrow}$ in Eq. (191). The final expression for the SPTF self-energy is given by

$$\Sigma = \Sigma^{(TH)} + \Sigma^{(TF)} + \Sigma^{(\mathrm{ph})}. \tag{195}$$

Due to off-diagonal spin structure of the self-energy $\Sigma^{(\mathrm{ph})}$, this method can be used to consider the nonquasiparticle states in HMFs. A more detailed justification and description of the method has been given by Katsnelson and Lichtenstein (2002). This approach was also generalized to the case of strong spin-orbit coupling and used for actinide magnets (Pourovskii *et al.*, 2005, 2006). In that case, separation into density and magnetic channels is not possible and one should work with the 4×4 supermatrices for the effective interaction.

Recently, several LDA+DMFTcalculations of different HMF materials have been carried out. Now we review the results of these calculations, focusing mainly on nonquasiparticle states resulting from the electron-magnon interactions. LDA+DMFT is the only contemporary practical way to consider them in the electronic-structure calculations.

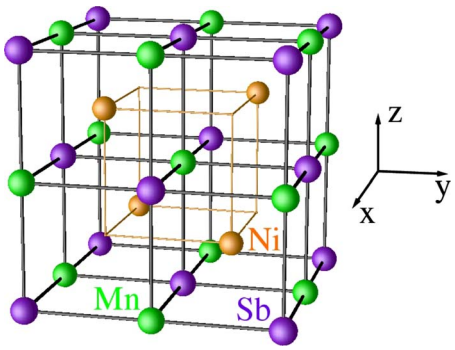

FIG. 14. (Color online) $C1_b$ structure with the fcc Bravais lattice (space group $F\bar{4}3m$). Mn (green) and Sb (purple) atoms are located at (0,0,0) and $(\frac{1}{2}, \frac{1}{2}, \frac{1}{2})$ forming the rocksalt structure arrangement. Ni (orange) atom is located in the octahedrally coordinated pocket, at one of the cube center positions $(\frac{3}{4}, \frac{3}{4}, \frac{3}{4})$ leaving the other $(\frac{1}{4}, \frac{1}{4}, \frac{1}{4})$ empty. This creates voids in the structure (Yamasaki *et al.*, 2006).

V. ELECTRONIC STRUCTURE OF SPECIFIC HALF-METALLIC COMPOUNDS

A. Heusler alloys

1. NiMnSb: Electronic structure and correlations

The intermetallic compound NiMnSb crystallizes in the cubic structure of MgAgAs type ($C1_b$) with the fcc Bravais lattice (space group $F\bar{4}3m = T_d^2$). The crystal structure is shown in Fig. 14. This structure can be described as three interpenetrating fcc lattices of Ni, Mn, and Sb. A detailed description of the band structure of semi-Heusler alloys was given using electronic-structure calculations analysis (de Groot, Mueller, v. Engen, *et al.*, 1983; Öğüt and Rabe, 1995; Galanakis *et al.*, 2002a; Kulatov and Mazin, 2003; Nanda and Dasgupta, 2003; Galanakis and Mavropoulos, 2007); we briefly summarize the results.

To obtain the minority spin gap, not only the Mn-d-Sb-p interactions but also Mn-d-Ni-d interactions must be taken into account. Moreover, the loss of inversion symmetry produced by $C1_b$ structure (the symmetry lowering from O_h in the $L2_1$ structure to T_d in the $C1_b$ structure at Mn site) is an essential additional ingredient. All above interactions combined with the T_d symmetry lead to a nonzero anticrossing of bands and to gap opening.

The large exchange splitting of the Mn atom (producing the local Mn magnetic moment of about $3.7\mu_B$) is crucial to induce a half-metallic structure. In the spin-polarized calculation, the position of t_{2g} and e_g Ni states is changed slightly, so that the exchange splitting on Ni is not large. The local Ni magnetic moment calculation gives a value around $0.3\mu_B$.

The non-spin-polarized result has a striking resemblance to the majority-spin-polarized calculations, presented in Fig. 15. Kulatov *et al.* explained the half metallicity of NiMnSb by the extended Stoner factor

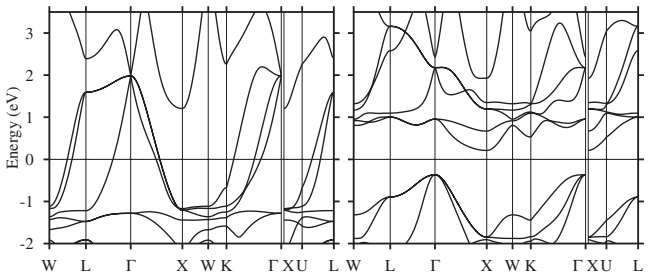

FIG. 15. Full basis-set spin-polarized (ferromagnetic) bands for NiMnSb; majority spin (left) and minority spin (right). The high-symmetry points are $W(\frac{1}{2},1,0)$, $L(\frac{1}{2},\frac{1}{2},\frac{1}{2})$, $\Gamma(0,0,0)$, $X(0,1,0)$, and $K(\frac{3}{4},\frac{3}{4},0)$ in the W-L-Γ-X-W-K-Γ line, and $X(0,0,1)$, $U(\frac{1}{4},\frac{1}{4},1)$, and $L(\frac{1}{2},\frac{1}{2},\frac{1}{2})$ in the X-U-L line (Yamasaki *et al.*, 2006).

calculations in the rigid-band approximation (Kulatov and Mazin, 2003): the minority spin-band gap opens due to the exchange splitting, which shifts minority bands, so that they become empty.

There is excellent agreement between the first band-structure calculation (de Groot, Mueller, v. Engen, *et al.*, 1983) and Nth-order muffin-tin orbital (NMTO) investigations (Andersen and Saha-Dasgupta, 2000; Zurek *et al.*, 2005; Yamasaki *et al.*, 2006). NMTO Wannier Mn d orbitals are shown in Fig. 16. The triply degenerate manganese t_{2g} orbitals are complicated due to the hybridization with Ni d and Sb p states. The d_{xy} orbital at the Mn site is deformed by antibonding with the Ni d state directed tetrahedrally to $[11\bar{1}]$, $[\bar{1}\bar{1}\bar{1}]$, $[1\bar{1}1]$, and $[\bar{1}11]$. The same Ni d orbitals couple with Sb p states. The direct Mn-d_{xy}-Sb-p π coupling is not seen since the distance is $d(\text{Mn-Sb}):d(\text{Ni-Sb})=1:\sqrt{3}/2$. Therefore, the Ni-$d$-Sb-$p$ interactions are more favorable. The dispersion of the Mn t_{2g} bands is mainly due to hopping via the tails of Sb p and Ni d orbitals. On the other hand, the next-nearest-neighbor (NNN) d-d hopping of the t_{2g} orbital is small. The e_g orbitals at the Mn site are much easier to understand: they point toward Sb atoms, and a strong $pd\sigma$ coupling between Sb p and Mn e_g states is seen. This induces large NNN d-d hoppings.

The Wannier orbital analysis for NiMnSb (Yamasaki *et al.*, 2006) confirms the previous conclusions of (de Groot, Mueller, v. Engen, *et al.*, 1983) about the role of p-d hybridization as well as the role of d-d hybridization (Galanakis *et al.*, 2002a). The LDA partial density of states for half-metallic NiMnSb and the fat-band structure that marks the main orbital character of va-

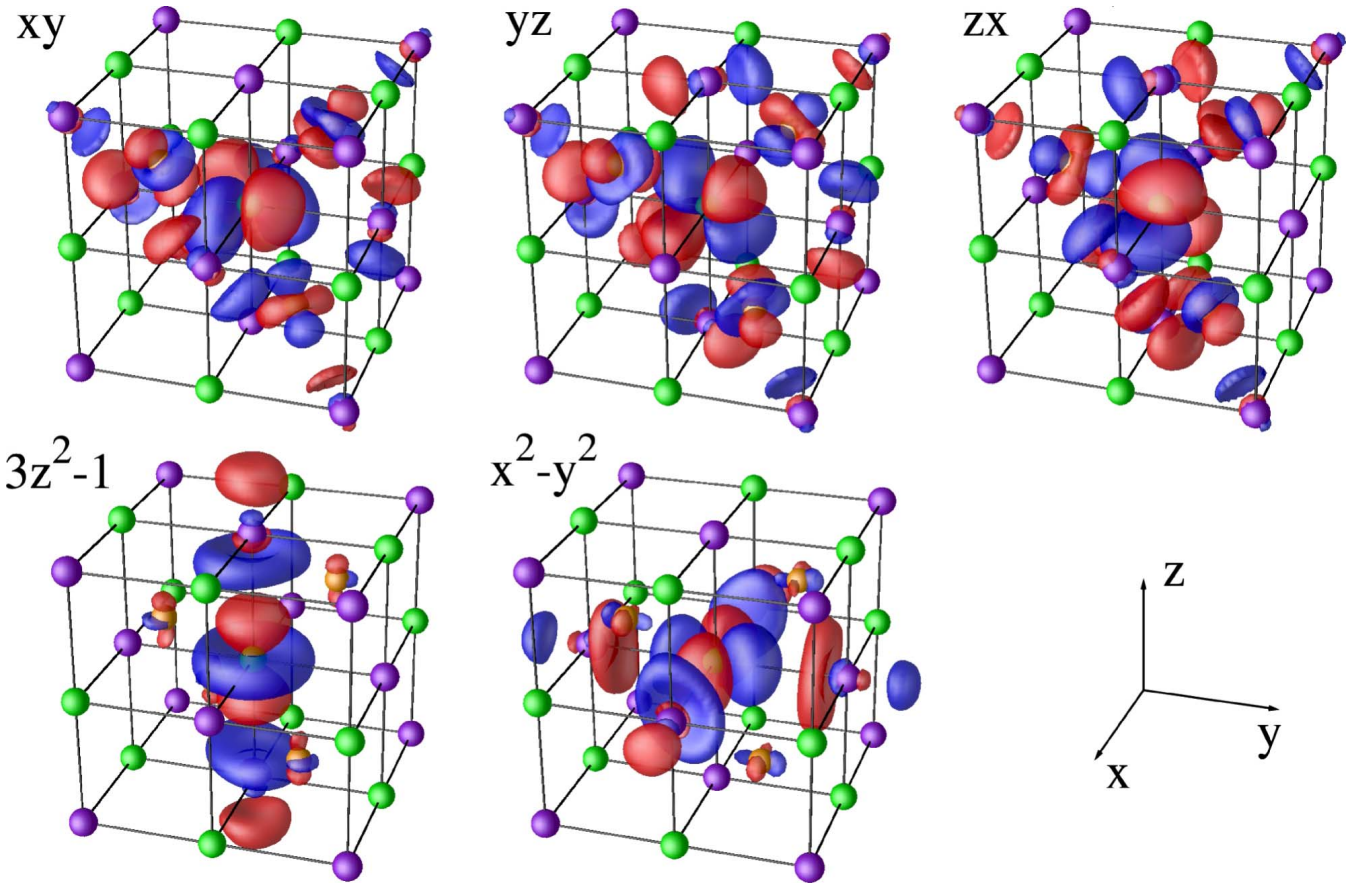

FIG. 16. (Color online) NMTO Mn-d Wannier orbitals of NiMnSb. Ni is orange, Mn is green, and Sb is purple. Red (blue) indicates a positive (negative) sign. Upper panel: t_{2g} orbitals; d_{xy} (left), d_{yz} (middle), d_{zx} (right). The triply degenerate t_{2g} orbitals can be obtained by the permutation of axes. Lower panel: e_g orbitals; d_{3z^2-1} (left), $d_{x^2-y^2}$ (middle). These e_g orbitals are doubly degenerated (Yamasaki *et al.*, 2006).

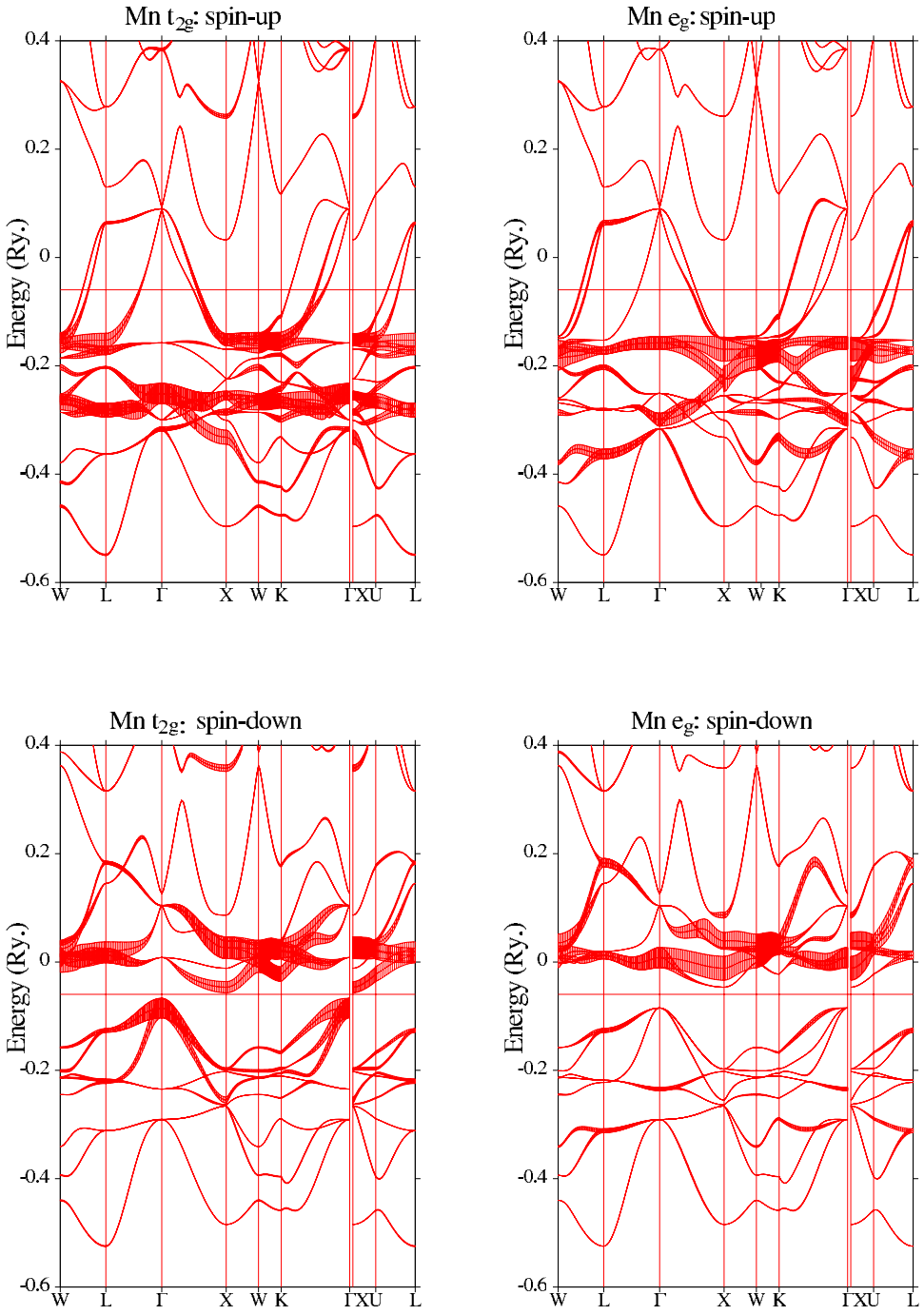

FIG. 17. (Color online) Decorated (fat) bands for the spin-polarized (ferromagnetic) NiMnSb; Mn majority spin (up) and minority spin (down). The high-symmetry points are $W(\frac{1}{2},1,0)$, $L(\frac{1}{2},\frac{1}{2},\frac{1}{2})$, $\Gamma(0,0,0)$, $X(0,1,0)$, and $K(\frac{3}{4},\frac{3}{4},0)$ in the W-L-Γ-X-W-K-Γ line, and $X(0,0,1)$, $U(\frac{1}{4},\frac{1}{4},1)$, and $L(\frac{1}{2},\frac{1}{2},\frac{1}{2})$ in the X-U-L line (Yamasaki, 2006).

lence states are presented in Figs. 17–19. One can see that the spin-up Mn d and Ni d states are located at the same energy region, while spin-down bands are separate due to the significant Mn exchange splitting. The top of the valence spin-down bands forms by the Mn t_{2g}, Sb p, and Ni t_{2g} orbitals, while the bottom of the conduction bands is due to the Mn e_g and t_{2g} states. This means that large Mn spin splitting and Sb-mediated indirect Mn-Ni interactions are responsible for the formation of the half-metallic gap. One can see these complicated Mn t_{2g} valence orbitals with large contributions of Sb p and Ni t_{2g} states in Fig. 15. The physical picture of the down-folding analysis should not change very much if one explicitly includes Sb p and Ni d orbitals.

We now discuss the prototype half-metallic ferromag net NiMnSb where the gap is situated in the spin-down (minority) channel. The temperature dependence of the HMF electronic structure and the stability of half metallicity against different spin excitations are crucial for practical applications in spintronics. A simple attempt to incorporate finite-temperature effects (Skomski and Dowben, 2002; Dowben and Skomski, 2003), leading to static noncollinear spin-configurations, shows a mixture of spin-up and spin-down density of states that destroy the half-metallic behavior. Chioncel, Katsnelson, de Groot, *et al.* (2003) used a different more natural approach to investigate the proper effect of dynamical spin

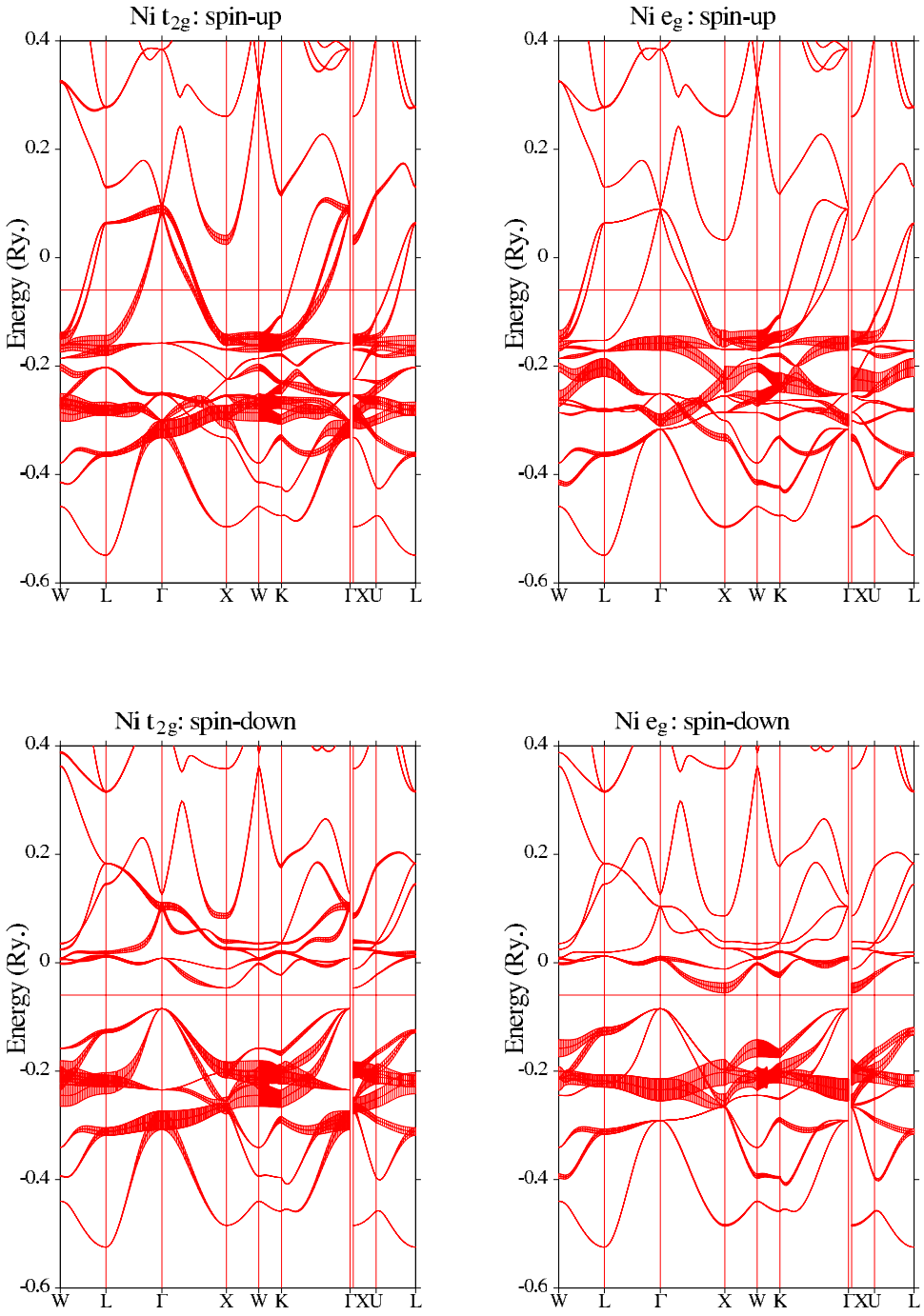

FIG. 18. (Color online) Decorated (fat) bands for the spin-polarized (ferromagnetic) NiMnSb; Ni majority spin (up) and minority spin (down) (Yamasaki, 2006).

fluctuations on the electronic structure at $T < T_C$, within the half-metallic ferromagnetic state.

The LDA+DMFT calculation for NiMnSb (Chioncel, Katsnelson, de Groot, *et al.*, 2003) was the first application of the combined electronic structure and many-body technique to HMF. Aryasetiawan *et al.* (2004) pointed out that a rigorous way to define the screened frequency-dependent on-site Coulomb interaction matrix elements for correlated states is related to the generalized *GW* scheme in which *d-d* screening is suppressed to preserve the double counting in the model approach. However, in practice for realistic materials, the elimination of degrees of freedom is a difficult procedure. To find the average Coulomb interaction on the *d* atoms U and corresponding exchange interactions J, a simpler approach, the constrained LDA scheme (Dederichs *et al.*, 1984; Norman and Freeman, 1986; McMahan *et al.*, 1988; Gunnarsson *et al.*, 1989; Hybertsen *et al.*, 1989; Anisimov and Gunnarsson, 1991), can be used. In this approach, the Hubbard U is calculated from variation of the total energy with respect to the occupation number of the localized orbitals. In such a scheme, the metallic screening is rather inefficient for 3*d* transition metals, and effective U is of the order of 6 eV (Anisimov and Gunnarsson, 1991). The perfect metallic screening will lead to a smaller value of U. Unfortunately, there are no reliable schemes to calculate U

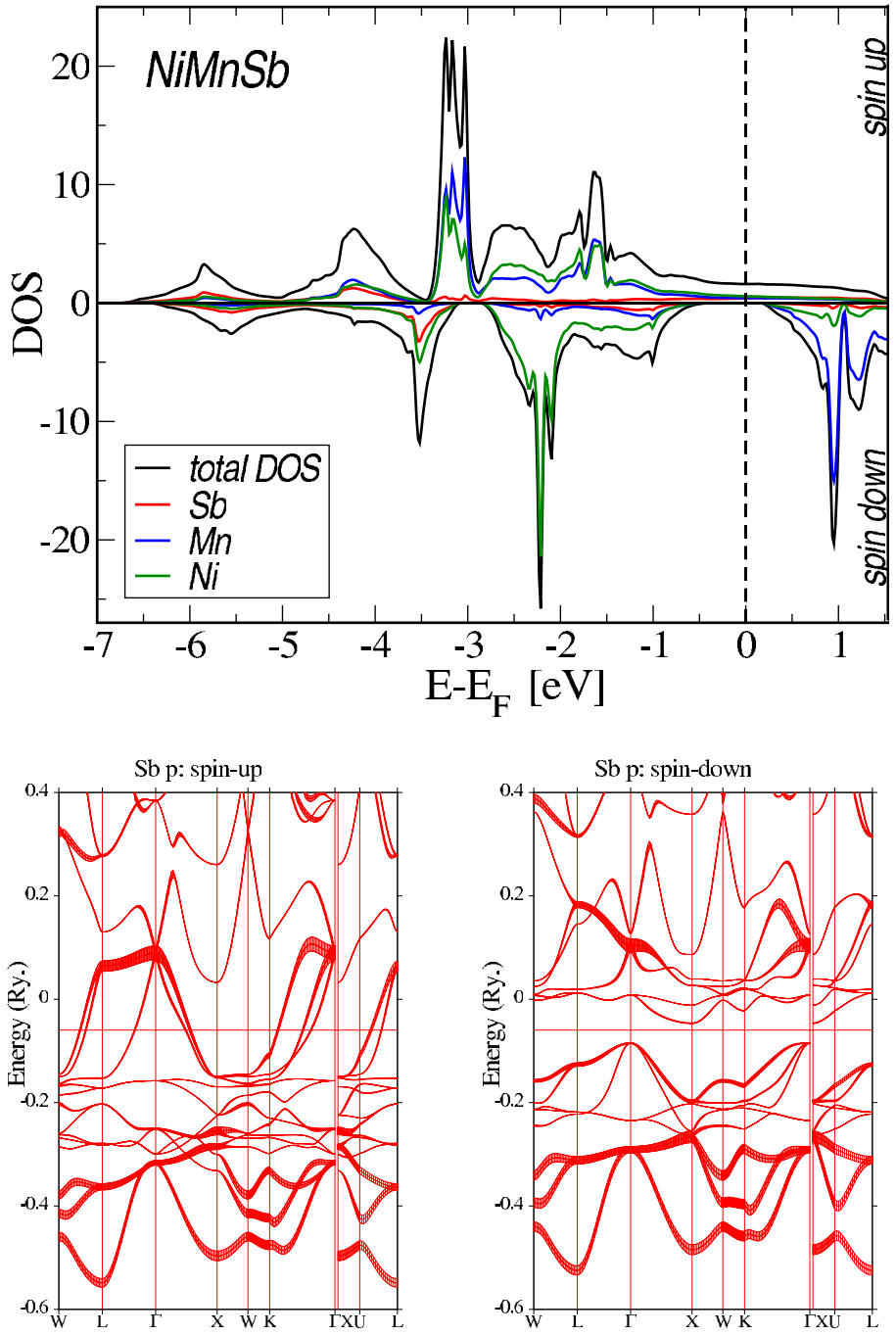

FIG. 19. (Color online) Electronic structure of NiMnSb. Upper figure: FLAPW calculation of spin-polarized NiMnSb (Lezaic, 2006). Lower figures: Decorated (fat) bands for the spin-polarized (ferromagnetic) NiMnSb; Sb majority spin (up) and minority spin (down) (Yamasaki, 2006).

within the constrained LDA for metals (Solovyev and Imada, 2005), and in the works of Chioncel, Katsnelson, de Groot, *et al.* (2003), Chioncel, Arrigoni, Katsnelson, *et al.* (2005); Chioncel, Katsnelson, de Wijs, *et al.* (2005), and Chioncel, Mavropoulos, Lezaic, *et al.* (2006), some intermediate values were chosen, $U=2-4$ eV and $J=0.9$ eV. Recent analysis of angle-resolved photoemission and the LDA theory indicates a shift of spectral function of the order of 0.5–1 eV, which can be attributed to correlation effects beyond the LDA (Correa *et al.*, 2006). The first angle-resolved photoemission results (Kisker *et al.*, 1987) generally agree with the LDA band structure, but demonstrate the same shift of quasiparticle dispersion of the order of 0.5 eV below the Fermi level for spin-down Mn t_{2g} bands. This can easily lead to the effective Hubbard interactions in the static mean-field approximation of the order of $U^*=1$ eV, although one should carefully investigate the effects of spin-orbital splitting. Since the spherically averaged effective Hubbard interaction is $U^*=U-J$ and the value of

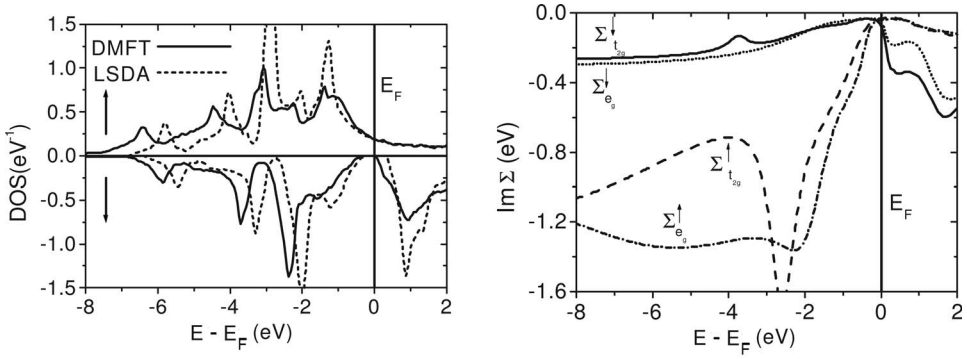

FIG. 20. Density of states for HMF NiMnSb in LSDA scheme (dashed line) and in LDA+DMFT scheme (solid line) with effective Coulomb interaction $U=3$ eV, exchange parameter $J=0.9$ eV, and temperature $T=300$ K. The nonquasiparticle state is evidenced just above the Fermi level. The imaginary part of self-energies $\mathrm{Im}\,\Sigma_d^{\downarrow}$ for t_{2g} (solid line) and e_g (dotted line), and $\mathrm{Im}\,\Sigma_d^{\uparrow}$ for t_{2g} (dashed line) and e_g (dash-dotted line), respectively.

intra-atomic exchange interactions is not screened much in solids being of the order of $J=1$ eV, we can conclude from the photoemission experiments (Kisker *et al.*, 1987) and resonant x-ray scattering (Yablonskikh *et al.*, 2001) that the Hubbard interaction $U=2$ eV is quite reasonable. An account of the correlation effects in the framework of the LDA+DMFT method also improves the description of magneto-optical properties of NiMnSb (Chadov *et al.*, 2006).

Typical results for the density of states using the LDA and LDA+DMFT are presented in Fig. 20. The LDA+DMFT density of states shows the existence of nonquasiparticle states in the LDA gap of the spin-down channel just above the Fermi level.

It is important to note that the magnetic moment per formula unit is not sensitive to the U values. For a temperature $T=300$ K, the calculated magnetic moment, $\mu=3.96\mu_B$, is close to the zero-temperature LDA value, which is integer, $\mu=4\mu_B$. This means that the half-metallic state is stable with respect to switching on correlation effects. The DMFT gap in the spin-down channel, defined as the distance between the occupied part and the starting point of the NQP tail, is also not very sensitive to U. The total DOS is also weakly U dependent due to the T-matrix renormalization effects.

In comparison with the LDA result, a strong spectral weight transfer is present for the unoccupied part of the band structure due to the appearance of the nonquasiparticle states in the energy gap above the Fermi energy (Sec. III.B). Their spectral weight is not too small and has a relatively weak dependence on the U value (Fig. 21), which is also a consequence of the T-matrix renormalization (Katsnelson and Lichtenstein, 2002).

For spin-up states, we have a normal Fermi-liquid behavior $-\mathrm{Im}\Sigma_d^{\uparrow}(E)\propto(E-E_F)^2$ with a typical energy scale of the order of several eV. The spin-down self-energy behaves in a similar way below the Fermi energy, with a bit smaller energy scale. At the same time, a significant increase in $\mathrm{Im}\,\Sigma_d^{\downarrow}(E)$ with a much smaller energy scale (tenths of an eV) is observed right above the Fermi level, which is more pronounced for t_{2g} states (Fig. 20). The NQP states are visible in the spin-down DOS (Fig. 20) at the same energy scale as the imaginary part of $\Sigma^{\downarrow}$. Similar behavior is evidenced in the model calculation of Fig. 13. The NQP spectral weight in the density of states (Fig. 21) is proportional to the imaginary part of the self-energy.

From the general many-body theory, the DMFT approach neglects the momentum dependence of the electron self-energy. In many cases, such as the Kondo effect and the Mott metal-insulator transition, the energy dependence of the self-energy is more important than the momentum dependence, and therefore the DMFT scheme is adequate to consider these problems (Georges *et al.*, 1996). In the case of itinerant electron ferromagnetism, the situation is much less clear. However, the LDA+DMFT treatment of finite-temperature magnetism and electronic structure in Fe and Ni appeared to be quite successful (Lichtenstein *et al.*, 2001). Experimentally, even in itinerant electron paramagnets that are close to ferromagnetic instability, such as Pd, the momentum dependence of the self-energy does not seem to be essential (Joss *et al.*, 1984). One can expect that in magnets with well-defined local moments such as half-metallic ferromagnets, the local DMFT approximation

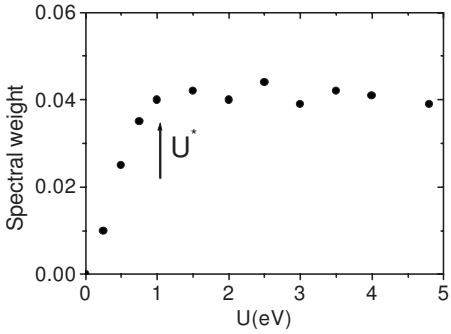

FIG. 21. Spectral weight of the nonquasiparticle state, calculated as a function of average on-site Coulomb repulsion U at temperature $T=300$ K (Chioncel, Katsnelson, de Groot, *et al.*, 2003).

for the self-energy should be even more accurate. In particular, as discussed above, it can be used for calculations of spin-polaronic or nonquasiparticle effects in these materials.

2. Impurities in HMF: Lanthanides in NiMnSb

Here we discuss the inroduction of nonintrinsic deffects in NiMnSb, which preserves the half-metallic properties, on the one hand, while optimizing the magnetic disorder, on the other hand (Attema *et al.*, 2004). Good candidates are the rare-earth impurities in NiMnSb (Attema *et al.*, 2004; Chioncel, 2004). The motivation of this choice is connected with the substantial spin-orbit interaction in the rare-earth localized f shell. Besides that, the origin of the band gap in NiMnSb is closely related to the band gap in III-V semiconductors: it is expected that substitution of some of the tetravalent elements in NiMnSb by a lanthanide preserves the essential feature of the half-metal, namely, the band gap for one spin direction.

These systems can be really synthesized, compounds RNiSb (for heavy rare-earth elements R) existing with exactly the same crystal structure as NiMnSb. The rare-earth atoms, which show both a large spin and orbital moment, can be expected to introduce a large spin-orbit interaction, in other words around 1/4 (Nd) and 3/4 (Er) in the lanthanides series. Total energy calculations allow one to evaluate the coupling between the rare-earth ($4f$) impurity spins and the manganese ($3d$) conduction electron spins. For substantial coupling, the fluctuations of the Mn ($3d$) conduction electron spins, i.e., the spin wave, might be blocked, thus the magnon branch is qualitatively changed. In contrast with the clean limit (pure NiMnSb), the magnon spectra of $NiMn_{1-x}R_xSb$ present a fragmented structure with several gaps in the Brillouin zone. This fragmentation implies that the finite-temperature effects are diminished for a suitably chosen rare-earth element.

The *ab initio* electronic-structure calculations were carried out using the scalar relativistic linear muffin-tin orbital (LMTO) method within the atomic-sphere approximation in two flavors: LDA and LDA+U (Andersen, 1975; Andersen and Jepsen, 1984; Anisimov, Aryasetiawan, and Lichtenstein 1997). To evaluate the coupling between the rare-earth and the Mn sublattices, ferromagnetic and ferrimagnetic structures were taken as the initial state of the calculation and they were preserved after the self-consistent calculation.

A simplified model was used that captures the complex interplay of the Mn ($3d$) itinerant conduction-band electrons and the localized $4f$ electrons, the latter carrying a strong magnetic moment. This model deals with a mean-field decoupling, in which the Mn $3d$ and the R f states are described by the LDA+U whereas the $3d$-$4f$ interaction is treated as perturbation. The corresponding mean-field Hamiltonian can be written in the form

$$\mathcal{H} \simeq \mathcal{H}_{\mathrm{LDA}+U} - J\sum_i \sigma_i^{3d} S_{i+\delta}^f, \tag{196}$$

where the spin of the conduction electron at site R_i is denoted by σ_i^{3d} and $S_{i+\delta}^f$ represents the spin of the $4f$ shell at the $R_{i+\delta}$ site. The Mn d local moment fluctuations could be quenched by a strong f-d coupling, which affects the magnon excitations. The strength of such a coupling was evaluated by calculating in an *ab initio* fashion the total energy of $NiMn_{1-x}R_xSb$ compounds for a parallel or antiparallel f-d coupling (Attema *et al.*, 2004; Chioncel, 2004). Given the geometry of the cell, the lanthanide substitution is realized in the fcc-Mn sublattice, so 12 pairs of $R(4f)$-Mn($3d$) are formed. The f-d coupling is calculated as the $E_{\uparrow\uparrow}-E_{\downarrow\uparrow}$ energy corresponding to a pair.

Adopting a two-sublattice model described by the Hamiltonian (196), i.e., the sublattice of lathanides $R(4f)$ being antiferromagneticaly and ferromagnetically oriented with respect to the Mn($3d$) sublattice, the J values correspond to the intersublattice couplings. In pure NiMnSb, the ferromagnetic Curie temperature T_C =740 K is determined by the strength of the Mn-Mn ($3d$-$3d$) sublattice interaction. For a small lanthanide content, one can expect this interaction in $NiMn_{1-x}R_xSb$ compounds is on the same scale as in pure NiMnSb. Therefore, the substitution introduces competition between the intrasublattice and intersublattice interactions, which are crucial parameters for any practical application. In the case of Nd, there is a large $3d$-$4f$ coupling that should dominate over the $3d$-$3d$ coupling. For temperatures lower than the Curie temperature corresponding to the $Ni_8Mn_7NdSb_8$ compound, T_C^{Nd}, the $3d$-$4f$ coupling interaction will lock the Mn ($3d$)magnetic moment fluctuations decreasing the available number of magnon states. Above T_C^{Nd}, the thermal fluctuations already removed the long-range order of the Mn ($3d$) sublattice, and there are no available magnon states. As a consequence, the Nd substitution can be attractive for high-temperature applications where the $3d$-$4f$ coupling might play an important role. In the cubic structure of NiMnSb, the uniaxial anisotropy is completely missing. Nevertheless, the $4f$ impurity spin-orbit coupling lifts the degeneracy in the Γ point. The lowest $3d$-$4f$ coupling is realized in the case of Ho.

The LDA+U density of states for $HoNi_8Mn_7Sb_8$ for $3d$-$4f$ antiparallel and parallel couplings and the U_f =9 eV value of the on-site Coulomb interaction is presented in Fig. 22. On the one hand, for the antiparallel coupling the magnetic moments are $\mu_{\mathrm{Ho}}^{\mathrm{AF}}=-4.09\mu_B$, $\mu_{\mathrm{Mn1}}^{\mathrm{AF}}=3.73\mu_B$, $\mu_{\mathrm{Mn2}}^{\mathrm{AF}}=3.80\mu_B$ and the gap of 0.55 eV is situated in the majority spin channel. On the other hand, for parallel coupling the magnetic moments have almost the same magnitude $\mu_{\mathrm{Ho}}^{F}=3.96\mu_B$, $\mu_{\mathrm{Mn1}}^{F}=3.72\mu_B$, μ_{Mn2}^{F} $=3.80\mu_B$ with a similar gap situated in the minority spin channel. It is important to note that in the case of $Ni_8Mn_7HoSb_8$, the Ho($4f$) orbitals do not hybridize with the Mn($3d$) orbitals near the Fermi level. As one can see in Fig. 22, the behavior of the DOS near the Fermi level

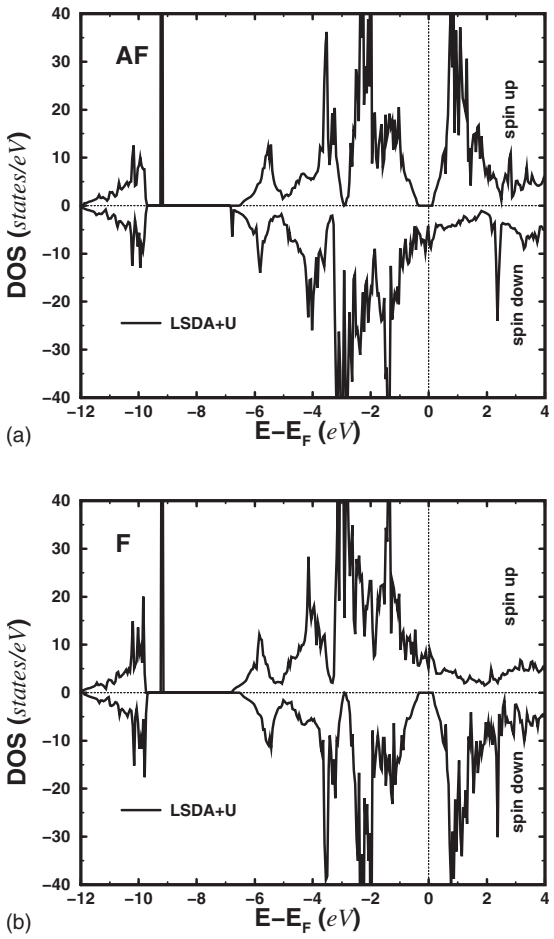

FIG. 22. Density of states for the half-metallic ferromagnet $Ni_8Mn_7HoSb_8$ in the case of antiparallel 3*d*-4*f* coupling (a) and parallel coupling (b).

is very similar, so that the nature of carriers around E_F is not changed.

The electronic-structure calculation for the antiferromagnetic HoNiSb compound was performed by Attema *et al.* (2004) and Chioncel (2004) (see Fig. 23). This is known to be a semiconducting material with interesting transport properties [giant magnetoresistance effect (Karla, Pierre, and Ouladdiaf, 1998; Karla, Pierre, and Skolozdra, 1998; Karla *et al.*, 1999; Pierre and Karla, 2000)]. The inverse susceptibility curves show a Curie-Weiss behavior down to 10 K (Karla, Pierre, and Ouladdiaf, 1998; Karla, Pierre, and Skolozdra, 1998; Karla *et al.*, 1999; Pierre and Karla, 2000). The onset of the antiferromagnetic ordering was estimated from susceptibility measurements between 1.5 and 2.5 K, and the neutron-diffraction data indicated an antiferromagnetic propagation vector (1/2,1/2,1/2) (Karla, Pierre, and Ouladdiaf, 1998; Karla, Pierre, and Skolozdra, 1998; Karla *et al.*, 1999, Pierre and Karla, 2000). In order to describe the antiferromagnetic ground state, a rhombohedral description of the $Ho_2Ni_2Sb_2$ unit cell was used. The atoms $Ho_1(0,0,0)$ and $Ho_2(1,1,1)$ acquire magnetic moments of $\mu_{Ho_1}=4.0\mu_B$ and $\mu_{Ho_2}=-4.0\mu_B$, respectively. The antiferromagnetic insulating state shows a gap of 0.29 eV in agreement with the experimental results. There are some qualitative features that are similar for the antiferromagnetic $Ho_2Ni_2Sb_2$ and the $HoNi_8Mn_7Sb_8$ compounds, namely the almost identical magnetic moment μ_{Ho} and positions of occupied and unoccupied Ho(4*f*) peaks in DOS. Perhaps the most important observation is that the spin-down channel in $Ho_2Ni_2Sb_2$ is isoelectronic to that in NiMnSb, so that the Ho substitution would preserve the half metallicity of $HoNi_8Mn_7Sb_8$ in the minority spin channel.

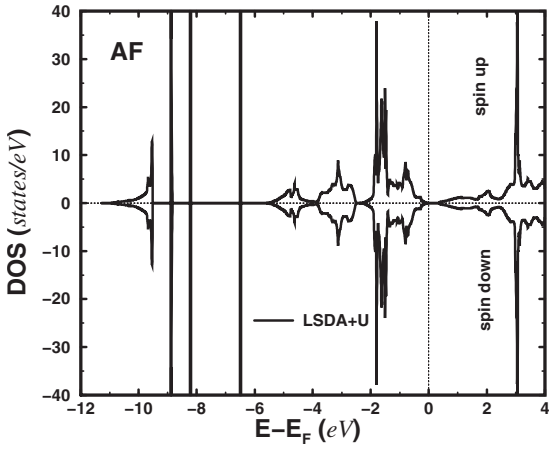

FIG. 23. Density of states of semiconducting HoNiSb (Chioncel, 2004).

3. FeMnSb: A ferrimagnetic half-metal

Early theoretical studies demonstrated that the gap in the minority spin channel is stable with respect to change of the 3*d* atom X=Fe,Co,Ni in the *X*MnSb compounds (Kübler, 1984; de Groot *et al.*, 1986). A noticeable difference between Ni- and Fe-based Heusler alloys is that NiMnSb is a half-metallic ferromagnet with a very small value of Ni magnetic moment ($0.2\mu_B$), whereas in FeMnSb the antiferromagnetic coupling between Fe ($-1\mu_B$) and Mn ($3\mu_B$) moments stabilizes the gap and the half-metallic ferrimagnetic electronic structure (de Groot *et al.*, 1986). Unfortunately, the ternary compound FeMnSb does not exist, but indications of its magnetic and crystallographic properties were obtained by extrapolating the series of $Ni_{1-x}Fe_xMnSb$ (de Groot *et al.*, 1986) to high Fe concentration.

In the nonrelativistic approximation, there are two essentially different sources for states in the gap at finite temperatures. First, there is the simple effect of gap filling due to disorder, i.e., due to scattering on static (classical) spin fluctuation or thermal magnons; this is symmetric with respect to the Fermi energy. On the contrary, the correlation effects result in an asymmetry in the gap filling, spin-down nonquasiparticle states appearing above the Fermi level. One has to take into account also spin-orbit coupling effects mixing the spin-up and spin-down states due to nonzero elements of spin-orbital interactions $V_{SO}^{\sigma,\sigma'}$ (see the discussion in Sec.

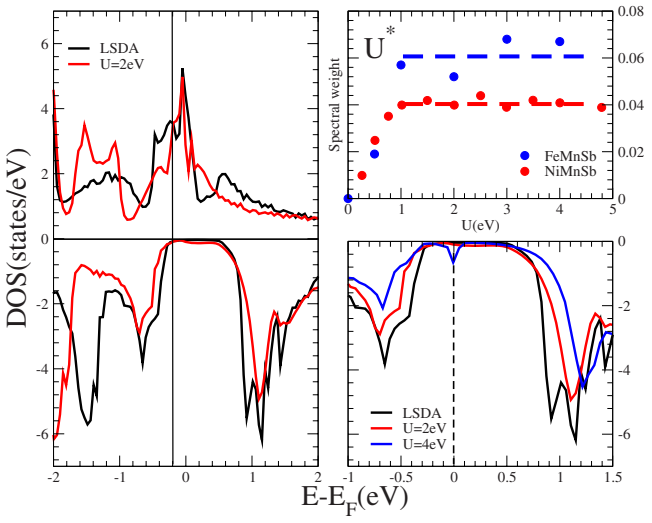

FIG. 24. (Color online) Electronic structure of FeMnSb. Left: Density of states of half-metallic FeMnSb, LSDA (black line), and LSDA+DMFT (red line) for the effective Coulomb interaction $U=2$ eV exchange parameter $J=0.9$ eV and temperature $T=300$ K. Lower right panel: Zoom around E_F for different values of U. Upper right panel: Spectral weight of the NQP states calculated as a function of U. The values obtained for NiMnSb (Chioncel, Katsnelson, de Groot, 2003) are plotted for comparison (Chioncel, Arrigoni, Katsnelson, *et al.*, 2006).

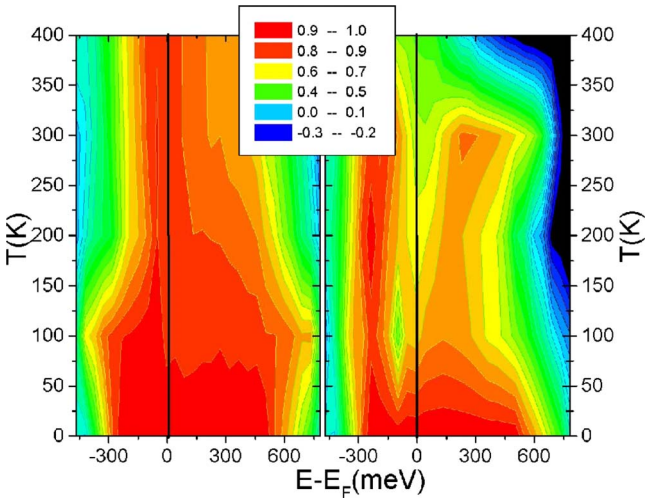

FIG. 25. (Color online) Contour plots of polarization as a function of energy and temperature for different values of local Coulomb interaction U. Left, $U=2$ eV; right, $U=4$ eV. The LSDA polarization is plotted as the $T=0$ K temperature result. The asymmetry of the NQP states is clearly visible for $U=4$ eV (Chioncel, Arrigoni, Katsnelson, *et al.*, 2006).

III.B). To illustrate the differences between the static and dynamic effects, we plot the DOS of the LDA+DMFT calculations compared with recent results including SO coupling (de Groot *et al.*, 1986; Mavropoulos *et al.*, 2004).

A relatively weak dependence of the NQP spectral weight on U (Fig. 24) is evidenced for both NiMnSb and FeMnSb compounds. A "saturation" of the spectral weight for FeMnSb takes place for almost the same value, $U^* \simeq 1$ eV, as in the case of NiMnSb, which is in agreement with experimental observation of relatively weak correlation effects in Heusler HMFs like PtMnSb (Kisker *et al.*, 1987). The small value of the effective Hubbard parameter can be understood in terms of the large T-matrix renormalization of the Coulomb interactions (Katsnelson and Lichtenstein, 1999, 2002). The spectral weight values for FeMnSb are larger in comparison with those obtained for NiMnSb (Chioncel, Katsnelson, de Groot, *et al.*, 2003; Chioncel *et al.*, 2003), which can be attributed to a larger majority spin DOS at the Fermi level.

The spin-orbit coupling produces a peak in the minority-spin channel close to the Fermi level (Mavropoulos *et al.*, 2004), which is an order of magnitude smaller than the spectral weight of the NQP states. According to the SO results, the polarization at the Fermi level for NiMnSb and FeMnSb is almost the same. In contrast, calculation (Chioncel, Arrigoni, Katsnelson, *et al.*, 2006) shows that the spectral weight of the NQP states in FeMnSb is almost twice as large as the value for NiMnSb.

To discuss the influence of temperature and local Coulomb interactions on the polarization in the FeMnSb compound, we present results of LDA+DMFT calculations for $T \leq 400$ K and different U's. Figure 25 presents the contour plot of spin polarization $P(E,T)$ as a function of energy E and temperature T for $U=2$ and 4 eV. The LDA value, plotted for convenience as the $T=0$ K result, shows a gap with magnitude 0.8 eV, in agreement with previous calculations (Mavropoulos *et al.*, 2004).

One can see a peculiar temperature dependence of the spin polarization. The NQP features appear for $E-E_F \geq 0$ and are visible in Fig. 24 for $U=2$ eV and $T=300$ K. Increasing the value of U from 2 to 4 eV, the NQP contribution in depolarization becomes more significant. When the tail of the NQP states crosses the Fermi level, a drastic depolarization at the Fermi level takes place, the NQP contribution being pinned to the Fermi level for $U=4$ eV.

One can see a clear distinction between the finite-temperature behavior of the polarization and magnetization, shown in Fig. 26 for different values of U. For $U=4$ eV, already at 100 K there is a strong depolarization about 25%. On the contrary, it is interesting to note that the reduced magnetization $M(T)/M(0)$ decreases slowly in the temperature range shown in Fig. 25. This reduction is a consequence of the finite-temperature excitations, i.e., spin-flip processes, affecting both spin channels. In the minority-spin channel, NQP states are formed, and in the majority channel a spectral weight redistribution around the Fermi level (Fig. 24) contributes to the depolarization. The corresponding depolarization increases with the strength of correlations. The density of NQP states displays a rather strong temperature dependence (Sec. III.C) and results in an asymmetry that is visible in Figs. 24 and 25.

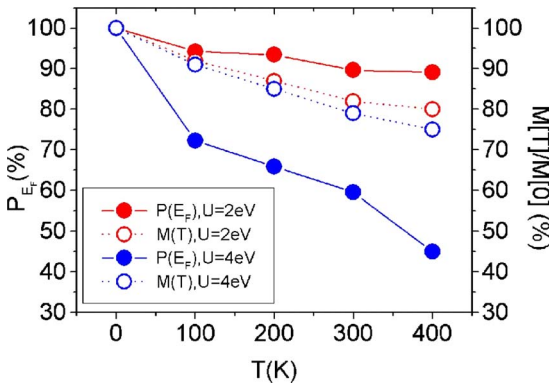

FIG. 26. (Color online) Temperature-dependent polarization at the Fermi level; $P(E=E_F,T)$ (solid line) and magnetization (dashed line) for different values of local Coulomb interaction U (Chioncel, Arrigoni, Katsnelson, *et al.*, 2006).

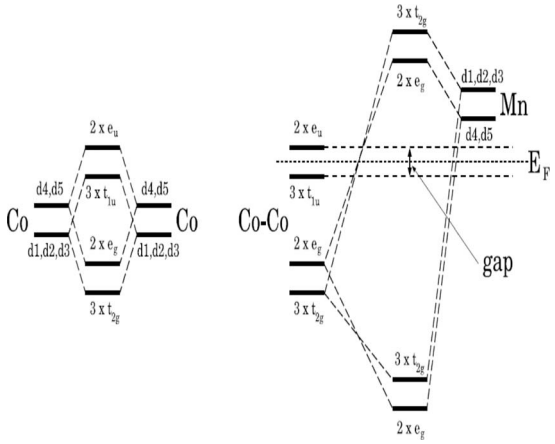

FIG. 27. Schematic illustration of the gap formation in Co_2MnZ compounds with Z=Al,Si,Ge,Sn (Galanakis *et al.*, 2006).

NQP states dominate in the depolarization of this class of Heusler compounds, while spin-orbit contributions are much smaller. In addition, many-body effects are more pronounced in FeMnSb than in NiMnSb. This is connected with the larger DOS in the majority spin channel in the former material. Therefore, doping of NiMnSb by Fe could be an interesting issue to investigate the interplay between alloying and many-body effects. The LDA+DMFT calculations for the NiMnSb supercell containing 25% Fe impurities show a half-metallic character at the LDA level, with the same strong correlation-induced depolarization effects as in pure FeMnSb. Therefore, many-body effects for this material are of primary importance even in the presence of disorder. Correlation effects on surfaces of half metals were discussed recently, and it was shown that these states can be probed both directly and via their effect on surface states (Irkhin and Katsnelson, 2006).

4. Co_2MnSi: A full-Heusler ferromagnet

The origin of the minority band gap in full Heuslers was discussed by Galanakis *et al.* (Galanakis *et al.*, 2006; Galanakis and Mavropoulos, 2007). Based on the analysis of the band-structure calculations, it was shown that the 3*d* orbitals of Co atoms from the two different sublattices, $Co^1(0,0,0)$ and $Co^2(1/2,1/2,1/2)$, couple and form bonding hybrids $Co^1(t_{2g}/e_g)$-$Co^2(t_{2g}/e_g)$. In other words, the t_{2g}/e_g orbitals of one of the Co atoms can couple only with the t_{2g}/e_g orbitals of the other Co atom. Furthermore, the Co-Co hybrid bonding orbitals hybridize with the Mn(d)-t_{2g},e_g manifold, while the Co-Co hybrid antibonding orbitals remain uncoupled owing to their symmetry. The Co-Co hybrid antibonding t_{2g} is situated below the Fermi energy E_F and the Co-Co hybrid antibonding e_g is unoccupied and lies just above the Fermi level. Thus, due to the missing Mn(d)-t_{2g},e_g and Co-Co hybrid antibonding hybridization, the Fermi energy is situated within the minority gap formed by the triply degenerate Co-Co antibonding t_{2g} and the doubly degenerate Co-Co antibonding e_g (see Fig. 27).

Figure 28 shows the results of DOS calculations using the LDA and LDA+DMFT schemes. The inset presents the spin polarization $P(E_F)=[N_\uparrow(E_F)-N_\downarrow(E_F)]/[N_\uparrow(E_F)+N_\downarrow(E_F)]$. One can see that in the minority spin channel asymmetric NQP states are formed, while in the majority a spectral weight redistribution takes place, which contributes to the depolarization. Contrary to the FeMnSb (Chioncel, Arrigoni, Katsnelson, *et al.*, 2006), where the density of NQP states shows a rather strong temperature dependence, in the full-Heusler Co_2MnSi the temperature dependence is not so significant, similar

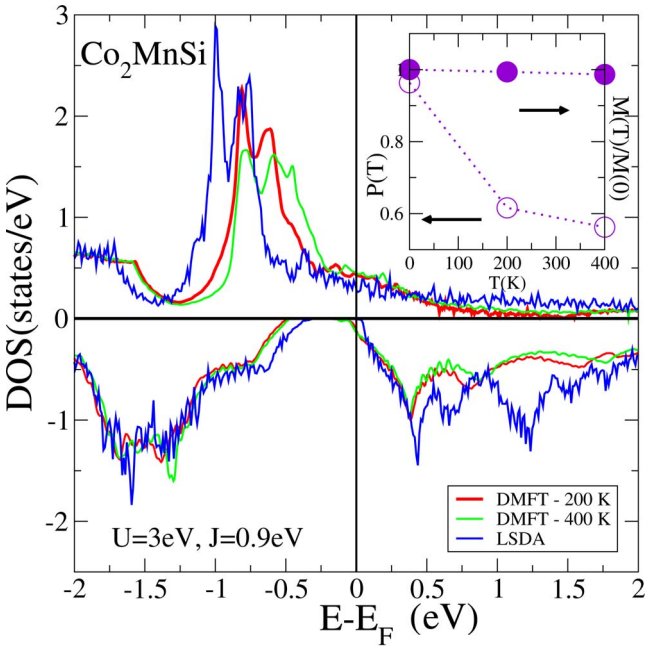

FIG. 28. (Color online) Total density of states of Co_2MnSi full-Heusler alloy. Notice that the gap is formed between the occupied Co-Co antibonding t_{2g} orbitals and empty Co-Co antibonding e_g orbitals. The LDA+DMFT results are presented as well for U=3 eV, J=0.9 eV, and different temperatures. The inset shows the finite-temperature spin polarization.

to the result obtained for NiMnSb (Chioncel, Katsnelson, de Groot, *et al.*, 2003).

B. Half-metallic materials with zinc-blende structure

One of the strongest motivations to investigate magnetic semiconductors and half-metallic ferromagnets is the possibility to design and produce stable structures on semiconducting substrates with interesting properties. From this point of view, first-principles studies are an excellent starting point to predict new systems having the desired properties. Using the full-potential density-functional method, all 3*d* transition metal pnictides and chalcogenides with wurtzite structure were investigated systematically by Xie, Liu, and Pettifor (2003) in order to find half-metallic ferromagnets. These can be fabricated as thin films with large thickness for real spintronic applications. Nine of the wurtzite phases (MnSb, CrAs, CrSb, VAs, VSb, CrSe, CrTe, VSe, and VTe) were found to be robust half-metallic ferromagnets with large half-metallic gaps (0.2–1 eV). Being compatible with the III-V and II-VI semiconductors, these half-metallic ferromagnetic phases, when realized experimentally, would be useful in spintronic and other applications. At the same time, zinc-blende (ZB) phases of MnAs, CrAs, and CrSb have been fabricated successfully in the form of nanodots, ultrathin films, and multilayers, respectively. A study within density-functional theory (Liu, 2003) for the ZB predicted CrSb half-metallic ferromagnetism with a magnetic moment of $3.0\mu_B$ per formula.

1. CrAs: Tunable spin transport

Akinaga *et al.* (2000) have found the possibility to fabricate ZB-type CrAs half-metallic ferromagnetic material. Experimental data confirmed that this material is ferromagnetic with the magnetic moment of $3\mu_B$, in agreement with theoretical predictions (Akinaga *et al.*, 2000). According to this calculation, this half-metallic material has a gap of about 1.8 eV in the minority spin channel, which has attracted much attention to this potential candidate for spintronic applications, keeping in mind also its high Curie temperature T_C about 400 K. Recent experiments on CrAs epilayers grown on GaAs(001) evidenced an orthorhombic structure, different from the ZB one, so the structure is rather sensitive to the preparation process (Etgens *et al.*, 2004). However, it is highly desirable to explore the possibility of the existence of half-metallic ferromagnetism in materials that are compatible with practically important III-V and II-IV semiconductors. For this purpose, efforts have been made to investigate metastable ZB structures, such as CrAs (Akinaga *et al.*, 2000; Mizuguchi *et al.*, 2002).

It is interesting to explore the mechanisms of half-metallic ferromagnetism at finite temperature from a realistic electronic-structure point of view. Theoretical studies (Shirai, 2003) of the 3*d* transition-metal monoarsenides have shown that the ferromagnetic phase of ZB structure CrAs compound should be more stable than the antiferromagnetic one. The many-body effects (see Fig. 29) are very sensitive to structural properties of the artificially produced CrAs compound (Chioncel *et al.*, 2005). Similar electronic-structure calculations concerning the stability of the half-metallic ferromagnetic state in the ZB structure have been carried out (Xie, Xu, Liu, *et al.*, 2003). The LDA+DMFT calculations were carried out for three lattice constants: the GaAs (5.65 Å), InAs (6.06 Å), and the equilibrium value (a_{eq}=5.8 Å) obtained by density-functional calculations (Shirai, 2003). The corresponding LDA computational results agree with previous ones (Akinaga *et al.*, 2000; Galanakis and Mavropoulos, 2003; Shirai, 2003). In order to evaluate the average Coulomb interaction on the Cr atoms and the corresponding exchange interactions, the constrained LDA method (Anisimov and Gunnarsson, 1991) was used by Chioncel *et al.* (2005), which yielded U=6.5 eV and J=0.9 eV. It is important to note that the values of the average Coulomb interaction parameter decrease slightly going from the GaAs (U=6.6 eV) to InAs (U=6.25 eV) lattice constants (Chioncel *et al.*, 2005), which is in agreement with a naive picture of a less effective screening due to increasing the distances between atoms.

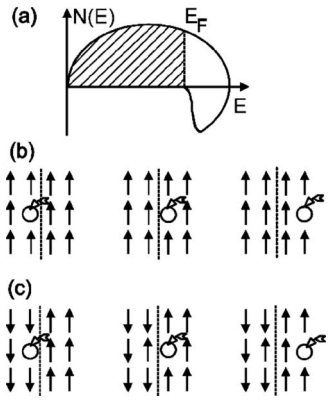

FIG. 29. The tunneling transport between strongly correlated ferromagnets. (a) The density of states in the lower Hubbard band is provided by standard current states for majority-spin electrons (above) and by nonquasiparticle states for minority-spin electrons (below), the latter contribution nonzero only above the Fermi energy (occupied states are shadowed). However, the tunneling is possible both for (b) parallel and (c) antiparallel magnetization directions (Chioncel *et al.*, 2005).

The typical insulating screening used in the constraint calculation (Anisimov and Gunnarsson, 1991) should be replaced by a metallic kind of screening. The metallic screening will lead to a smaller value of U. Since there are no reliable schemes to calculate U in metals, some intermediate values were chosen, U=2 eV and J=0.9 eV. It is important to realize that there are no significant changes in the values of the average Coulomb interaction for the lattice structures studied, the exchange interaction being practically constant. Note that the physical results are not very sensitive to the value of U, as was demonstrated for NiMnSb (Chioncel, Katsnelson, de Groot, *et al.*, 2003).

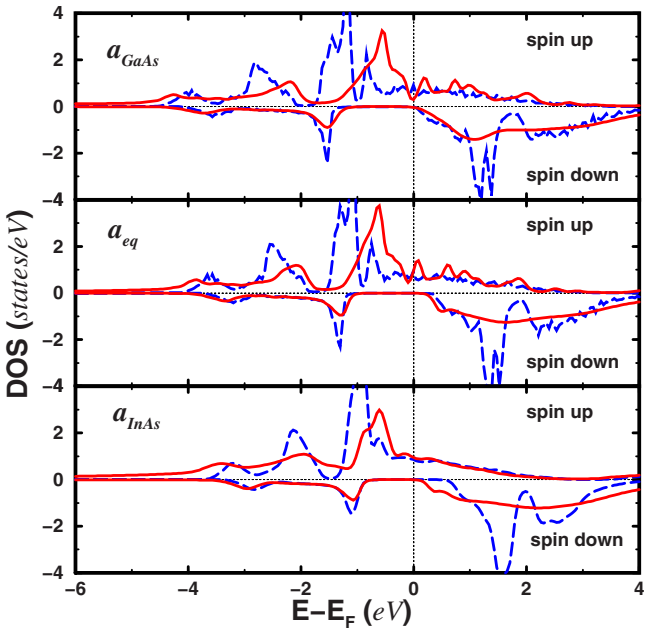

FIG. 30. (Color online) Cr density of states calculated in LSDA (dashed line) and LSDA+DMFT (solid line) methods corresponding to temperature $T=200$ K, average Coulomb interaction parameter $U=2$ eV, and exchange $J=0.9$ eV. The nonquasiparticle states are clearly visible for lattice parameters larger than $a_{eq}=5.8$ Å, in the unoccupied part for the minority-spin channel just above the Fermi level, around 0.5 eV (Chioncel *et al.*, 2005).

The LSDA and LSDA+DMFT calculation for the density of states, is presented in Fig. 30. Depending on the lattice constant, the Cr and As atoms lose electrons and this charge is gained by the vacant sites. As a result, the Fermi level is moved from the right edge of the gap (for the GaAs substrate) toward the middle of the gap (for the InAs substrate). The Cr moments are well localized due to a mechanism similar to localization of the magnetic moment on the Mn atom in NiMnSb (de Groot, Mueller, v. Engen, *et al.*, 1983). The local Cr spin moment is more than $3\mu_B$, and the As atom possesses a small induced magnetic moment (of order of $-0.3\mu_B$) coupled antiparallel to the Cr one. The results are presented in Table I. Cr magnetic moments calculated in DMFT increase in comparison with the LDA results due to the localization tendency of the Cr $3d$ states, which is a consequence of correlation effects.

According to the calculations of Chioncel *et al.* (2005), the system remains half metallic with a rather large band gap (about 1.8 eV) for all lattice constants compared with the band gap of the NiMnSb, which is only 0.75 eV (de Groot, Mueller, v. Engen, *et al.*, 1983). In Fig. 30, the nonquasiparticle states are visible for a lattice parameter higher than the equilibrium one, with a considerable spectral weight in the case of the InAs substrate. This situation is favorable for the experimental investigation of the NQP states.

Comparing the electronic structure of CrAs growing on InAs or GaAs substrates, we conclude that the most

TABLE I. Summary of the results of calculations (Chioncel *et al.*, 2005). CrAs magnetic moments corresponding to the GaAs, InAs, and the equilibrium lattice constant a_{eq}. For the latter one, the value $a_{eq}=5.8$ Å was used. Parameters of the DMFT calculations are presented in the last three columns (Chioncel *et al.*, 2005).

	Cr (μ_B)	As (μ_B)	E (μ_B)	$E1$ (μ_B)	Total (μ_B)	T (K)	U (eV)	J (eV)
μ_{LDA}^{GaAs}	3.191	−0.270	−0.009	0.089	3.00			
μ_{DMFT}^{GaAs}	3.224	−0.267	−0.023	0.067	3.00	200	2	0.9
μ_{LDA}^{eq}	3.284	−0.341	−0.018	0.076	3.00			
μ_{DMFT}^{eq}	3.290	−0.327	−0.024	0.068	3.00	200	2	0.9
μ_{LDA}^{InAs}	3.376	−0.416	−0.025	0.066	3.00			
μ_{DMFT}^{InAs}	3.430	−0.433	−0.033	0.043	3.00	200	2	0.9

significant change in the electronic structure is related with the As p states. Having a larger lattice constant in the case of InAs substrates, the Cr atom acquires a slightly larger magnetic moment. Nevertheless, in the LDA calculations the magnetic moment per unit cell is integer, $3\mu_B$. Expanding the lattice constant from the GaAs to the InAs lattice, the Cr states become more "atomic," and therefore the spin magnetic, moment increases. This is reflected equally in the charge transfer, which is smaller for the InAs lattice parameters. A larger Cr moment induces a large spin polarization of the As p states, compensating the smaller p-d hybridization, the total moment retaining its integer value of $3\mu_B$ (Galanakis and Mavropoulos, 2003).

The essential difference of the many-body electronic structure for the lattice constants of GaAs and InAs is due to the difference in the position of the Fermi energy with respect to the minority-spin band gap, whereas the self-energy characterizing the correlation effects is not changed much (Fig. 31). The total density of states $N(E)$ is rather sensitive to the difference between the band edge E_c and the Fermi energy E_F. If this difference is very small (i.e., the system is close to the electronic topological transition $E_c \to E_F$), one can use a simple expression for the singular contribution to the bare density of states, $\delta N_0(E) \propto \sqrt{E-E_c}$ $(E>E_c)$. The appearance of the complex self-energy $\Sigma(E)=\Sigma_1(E)-i\Sigma_2(E)$ changes the singular contribution as

$$\delta N(E) \propto [\sqrt{Z_1^2(E)+\Sigma_2^2(E)}+Z_1(E)]^{1/2}, \tag{197}$$

where $Z_1(E)=E-E_c-\Sigma_1(E)$ [cf. Katsnelson and Trefilov (1990)]. Assuming that the self-energy is small in comparison with $E-E_c$, one can find for the states in the gap $\delta N(E) \propto \Sigma_2(E)/\sqrt{E_c-E}$ $(E<E_c)$. One can see that the shift of the gap edge changes drastically the density of states for the same $\Sigma_2(E)$.

A practical use of tunable properties of NQP states in CrAs grown on different substrates is possible. For most applications, room temperature and the stability of the ferromagnetic state are important prerequisites. The ferromagnetic CrAs might be grown on III-V semiconduc-

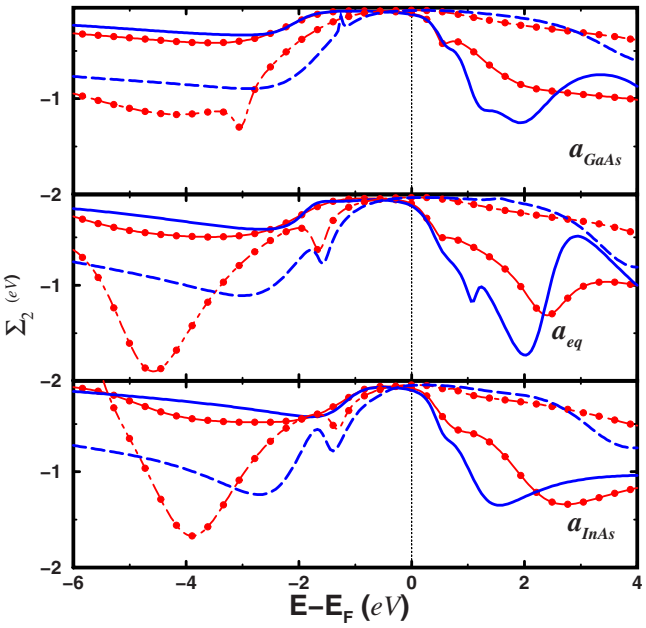

FIG. 31. (Color online) Energy dependences of imaginary parts of the electron self-energy $\Sigma_2(E)$, for lattice constants of GaAs, equilibrium, and InAs: e_g down solid line, t_{2g} down decorated solid line, e_g up dashed line, t_{2g} up decorated dashed line (Chioncel *et al.*, 2005).

tors similar to the zinc-blende CrSb (Zhao *et al.*, 2001). The presence of the NQP states was obtained by Chioncel *et al.* (2005) for CrAs lattice parameters larger than 5.8 Å. It was found experimentally that at 300 K, around this value of the lattice parameter, a stable solid solution of $Ga_{0.65}In_{0.35}As$ is formed (Harland and Woolley, 1966). Thus, from a practical point of view, 65% of gallium in a $Ga_xIn_{1-x}As$ compound would constitute the ideal substrate for the CrAs half metal. This could be a part of the epitaxial III-V structure providing an easy way to integrate with the existing semiconductor technology.

To determine possible substrates for growth of layered half-metallic materials, electronic-structure calculations were carried out for lattice parameters in the range 5.60–6.03 Å (Fong *et al.*, 2004). According to these calculations, growth with minimal strain might be accomplished in a half-metallic multilayer system grown on InAs substrate, which would be the best choice to evidence the NQP states, since the Fermi energy is situated in this case far enough from the bottom of the conduction band.

A high sensitivity of the minority-electron DOS near E_F to the lattice constant opens a new opportunity. Suppose we have an antiparallel orientation of the magnetizations in the CrAs-based tunnel junction [such as shown in Fig. 29(c)]. Then the $\mathcal{I}-V$ characteristic is determined by the density of the NQP states. Thus if we will influence the lattice constant (e.g., using a piezoelectric material), we can modify the differential conductivity. This makes CrAs a very promising material with tunable characteristics, which opens new ways for applications in spintronics.

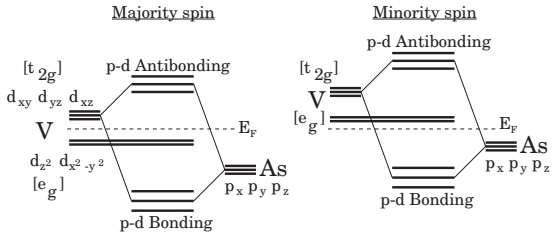

FIG. 32. Schematic representation of the *p-d* hybridization and bonding-antibonding splitting in VAs (Chioncel, Mavropoulos, Lezaic, *et al.*, 2006).

2. VAs: Correlation-induced half-metallic ferromagnetism?

Interesting materials for spintronics applications are ferromagnetic semiconductors (Nagaev, 1983; Ohno, 1998a, 1998b). Candidate systems are ordered compounds such as europium chalcogenides (e.g., EuO) and chromium spinels (e.g., $CdCr_2Se_4$) (Nagaev, 1983), as well as diluted magnetic semiconductors (e.g., $Ga_{1-x}Mn_xAs$) (Ohno, 1998a, 1998b). Unfortunately, all have Curie temperatures much lower than room temperature. On the other hand, VAs in the zinc-blende structure is, according to density-functional calculations (Galanakis and Mavropoulos, 2003), a ferromagnetic semiconductor with a high Curie temperature. Unlike CrAs (Akinaga *et al.*, 2000), CrSb (Zhao *et al.*, 2001), and MnAs (Okabayashi *et al.*, 2004), VAs has not yet been experimentally fabricated in the zinc-blende structure, but the increasing experimental activity in the field of the (structurally metastable) zinc-blende ferromagnetic compounds is promising in this respect.

The main result including many-body correlation effects is displayed in Fig. 33. While this material is expected to be a ferromagnetic semiconductor from density-functional theory (LSDA or GGA) or static LSDA+U calculations, the inclusion of dynamic Coulomb correlations within the LSDA+DMFT approach predicts a majority-spin band metallic behavior due to the closure of the gap (≈50 meV). However, since the minority-spin band gap (≃1 eV) remains finite, the material is found to be a half-metallic ferromagnet. To our knowledge, this is the first example in which dynamic correlations transform a semiconductor into a half-metal (Chioncel, Mavropoulos, Lezaic, *et al.*, 2006). This result demonstrates the relevance of many-body effects for spintronic materials.

Important features of the electronic structure of VAs (Galanakis and Mavropoulos, 2003) are shown schematically in Fig. 32. The t_{2g} states hybridize with the neighboring As p states, forming wide bonding and antibonding hybrid bands. In contrast, the e_g states form mainly nonbonding narrowbands. The Fermi level lies between e_g and antibonding t_{2g} states in the majority-spin bands, and between bonding t_{2g} and e_g in the minority-spin bands. The spin moment, concentrated mainly at the V atoms, is an integer of exactly $M=2\mu_B$ per unit formula, which is obvious from counting the occupied bands for two spin directions.

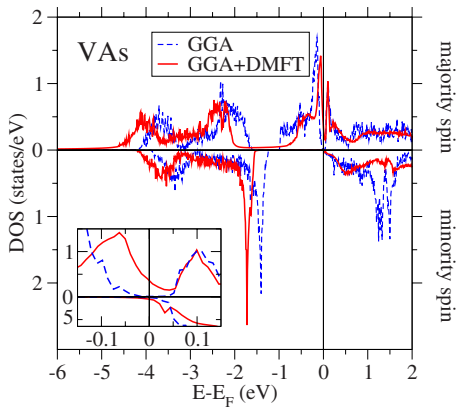

FIG. 33. (Color online) DOS of VAs within the GGA (dashed blue line) and GGA+DMFT (solid red line) for temperature $T=200$ K, $U=2$ eV, and $J=0.9$ eV. Inset: Focus around E_F showing the semiconducting gap within the GGA. To illustrate the minority-spin NQP states, a ten times larger scale for the spin down channel is used (Chioncel, Mavropoulos, Lezaic, *et al.*, 2006).

The exchange constants of VAs were calculated within the GGA and the adiabatic spin dynamics approach, similar to the one used by Halilov *et al.* (1998). Using these exchange parameters in a Monte Carlo simulation of the corresponding classical Heisenberg Hamiltonian yields a Curie temperature $T_C=820$ K (Chioncel, Mavropoulos, Lezaic, *et al.*, 2006) by the fourth-order cumulant crossing point. This result agrees with the value of $T_C=830$ K calculated by Sanyal *et al.* (2003) using a similar method. The high Curie point is well above room temperature, which makes VAs a promising candidate for applications in spintronics.

Static correlations were taken into account within the LDA+U method using similar values for the effective interaction parameters $U=2$ eV and $J=0.9$ eV, as in the case of Heusler alloys. This gives an estimation of correlation effects in VAs, since for an exact value of U one would need to perform a complicated analysis of screening effects in this compound (Aryasetiawan *et al.*, 2004; Kotliar *et al.*, 2006). The theoretically determined equilibrium lattice parameter, $a=5.69$ Å, and a broadening δ of about 15 K, which allows the majority spin gap to be clearly resolved, were used. For different lattice parameters (e.g., as for InAs) the LDA results agree with the previous ones (Galanakis and Mavropoulos, 2003; Sanyal *et al.*, 2003). The GGA DOS is shown in Fig. 33. The main difference in the GGA+U spectrum is that the occupied localized majority e_g states are expected to shift to even lower energy, while the unoccupied minority e_g states to higher energy. The semiconducting character does not change, since the e_g and t_{2g} bands remain separated for both spins; the majority-spin gap increases slightly, but remains small.

In order to investigate dynamic correlation effects in VAs, the fully self-consistent in spin, charge, and self-energy LSDA+DMFT scheme (Chioncel, Katsnelson, de Groot, *et al.*, 2003; Chioncel, Vitos, Abrikosov, *et al.*, 2003; Chioncel *et al.*, 2005) was used. Computational results for the DFT in the GGA approximation and LDA+DMFT densities of states are presented in Fig. 33. The nonquasiparticle states in the minority spin band are visible just above the Fermi level (inset), also predicted by previous calculations (Chioncel, Katsnelson, de Groot, *et al.*, 2003; Chioncel *et al.*, 2005). The weak spectral weight of NQP states is due to the fact that the Fermi level is close to the right edge of the minority-spin gap, as discussed for CrAs having a similar structure (Chioncel *et al.*, 2005). The local spin moments at V atoms do not change significantly (by less than 5%). However, in the case of VAs, another correlation effect appears: the small majority-spin gap at E_F closes, making the material half metallic (Chioncel, Mavropoulos, Lezaic, *et al.*, 2006).

In order to investigate the mechanism of the gap closing for the majority-spin channel, the behavior of the electron self-energy has been investigated (Chioncel, Mavropoulos, Lezaic, *et al.*, 2006). For the majority spin, $\mathrm{Im}\,\Sigma_\uparrow(E)\sim(E-E_F)^2$, which indicates Fermi-liquid behavior, as opposed to $\mathrm{Im}\,\Sigma_\downarrow(E)$, which shows a suppression around E_F due to the band gap, as well as a peculiar behavior for $E>E_F$ related to the existence of NQP states.

From the Dyson equation (166), one can see that the real part $\mathrm{Re}\,\Sigma_\sigma(E)$ causes a shift of the LDA energy levels. Therefore, due to the nonzero $\Sigma_\uparrow^{e_g}$, the e_g orbitals in the close vicinity of the Fermi level are pushed closer to E_F. This renormalization is connected with the large absolute value of $\mathrm{Re}(\partial\Sigma/\partial E)_{E_F}<0$. This causes occupied levels to be shifted to higher energy and unoccupied levels to lower energy. Note that this effect is completely opposite to the LDA+U results discussed above. In addition to this shift, the e_g peak is broadened by correlations, its tail reaching over the Fermi level (Fig. 33, inset). Thus the finite-temperature LDA+DMFT calculations demonstrate the closure of the narrow gap in the spin-up channel, which is produced by the correlation-induced Fermi-liquid renormalization and spectral broadening. At the same time, NQP states appear for the minority-spin channel just above E_F.

The slope of the majority-spin self-energy is almost a constant as a function of temperature at low T: $\mathrm{Re}(\partial\Sigma_\uparrow/\partial E)_{E_F}\simeq-0.4$ between 200 and 500 K. The quasiparticle weight, which measures the overlap of the quasiparticle wave function with the original one-electron one for the same quantum numbers, is $Z=(1-\partial\,\mathrm{Re}\,\Sigma_\uparrow/\partial E)^{-1}\simeq0.7$. As a consequence, the closure of the gap in the majority channel is a quantum effect originating from the multiorbital nature of the local Coulomb interaction (energy states are shifted toward E_F) rather than an effect of temperature. A similar gap closure is obtained for larger values of U, namely, $U=4$ and 6 eV, although the latter values should be taken with some caution in the FLEX calculation, which is in principle appropriate only in weak to intermediate coupling. As a general tendency, increasing $U^*=U-J$ produces a stronger Fermi-liquid renormalization in the majority-

spin channel, the same effect being evidenced for $J=0$.

On the one hand, density-functional theory calculations within the GGA (Chioncel, Mavropoulos, Lezaic, *et al.*, 2006) predict this material to be a ferromagnetic semiconductor with a tiny gap of about 50 meV in the majority-spin states and a large gap of the order of 1 eV for minority-spin states. Quantum effects, such as spin and orbital fluctuations, described by LDA+DMFT destroy the narrow gap and turn the material into a half-metallic ferromagnet.

On the other hand, several other mechanisms could contribute to the band-gap narrowing with increasing temperature. A well studied example is electron-phonon interaction. In another semiconductor with the zinc-blende structure, GaAs, it amounts to 50 meV at 200 K (Paessler, 1999). Also spin-orbit coupling can be essential when considering closing of the gap.

The LDA-GGA calculation supplemented by a Monte Carlo simulation also predicts a high Curie temperature of 830 K (Sanyal *et al.*, 2003), which makes this material of interest for technological applications. One can expect that T_C is not strongly affected by dynamical correlation, for the same reason as the effective exchange interaction parameters [see works of Katsnelson and Lichtenstein (2002)].

The revealed half-metallic (instead of semiconducting) behavior has important consequences in the potential applications of VAs in spintronics. In contrast to all semiconductor-based spin-injection devices (Zutic *et al.*, 2004) that avoid the resistivity mismatch problem, half metals can be applied to obtain giant magnetoresistance or, provided that interface states are eliminated (Mavropoulos *et al.*, 2005), tunneling magnetoresistance effects. We see that correlation effects play a decisive role in the prediction of new spintronic materials. The metallic nature of the majority spin channel would be visible in resistivity measurements. Therefore, the experimental realization of zinc-blende VAs would provide a test of this prediction. Further research should address the stability issue of the half-metallic ferromagnetic state in a zinc-blende structure. Some work in this direction has already been done (Shirai, 2003; Xie, Xu, Liu, *et al.*, 2003).

C. Half-metallic transition-metal oxides

1. CrO_2: A rutile structure half-metallic ferromagnet

Chromium dioxide CrO_2 has a rutile structure with $a=4.421$ Å, $c=2.916$ Å ($c/a=0.65958$), and internal parameter $u=0.3053$. (Porta *et al.*, 1972). The Cr atoms form a body-center tetragonal lattice and are surrounded by a slightly distorted octahedron of oxygen atoms. The space group of this compound is nonsymmorphic ($P4_2/mnm=D_{4h}^{14}$). The Cr ions are in the center of CrO_6 octahedra, so that the $3d$ orbitals are split into a t_{2g} triplet and an excited e_g doublet. The e_g states with only two valence $3d$ electrons are irrelevant, and only the t_{2g} orbitals are to be considered. The tetragonal symmetry distorts the octahedra, which lifts the degeneracy

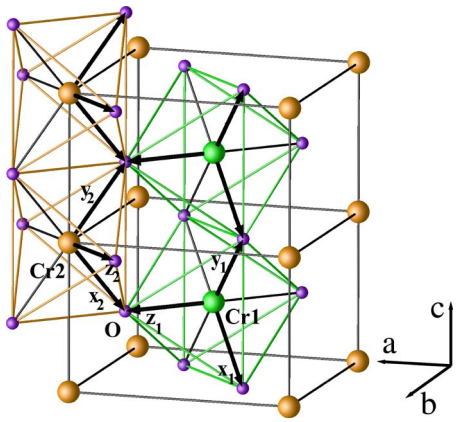

FIG. 34. (Color online) CrO_2 (rutile) structure. Cr1 (green) and Cr2 (orange) are located at (0, 0, 0) and $(\frac{1}{2},\frac{1}{2},\frac{1}{2})$. Cr atoms are octahedrally coordinated by oxygen atoms (purple). The local coordinate system is used for each Cr atom; $\hat{\mathbf{x}}_1=-\frac{1}{2}\hat{\mathbf{a}}+\frac{1}{2}\hat{\mathbf{b}}-\frac{1}{\sqrt{2}}\hat{\mathbf{c}}$, $\hat{\mathbf{y}}_1=-\frac{1}{2}\hat{\mathbf{a}}+\frac{1}{2}\hat{\mathbf{b}}+\frac{1}{\sqrt{2}}\hat{\mathbf{c}}$, $\hat{\mathbf{z}}_1=\frac{1}{\sqrt{2}}\hat{\mathbf{a}}+\frac{1}{\sqrt{2}}\hat{\mathbf{b}}$, and $\hat{\mathbf{x}}_2=-\frac{1}{2}\hat{\mathbf{a}}-\frac{1}{2}\hat{\mathbf{b}}-\frac{1}{\sqrt{2}}\hat{\mathbf{c}}$, $\hat{\mathbf{y}}_2=-\frac{1}{2}\hat{\mathbf{a}}-\frac{1}{2}\hat{\mathbf{b}}+\frac{1}{\sqrt{2}}\hat{\mathbf{c}}$, $\hat{\mathbf{z}}_2=-\frac{1}{\sqrt{2}}\hat{\mathbf{a}}+\frac{1}{\sqrt{2}}\hat{\mathbf{b}}$. $\hat{\mathbf{x}}_{1,2}$ and $\hat{\mathbf{y}}_{1,2}$ approximately point to O atom, and $\hat{\mathbf{z}}_{1,2}$ exactly point to O atom. The local axes are transformed into each other by a 90° rotation around the crystal c axis (Yamasaki *et al.*, 2006).

of the t_{2g} orbitals into a d_{xy} ground state and d_{yz+zx} and d_{yz-zx} excited states (Lewis *et al.*, 1997; Korotin *et al.*, 1998) (see Fig. 34; a local coordinate system is used for every octahedron). A double exchange mechanism for two electrons per Cr site has been proposed (Schlottmann, 2003). According to this, the strong Hund rule together with the distortion of CrO_6 octahedra leads to localization of one electron in the d_{xy} orbital, while the electrons in the d_{yz} and d_{xz} are itinerant.

Measurements of the magnetic susceptibility in the paramagnetic phase show a Curie-Weiss-like behavior indicating the presence of local moments (Chamberland, 1977), which suggests a mechanism of ferromagnetism beyond the standard band or Stoner-like model.

Several recent experimental investigations of photoemission (Tsujioka, 1997), soft-x-ray absorption (Stagarescu *et al.*, 2000), resistivity (Suzuki and Tedrow, 1998), and optics (Singley *et al.*, 1999) suggest that electron correlations are essential for the underlying physical picture in CrO_2. Schwarz (1986) first predicted the half-metallic band structure with a spin moment of $2\mu_B$ per formula unit for CrO_2. Lewis *et al.* (1997) used the plane-wave potential method and investigated the energy bands and transport properties, characterizing CrO_2 as a "bad metal" (a terminology applied earlier to high-temperature superconductors and to other transition-metal oxides, even ferromagnets like $SrRuO_3$). A decade later, the LSDA+U calculation (Korotin *et al.*, 1998) treated conductivity in the presence of large on-site Coulomb interactions and described CrO_2 as a negative charge-transfer gap material with self-doping. Contrary to the on-site strong correlation description, transport and optical properties obtained within the FLAPW method (LSDA and GGA) (Mazin *et al.*, 1999)

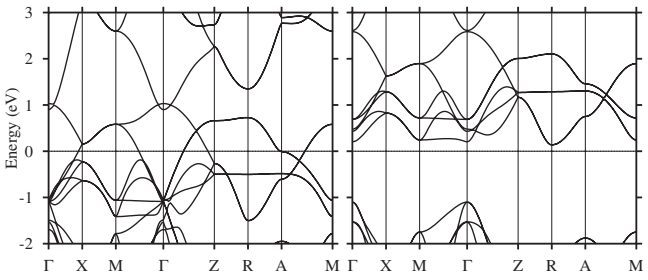

FIG. 35. Full basis-set spin-polarized (ferromagnetic) bands for CrO_2; majority spin (left) and minority spin (right). E_F is set to zero. The high-symmetry points are $\Gamma(0,0,0)$, $X(0,\frac{1}{2},0)$, $M(\frac{1}{2},\frac{1}{2},0)$, $Z(0,0,\frac{1}{2})$, $R(0,\frac{1}{2},\frac{1}{2})$, and $A(\frac{1}{2},\frac{1}{2},\frac{1}{2})$ (Yamasaki *et al.*, 2006).

suggested that the electron-magnon scattering is responsible for the renormalization of one-electron bands. More recent model calculations (Laad *et al.*, 2001; Craco *et al.*, 2003) propose even orbital correlations.

Chemical bonding in rutile-type compounds including CrO_2 has been analyzed by Sorantin and Schwarz (1992). One can see that around the Fermi level, the bands are primarily chromium $3d$ states of t_{2g} manifold, with e_g bands being situated higher in energy due to the crystal-field splitting. In the spin-polarized case, the exchange splitting shifts the minority spin d bands above the Fermi level (Fig. 35). For the majority t_{2g} bands, the Fermi level lies in a pseudogap. Oxygen $p-$ chromium d hybridization creates both bonding and antibonding hybrid orbitals, with the bonding orbital appearing in the occupied part and the antibonding hybrid orbital remaining in the Cr t_{2g} manifold. Half of the d_{yz} and d_{zx} components of t_{2g} are pushed upward by antibonding, which explains the d_{xy} dominance in the spin density. The nonmagnetic DOS shows a sharp peak at the Fermi level, which signals the magnetic instability according to the usual Stoner argument.

Although there is a significant difference between the t_{2g} and e_g orbitals (Schwarz, 1986; Sorantin and Schwarz, 1992; Korotin *et al.*, 1998; Mazin *et al.*, 1999), the analysis in the framework of the NMTO technique (Andersen and Saha-Dasgupta, 2000; Zurek *et al.*, 2005) shows that their interplay is important not only for the crystal-field splitting of t_{2g} states, but also for the general bonding in the rutile structure. The t_{2g} orbitals form the basis set used by Yamasaki *et al.* (2006) to evaluate the effective hopping Hamiltonian matrix elements.

In CrO_2, the bands around the Fermi level are primarily chromium $3d$ states of t_{2g} manifold, e_g bands occuring higher in energy due to the crystal-field splitting. The t_{2g} orbitals are further split into single d_{xy} and nearly degenerate $d_{yz\pm zx}$ bands due to the orthorhombic distortion of CrO_6 octahedra. Despite the differences between Cr t_{2g}-e_g orbitals, their interaction plays an important role not only in characterizing the crystal-field splitting, but also in the general picture of bonding in the rutile structure.

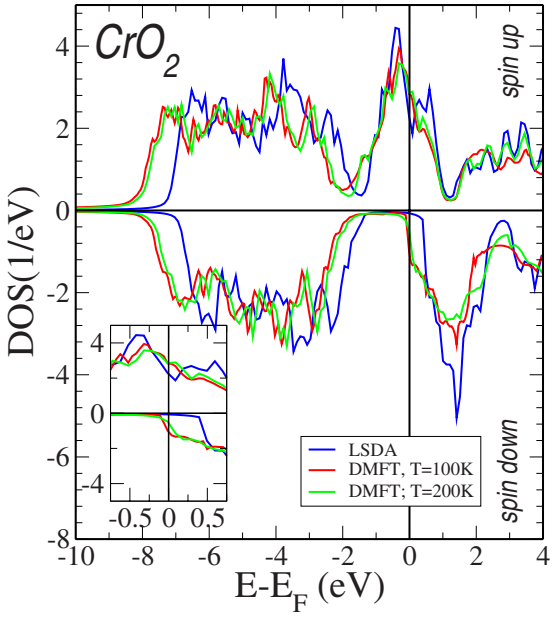

FIG. 36. (Color online) Density of states obtained within the LSDA and LSDA+DMFT calculations for different temperatures. The inset shows the results for a smaller energy window around the Fermi level (Chioncel *et al.*, 2007).

Concerning the Coulomb interaction U in CrO_2, the higher energy e_g bands, although making no noticeable contribution at the Fermi level, participate in the screening of the t_{2g} orbitals (Solovyev *et al.*, 1996; Pickett *et al.*, 1998), thereby giving the values $U=3$ eV and $J=0.87$ eV.

Previous LSDA+U (Korotin *et al.*, 1998; Toropova *et al.*, 2005) and DMFT (Laad *et al.*, 2001; Craco *et al.*, 2003) studies yielded independently a narrow almost flat band of d_{xy} character, which produces ferromagnetism in CrO_2. In contrast to these results, the fully self-consistent LSDA+DMFT (Chioncel *et al.*, 2007) yields, in agreement with a nonlocal variational cluster approach (Chioncel *et al.*, 2007), an itinerant d_{xy} orbital that crosses the Fermi level. Despite the nonlocalized character of the orbital, a ferromagnetic phase is obtained.

Results of the LSDA+DMFT calculation are presented in Fig. 36 for two different values of T and compared with the LSDA results. The LSDA Fermi level intersects the majority-spin bands near a local minimum and lies in the band gap of the minority spin. Finite temperatures and correlation effects close this pseudogap around the Fermi level, as can be seen from the LDA+DMFT results in Fig. 36. No differences can be observed between the two DMFT results at different temperatures, except for the smearing of DOS features at larger temperature. For both spin channels, the DOS is shifted uniformly to lower energies in the energy range −2 to −6 eV, where predominantly the O(p) bands are situated. This is due to the Cr(d) bands, which affect the O(p) states through the Cr(d)-O(p) hybridization, so

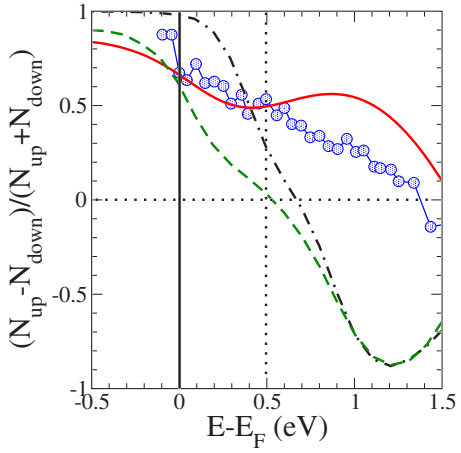

FIG. 37. (Color online) Energy dependence for the spin polarization of CrO_2. Experimental measurement (blue scattered line) (Huang *et al.*, 2003), LSDA calculation (black dot-dashed), DMFT (green dashed), and nonlocal variational approach (red solid line) (Chioncel *et al.*, 2007).

that O(p) states contribute actively to the ferromagnetic ground-state formation.

Figure 37 presents the experimentally measured spin polarization (Huang *et al.*, 2003) in comparison with the theoretical calculations within the LSDA and finite-temperature LDA+DMFT (T=200 K) (Chioncel, 2006). Resonant x-ray emission spectroscopy (Kurmaev *et al.*, 2003) showed the existence of nearly currentless minority spin states in the vicinity of the Fermi level, which can be connected to the nonquasiparticle states (Sec. III.J). As described in Secs. IV.A and V, the electronic structure of several half-metallic ferromagnets reveals the existence of such NQP states, which are important for description of spin polarization near the Fermi level. The LSDA+DMFT description, however, is not sufficient to capture the high-energy tail of the experimental spin polarization. This can be related to an improper description of unoccupied Cr e_g orbitals in the LSDA, and probably also to nonlocal exchange effects, which can be investigated within a cluster DMFT scheme (Kotliar *et al.*, 2006).

The NQP states occur around 0.25 eV in the spin-down channel. At zero temperature, the variational cluster results (Chioncel *et al.*, 2007) yield states in the minority channel that are actually far from E_F, but have a tail vanishing at E_F. This is in agreement with low-temperature experiments (Soulen *et al.*, 1998; Ji *et al.*, 2001) that support very high polarization of CrO_2.

The effects of local and nonlocal electronic correlations in CrO_2 (Chioncel *et al.*, 2007) change considerably the mean-field LSDA+U picture, despite the interaction is not too strong. In particular, in LSDA+U the single occupancy of the Cr d_{xy} orbital is determined by the exchange and crystal-field splitting. On the other hand, the competition of the latter with correlation effects, which is taken into account in the DMFT and variational cluster perturbation theory calculations, induces a ferromagnetic state with itinerant-type d_{xy} orbitals possessing a large effective mass rather than with localized moments, in contrast to previous results (Korotin *et al.*, 1998; Laad *et al.*, 2001; Craco *et al.*, 2003; Toropova *et al.*, 2005). In the minority-spin channel, correlations induce NQP states that are crucial for the occurrence of spin depolarization in CrO_2. However, a quantitative analysis of the depolarization requires the inclusion of additional effects, e.g., disorder or phonons (Sec. III.C).

VI. EXCHANGE INTERACTIONS AND CRITICAL TEMPERATURES IN HALF-METALLIC COMPOUNDS

Owing to the strong interest in the half-metallic ferromagnetism, the number of theoretical studies of exchange interactions and calculations of Curie temperatures in Heusler alloys has been drastically increased [see, e.g., Zhang *et al.* (2007)]. The first investigation of exchange interactions in half metals within the DFT formalism was by Kübler (Kübler *et al.*, 1983). The mechanisms of ferromagnetism in Heusler alloys were discussed on the basis of total-energy calculations for the ferro- and antiferromagnetic configurations. Since the antiferromagnetic state of the system is not half metallic, such an estimation gives only crude values of exchange parameters in HMFs. Therefore, a more precise evaluation of the exchange interactions from the first-principles theory is required. In this section, we present the real-space Green's function and frozen-magnon techniques to calculate the exchange parameters, and their applications to full-Heusler, semi-Heusler, and zinc-blende half metals.

A. The Green's function formalism

Within the first-principles Green's function approach, the exchange parameters (Liechtenstein *et al.*, 1987) are obtained by mapping the second variation of electronic band energy to the classical Heisenberg Hamiltonian and making use of the magnetic version of Andersen's local force theorem (Mackintosh and Andersen, 1980),

$$H_{\text{eff}} = -\sum_{\mu,\nu}\sum_{\mathbf{R}\mathbf{R}'} J^{\mu,\nu}_{\mathbf{R}\mathbf{R}'}\mathbf{s}^{\mu}_{\mathbf{R}}\mathbf{s}^{\nu}_{\mathbf{R}'}. \tag{198}$$

In Eq. (198), the indices μ and ν mark different sublattices, $\mathbf{R}$ and $\mathbf{R}'$ are the lattice vectors specifying the atoms within a sublattice, and $\mathbf{s}^{\mu}_{\mathbf{R}}$ is the unit vector in the direction of the magnetic moment. By introducing the generalized notation for site (i=μ,$\mathbf{R}$), a simple and transparent expression for the exchange interaction parameters is obtained in the following form (Liechtenstein *et al.*, 1987):

$$J_{ij} = \frac{1}{4\pi}\int_{-\infty}^{E_F} d\epsilon\, \mathrm{Im}\, \mathrm{Tr}_L\{\Delta_i G^{\uparrow}_{ij}\Delta_j G^{\downarrow}_{ji}\}, \tag{199}$$

where G^{σ}_{ij} is the real-space Green's function and Δ_i is the local exchange splitting for site i.

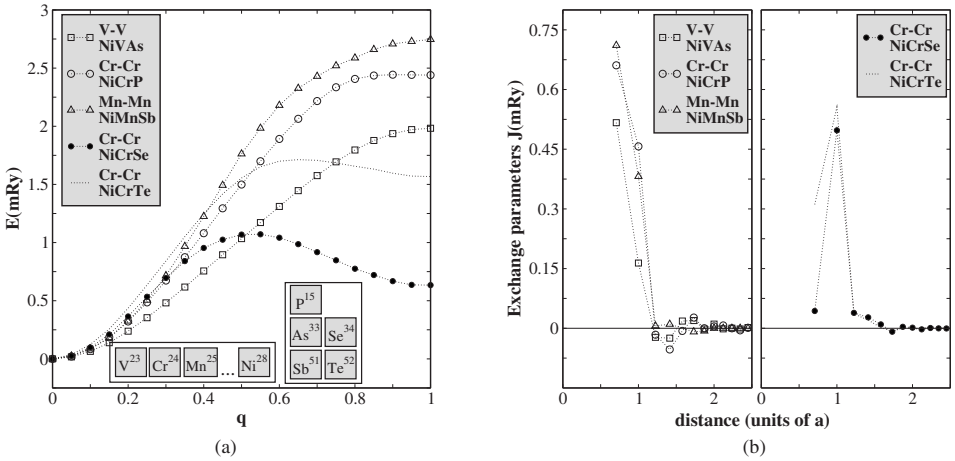

FIG. 38. (a) Frozen-magnon dispersion for NiCrZ (Z = P, Se, Te). (b) Interatomic exchange interactions (Sasioglu, Sandratskii, and Bruno, 2005).

B. The frozen-magnon approach and DFT calculations of spin spirals

The frozen-magnon approach is based on evaluation of the energy configurations defined by the following atomic polar and azimuthal angles:

$$\theta_{\mathbf{R}}^{\mu} = \theta; \quad \phi_{\mathbf{R}}^{\mu} = \mathbf{q}\cdot\mathbf{R} + \phi^{\mu}. \tag{200}$$

The angle θ defines the cone of the spin spiral, and the constant phase ϕ^{μ} is normally chosen to be zero. The magnetic moments of other sublattices are kept parallel to the z axis. Within the classical Heisenberg model (198), the energy of the spin-spiral configuration is

$$E^{\mu\mu}(\theta,\mathbf{q}) = E_0^{\mu\mu}(\theta) + J^{\mu\mu}(\mathbf{q})\sin^2\theta, \tag{201}$$

where $E_0^{\mu\mu}(\theta)$ does not depend on q and the Fourier transform $J^{\mu\mu}(\mathbf{q})$ is defined by

$$J^{\mu\nu}(\mathbf{q}) = \sum_{\mathbf{R}} J_{0\mathbf{R}}^{\mu\nu}\exp(i\mathbf{q}\cdot\mathbf{R}). \tag{202}$$

In the case in which $\nu=\mu$, the sum in Eq. (202) does not include the local interaction with $R=0$. Calculating $E^{\mu\mu}(\theta,\mathbf{q})$ for a regular $\mathbf{q}$-mesh in the Brillouin zone of the crystal and performing the inverse Fourier transformation, one gets exchange parameters $J_{0\mathbf{R}}^{\mu\mu}$ for sublattice μ.

The Curie temperature can be estimated within the mean-field approximation (MFA),

$$k_B T_C^{\mathrm{MFA}} = \frac{2}{3}\sum_{\mathbf{R}} J_{0\mathbf{R}}^{\mu\nu} = \frac{M}{6\mu_B}\frac{1}{N}\sum_{\mathbf{q}}\omega(\mathbf{q}), \tag{203}$$

and the random-phase approximation (RPA),

$$\frac{1}{k_B T_C^{\mathrm{RPA}}} = \frac{6\mu_B}{M}\frac{1}{N}\sum_{\mathbf{q}}\frac{1}{\omega(\mathbf{q})}, \tag{204}$$

with $\omega(\mathbf{q})$ the spin-wave dispersion, N the number of $\mathbf{q}$ points in the first Brillouin zone, and M the atomic magnetic moment. In the MFA, the Curie temperature is determined by the arithmetic average of the magnon energies, while in the RPA, T_C is determined by the harmonic average. Therefore, the value of T_C within the MFA is larger than the RPA one, the two values being equal only provided that the magnon spectrum is dispersionless.

C. First-principles calculations

1. Semi-Heusler $C1_b$ alloys

First-principles studies of exchange interactions and magnetic phase transitions for NiCrZ (Z=P, Se, Te), NiVAs, NiMnSb, and CoMnSb were carried out by many (Sasioglu, Sandratskii, and Bruno, 2005; Rusz *et al.*, 2006) In Fig. 38, the frozen-magnon dispersion and exchange interactions are presented (Sasioglu, Sandratskii, and Bruno, 2005). The exchange interactions are Fourier transforms of the frozen-magnon spectrum.

A remarkable feature of the exchange interactions is their short-range character, the Curie temperature determined by the interaction within the first two coordination spheres. The deviation from the collinear alignment of magnetic moments can also be characterized by magnon energies (Sandratskii, 1998; Sandratskii and Bruno, 2003). The deviation leads to the mixing of the majority and minority spin states, which makes half metallicity less favorable. A detailed discussion of different depolarization mechanisms is given in Sec. III.C.

2. Full-Heusler $L2_1$ alloys

Recently, studies of the interatomic exchange interactions in several full-Heusler compounds were reported by Kurtulus *et al.* (2005). Sasioglu *et al.* (2005) studied the exchange interactions in non-half-metallic Ni_2MnZ (Z=Ga, In, Sn, Sb) and half-metallic Mn_2VZ (Z=Al, Ge). The importance of the intersublattice exchange interactions has been demonstrated. For Mn_2VZ (Z=Al, Ge), it was shown that the ferrimagnetic coupling between the V and Mn moments stabilizes the ferromagnetic alignment of the Mn moments.

In Co_2MnZ (Z=Ga, Si, Ge, Sn), the presence of Co atoms makes the interaction more complicated (Kurtulus *et al.*, 2005). The interaction between Co atoms in the same sublattice, Co1(2)-Co1(2), and between Co atoms at different sublattices, Co1(2)-Co2(1), has to be taken into account. This approach gives results that go beyond

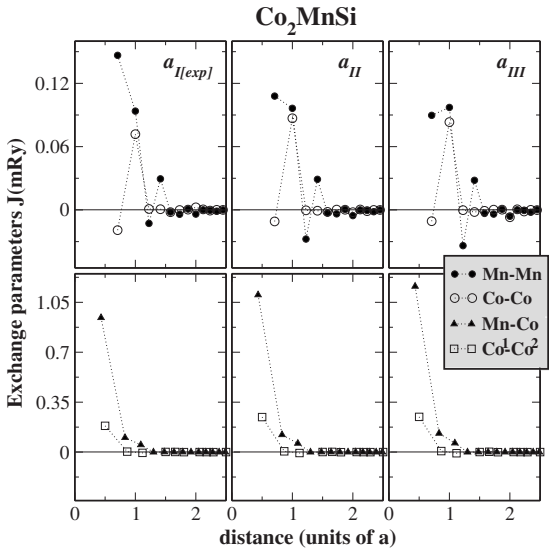

FIG. 39. Exchange constants for Co_2MnSi as a function of interatomic distance (Sasioglu, Sandratskii, and Bruno, *et al.*, 2005).

the initial approach of Kübler (Kübler *et al.*, 1983). From the J_{ij} values, it is clear that the exchange interactions are relatively short ranged and do not exceed the first four neighbors in each sublattice. The main exchange parameter corresponds to the nearest-neighbor Co(1)-Mn interaction. This already gives 70% of the total contribution to J and is about ten times larger than the Co-Co and Mn-Mn interactions (Kurtulus *et al.*, 2005). Thus, it was concluded that the Co-Mn interactions are responsible for the stability of ferromagnetism (see Fig. 39).

3. Zinc-blende half-metals

Besides the large number of results on the electronic properties of zinc-blende half metals, the exchange interactions constitute an important aspect to understand the stability of half metallicity in these structures. Shirai (2003) obtained that in VAs, CrAs and MnAs ferromagnetism is energetically favorable in comparison with the antiferromagnetic state, unlike FeAs, where an opposite effect was demonstrated. Sakuma (2002) predicted ferromagnetism in the isoelectronic MnSi, MnGe, and MnSn compounds. Similar to CrAs, the ferromagnetism in these systems is stabilized by short-range interactions (direct Mn-Mn and indirect through *sp* atoms), giving a Curie temperature of 1000 K (Sakuma, 2002). T_C for the VAs (CrAs and MnAs) was also calculated by Kübler (2003) yielding the same range of magnitudes. Using GaAs and InAs lattice constants, Sanyal *et al.* (2003) calculated T_C for the VAs CrAs and MnAs. Sasioglu, Galanakis, Sandratskii, *et al.* (2005) calculated the exchange parameters for a large number of pnictides.

MnC presents an interesting situation since its half-metallic gap is situated in the majority spin channel. The Curie temperature was found to be 500 K. Figure 40 represents the frozen-magnon energies for a selected direction in the Brillouin zone and the exchange constants. Ferromagnetism is stabilized by the direct Mn-Mn interactions and Mn-C ferromagnetic coupling. A remarkable feature of MnC is the small difference between the MFA and RPA values of T_C (Sasioglu, Galanakis, Sandratskii, *et al.*, 2005).

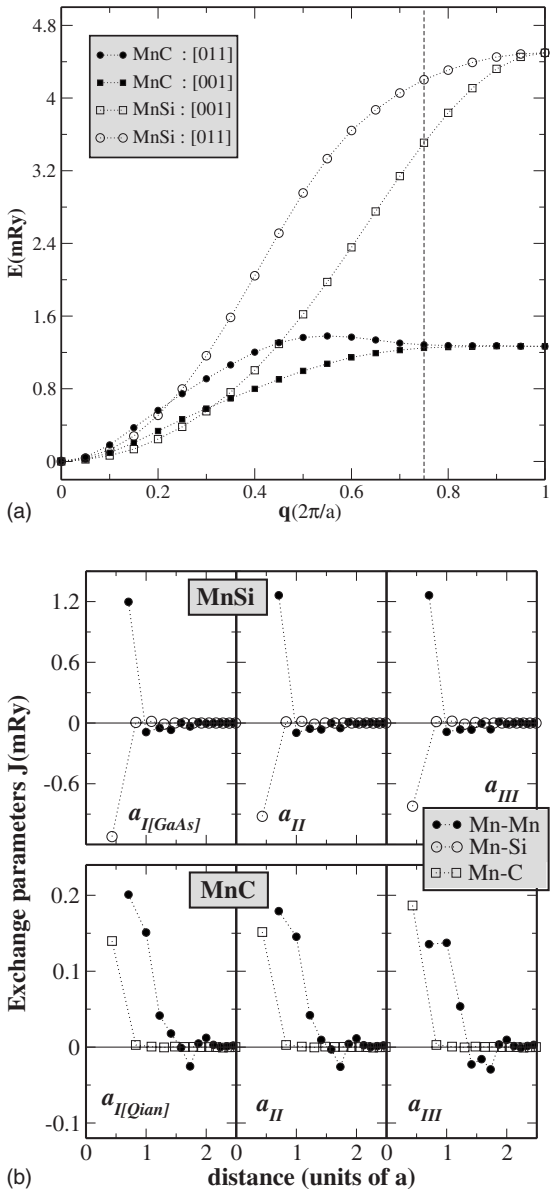

FIG. 40. Spin-wave spectrum and exchange interactions. Upper pannel: Frozen-magnon energies for MnC and MnSi in the $[00q]$ and $[0qq]$ directions. Vertical dotted line shows the Brillouin-zone boundary. Lower panel: Exchange constants as a function of interatomic distance (Sasioglu, Galanakis, Sandratskii, *et al.*, 2005).

VII. CONCLUSIONS

The idea of half-metallic ferromagnetism appeared as a result of band-structure calculations (de Groot, Mueller, v. Engen, *et al.*, 1983). For a long time, the dominant activity in this field was theoretical. Conceptually, HMFs

are of interest because they provide an opportunity to probe some essentially many-particle effects (Irkhin and Katsnelson, 1990). Whereas for a generic metallic system the Landau Fermi-liquid theory (Nozieres, 1964; Vonsovsky and Katsnelson, 1989) works, most correlation effects hidden in a parameter renormalization (such as effective mass, magnetic moment, etc.), in HMFs the spin-polaronic effects lead to a qualitatively new feature, namely, the occurrence of nonquasiparticle (incoherent) states in the energy gap for one of the spin projections near the Fermi level. On the contrary, similar effects for electron-magnon interactions in traditional itinerant-electron ferromagnets are mixed with other kinds of renormalization (e.g., electron-phonon, electron-electrons, etc.). The NQP states occur only above (below) E_F for a minority spin (majority-spin) gap. Therefore, HMFs are ideal objects to investigate the effects of electron-magnon interactions (Irkhin and Katsnelson, 1990).

An even stronger motivation to study HMFs is connected with the idea of using them in giant magnetoresistance and tunnel magnetoresistance (de Groot, Janner, and Mueller, 1983; Irkhin and Katsnelson, 1994; Prinz, 1998) devices. This initiated great theoretical activity in the field of heterostructures containing HMFs (Tkachov *et al.*, 2001; Irkhin and Katsnelson, 2002). At the same time, the interest in the search and prediction of new HMFs was growing on the basis of band-structure calculations, as well as attempts to better understand the features of electronic structure and chemical bonding, which are relevant for half metallicity (see Sec. V).

Recently, numerous attempts have been performed to build heterostructures with HMFs, such as Heusler alloys (Gercsi *et al.*, 2006; Sakuraba, Hattori, Oogane, *et al.* 2006; Sakuraba, Miyakoshi, Oogene, *et al.* 2006; Sakuraba *et al.*, 2007), CrO_2 (Miao *et al.*, 2006), and Fe_3O_4 (Rybchenko *et al.*, 2006; Zhao *et al.*, 2006). Therefore, the half metallicity predicted by electronic-structure calculations becomes practically applicable. Nevertheless, direct experimental evidence of half-metallic structure for specific compounds is still rather poor. Perhaps the unique method of testing genuine, bulk, half-metallic properties remains spin-resolved positron annihilation. This underexposed technique enables direct measurement of spin polarization in the bulk. Advanced techniques borrowed from semiconductor technologies that access spatially resolved spin polarization at the Fermi level would be interesting alternatives for positron annihilation. Although extensively used to characterize semiconductors, they are poorly known in the spintronics community.

Among other experiments expected to advance the field, we mention STM (Irkhin and Katsnelson, 2006), spin-polarized photoemission (Park *et al.*, 1998), and Andreev reflection (Soulen *et al.*, 1999). Investigations of the nuclear magnetic relaxation rate should be mentioned in particular since the absence of the Korringa relaxation is a clear sign of half metallicity (Irkhin and Katsnelson, 2001). NMR gives direct information on bulk properties that is not surface, sensitive. Also, the data of core-level spectroscopies, especially XMCD, would be very useful (see Sec. III.J). As for the band-structure calculations, application of state-of-art methods taking into account correlation effects, such as *GW* or DMFT (see Sec. IV.A), looks very promising. Another possible direction is the use of electron-structure calculations to search essentially new types of HMFs such as *sp* electron (or anionic) magnets (Attema *et al.*, 2005; Edwards and Katsnelson, 2006).

ACKNOWLEDGMENTS

We are grateful for enlightening discussions with O. K. Andersen, E. Arrigoni, V. Antonov, S. Blügel, P. Bruno, C. Carbone, P. H. Dederichs, P. A. Dowben, H. Ebert, D. M. Edwards, O. Eriksson, A. J. Freeman, P. Fulde, A. Georges, G. Kotliar, J. Kübler, Ph. Mavropoulos, I. I. Mazin, J. Minar, W. Nolting, W. E. Pickett, L. M. Sandratskii, G. Sawatzky, D. J. Singh, L. Vitos, D. Vollhardt, G. A. de Wijs, R. Wiesendanger, and A. Yamasaki. This work was supported by the Stichting voor Fundamenteel Onderzoek der Materie (FOM), the Netherlands, and by the Netherlands Organization for Scientific Research (Grant No. NWO 047.016.005). V.Yu.I. acknowledges support from the Russian Basic Research Foundation (Grant No. 4640.2006.2) and A.I.L. acknowledges support from the DFG (Grant No. SFB 668-A3). L.C. acknowledges financial support offered by the Austrian Science Foundation FWF Project No. P18505-N16 and the Romanian CNCSIS Project No. 96/2006.

REFERENCES

Abragam, A., 1961, *The Principles of Nuclear Magnetism* (Clarendon, Oxford).
Akinaga, H., T. Magano, and M. Shirai, 2000, Jpn. J. Appl. Phys., Part 2 **39**, L1118.
Almbladh, C.-O., U. V. Barth, and R. V. Leeuwen, 1999, Int. J. Mod. Phys. B **13**, 535.
Andersen, O. K., 1975, Phys. Rev. B **12**, 3060.
Andersen, O. K., and O. Jepsen, 1984, Phys. Rev. Lett. **53**, 2571.
Andersen, O. K., and T. Saha-Dasgupta, 2000, Phys. Rev. B **62**, R16219.
Anisimov, V. I., F. Aryasetiawan, and A. I. Lichtenstein, 1997, J. Phys.: Condens. Matter **9**, 767.
Anisimov, V. I., and O. Gunnarsson, 1991, Phys. Rev. B **43**, 7570.
Anisimov, V. I., A. I. Poteryaev, M. A. Korotin, A. O. Anokhin, and G. Kotliar, 1997, J. Phys.: Condens. Matter **9**, 7359.
Anisimov, V. I., I. V. Solovyev, M. A. Korotin, M. T. Czyżyk, and G. A. Sawatzky, 1993, Phys. Rev. B **48**, 16929.
Anokhin, A. O., and M. I. Katsnelson, 1996, Int. J. Mod. Phys. B **10**, 2468.
Antonov, V. N., V. P. Antropov, B. N. Harmon, A. N. Yaresko, and A. Y. Perlov, 1999, Phys. Rev. B **59**, 14552.
Antonov, V. N., P. M. Oppeneer, A. N. Yaresko, A. Y. Perlov, and T. Kraft, 1997, Phys. Rev. B **56**, 13012.

Aryasetiawan, F., M. Imada, A. Georges, G. Kotliar, S. Biermann, and A. I. Lichtenstein, 2004, Phys. Rev. B **70**, 195104.
Attema, J. J., G. de Wijs, G. R. Blake, and R. A. de Groot, 2005, J. Am. Chem. Soc. **127**, 16325.
Attema, J. J., G. A. de Wijs, and R. A. de Groot, 2006, J. Phys. D **39**, 793.
Attema, J. J., C. M. Fang, L. Chioncel, G. A. de Wijs, A. I. Lichtenstein, and R. A. de Groot, 2004, J. Phys.: Condens. Matter **16**, S5517.
Auslender, M. I., and V. Y. Irkhin, 1984a, Z. Phys. B: Condens. Matter **56**, 301.
Auslender, M. I., and V. Y. Irkhin, 1984b, Solid State Commun. **50**, 1003.
Auslender, M. I., and V. Y. Irkhin, 1985a, Z. Phys. B: Condens. Matter **61**, 129.
Auslender, M. I., and V. Y. Irkhin, 1985b, Solid State Commun. **56**, 701.
Auslender, M. I., V. Y. Irkhin, and M. I. Katsnelson, 1988, J. Phys. C **21**, 5521.
Auslender, M. I., and M. I. Katsnelson, 1982, Teor. Mat. Fiz. **51**, 436.
Auslender, M. I., M. I. Katsnelson, and V. Y. Irkhin, 1983, Physica B & C **119**, 309.
Auth, N., G. Jakob, T. Block, and C. Felser, 2003, Phys. Rev. B **68**, 024403.
Baym, G., and L. P. Kadanoff, 1961, Phys. Rev. **124**, 287.
Bickers, N. E., and D. J. Scalapino, 1989, Ann. Phys. (N.Y.) **193**, 206.
Biermann, S., F. Aryasetiawan, and A. Georges, 2003, Phys. Rev. Lett. **90**, 086402.
Bona, G. L., F. Meier, M. Taborelli, E. Bucher, and P. H. Schmidt, 1985, Solid State Commun. **56**, 391.
Borca, C. N., T. Komesu, H.-K. Jeong, P. A. Dowben, D. Ristoiu, C. Hordequin, J. P. Nozières, J. Pierre, S. Stadler, and Y. U. Idzerda, 2001, Phys. Rev. B **64**, 052409.
Bowen, M., M. Bibes, A. Barthelemy, J.-P. Contour, A. Anane, Y. Lemaitre, and A. Fert, 2003, Appl. Phys. Lett. **82**, 233.
Bratkovsky, A. M., 1997, Phys. Rev. B **56**, 2344.
Bratkovsky, A. M., 1998, Appl. Phys. Lett. **72**, 2334.
Brown, P. J., K. U. Neumann, P. J. Webster, and K. R. A. Ziebeck, 2000, J. Phys.: Condens. Matter **12**, 1827.
Carneiro, G. M., and C. J. Pethick, 1975, Phys. Rev. B **11**, 1106.
Ceperley, D. M., and B. J. Alder, 1980, Phys. Rev. Lett. **45**, 566.
Chadov, S., J. Minar, H. Ebert, A. Perlov, L. Chioncel, M. I. Katsnelson, and A. I. Lichtenstein, 2006, Phys. Rev. B **74**, 140411.
Chamberland, B. L., 1977, CRC Crit. Rev. Solid State Mater. Sci. **7**, 1.
Chiba, D., K. Takamura, F. Matsukura, and H. Ohno, 2003, Appl. Phys. Lett. **82**, 3020.
Chioncel, L., 2004, "Finite temperature electronic structure, beyond local density approximation," Ph.D. thesis (Radbout University, Nijmegen).
Chioncel, L., 2006, unpublished.
Chioncel, L., H. Allmaier, E. Arrigoni, A. Yamasaki, M. Daghofer, M. I. Katsnelson, and A. I. Lichtenstein, 2007, Phys. Rev. B **75**, 140406.
Chioncel, L., E. Arrigoni, M. I. Katsnelson, and A. I. Lichtenstein, 2006, Phys. Rev. Lett. **96**, 137203.
Chioncel, L., M. I. Katsnelson, R. A. de Groot, and A. I. Lichtenstein, 2003, Phys. Rev. B **68**, 144425.
Chioncel, L., M. I. Katsnelson, G. A. de Wijs, R. A. de Groot, and A. I. Lichtenstein, 2005, Phys. Rev. B **71**, 085111.
Chioncel, L., P. Mavropoulos, M. Lezaic, S. Blugel, E. Arrigoni, M. I. Katsnelson, and A. I. Lichtenstein, 2006, Phys. Rev. Lett. **96**, 197203.
Chioncel, L., L. Vitos, I. A. Abrikosov, J. Kollar, M. I. Katsnelson, and A. I. Lichtenstein, 2003, Phys. Rev. B **67**, 235106.
Chitra, R., and G. Kotliar, 2000, Phys. Rev. B **62**, 12715.
Chitra, R., and G. Kotliar, 2001, Phys. Rev. B **63**, 115110.
Correa, J. S., C. Eibl, G. Rangelov, J. Braun, and M. Donath, 2006, Phys. Rev. B **73**, 125316.
Craco, L., M. S. Laad, and E. Müller-Hartmann, 2003, Phys. Rev. Lett. **90**, 237203.
Craco, L., M. S. Laad, and E. Müller-Hartmann, 2006, Phys. Rev. B **74**, 064425.
Dagotto, E., 2003, *Nanoscale Phase Separation and Colossal Magnetoresistance: The Physics of Manganites and Related Compounds* (Springer, Berlin).
de Boer, P. K., and R. A. d. Groot, 1999, Phys. Rev. B **60**, 10758.
Dederichs, P. H., S. Blügel, R. Zeller, and H. Akai, 1984, Phys. Rev. Lett. **53**, 2512.
de Groot, F. M. F., J. C. Fuggle, B. T. Thole, and G. A. Sawatzky, 1990, Phys. Rev. B **42**, 5459.
de Groot, R. A., 1991, Physica B **172**, 45.
de Groot, R. A., A. G. M. Janner, and F. M. Mueller, 1983, Patents NL 19830000602, EP 198402000215.
de Groot, R. A., F. M. Mueller, P. G. v. Engen, and K. H. J. Buschow, 1983, Phys. Rev. Lett. **50**, 2024.
de Groot, R. A., A. M. van der Kraan, and K. H. J. Buschow, 1986, J. Magn. Magn. Mater. **61**, 330.
Delves, R., and B. Lewis, 1963, J. Phys. Chem. Solids **28**, 549.
de Wijs, G. A., and R. A. de Groot, 2001, Phys. Rev. B **64**, 020402.
Dowben, P. A., and R. Skomski, 2003, J. Appl. Phys. **93**, 7948.
Dowben, P. A., and R. Skomski, 2004, J. Appl. Phys. **95**, 7453.
Ebert, H., 1996, Rep. Prog. Phys. **59**, 1665.
Ebert, H., and G. Schutz, 1991, J. Appl. Phys. **69**, 4627.
Edwards, D. M., 1983, J. Phys. C **16**, L327.
Edwards, D. M., 2002, Adv. Phys. **51**, 1259.
Edwards, D. M., and J. A. Hertz, 1973, J. Phys. F: Met. Phys. **3**, 2191.
Edwards, D. M., and M. I. Katsnelson, 2006, J. Phys.: Condens. Matter **18**, 7209.
Eerenstein, W., T. T. M. Palstra, S. S. Saxena, and T. Hibma, 2002, Phys. Rev. Lett. **88**, 247204.
Egorushkin, V., S. Kulkov, and S. Kulkova, 1983, Physica B & C **123**, 61.
Etgens, V. H., P. C. de Camargo, M. Eddrief, R. Mattana, J. M. George, and Y. Garreau, 2004, Phys. Rev. Lett. **92**, 167205.
Fazekas, P., B. Menge, and E. Müller-Hartmann, 1990, Z. Phys. B: Condens. Matter **78**, 69.
Fecher, G. H., H. C. Kandpal, S. Wurmehl, C. Felser, and G. Schonhense, 2006, J. Appl. Phys. **99**, 08J106.
Flatte, M. E., and G. Vignale, 2001, Appl. Phys. Lett. **78**, 1273.
Folkerts, W., G. Sawatzky, C. Haas, R. de Groot, and F. Hillebrecht, 1987, J. Phys. C **20**, 4135.
Fong, C. Y., M. C. Qian, J. E. Pask, L. H. Yang, and S. Dag, 2004, Appl. Phys. Lett. **84**, 239.
Fujii, S., S. Ishida, and S. Asano, 1995, J. Phys. Soc. Jpn. **64**, 184.
Fukuda, R., T. Kotani, Y. Suzuki, and S. Yokojima, 1994, Prog. Theor. Phys. **92**, 833.
Furukawa, N., 2000, J. Phys. Soc. Jpn. **69**, 1954.
Galanakis, I., 2003, J. Phys.: Condens. Matter **14**, 6329.

Galanakis, I., 2004, J. Phys.: Condens. Matter **16**, 3089.
Galanakis, I., P. H. Dederichs, and N. Papanikolaou, 2002a, Phys. Rev. B **66**, 134428.
Galanakis, I., P. H. Dederichs, and N. Papanikolaou, 2002b, Phys. Rev. B **66**, 174429.
Galanakis, I., and P. H. Dederichs, 2005, Eds., *Lecture Notes in Physics* (Springer, Berlin).
Galanakis, I., and P. Mavropoulos, 2003, Phys. Rev. B **67**, 104417.
Galanakis, I., and P. Mavropoulos, 2007, J. Phys.: Condens. Matter **19**, 315213.
Galanakis, I., P. Mavropoulos, and P. H. Dederichs, 2006, J. Phys. D **39**, 765.
Galitski, V. M., 1958, Zh. Eksp. Teor. Fiz. **34**, 1011.
Garsia, J., and G. Sabias, 2004, J. Phys.: Condens. Matter **16**, R145.
Georges, A., G. Kotliar, W. Krauth, and M. J. Rozenberg, 1996, Rev. Mod. Phys. **68**, 13.
Gercsi, Z., A. Rajanikanth, Y. K. Takahashi, K. Hono, M. Kikuchi, N. Tezuka, and K. Inomata, 2006, Appl. Phys. Lett. **89**, 082512.
Goering, E., S. Gold, M. Lafkioti, and G. Schütz, 2006, Europhys. Lett. **73**, 97.
Golosov, D. I., 2000, Phys. Rev. Lett. **84**, 3974.
Grigin, A. P., and E. L. Nagaev, 1974, Phys. Status Solidi B **61**, 65.
Gunnarsson, O., O. K. Andersen, O. Jepsen, and J. Zaanen, 1989, Phys. Rev. B **39**, 1708.
Gyorffy, B. L., A. J. Pindor, J. Staunton, G. M. Stocks, and H. Winter, 1985, J. Phys. F: Met. Phys. **15**, 1337.
Halilov, S. V., H. Eschrig, A. Y. Perlov, and P. M. Oppeneer, 1998, Phys. Rev. B **58**, 293.
Hanssen, K. E. H. M., and P. E. Mijnarends, 1986, Phys. Rev. B **34**, 5009.
Hanssen, K. E. H. M., P. E. Mijnarends, L. P. L. M. Rabou, and K. H. J. Buschow, 1990, Phys. Rev. B **42**, 1533.
Harland, H., and J. C. Woolley, 1966, Can. J. Phys. **44**, 2715.
Harris, J., and R. Jones, 1974, J. Phys. F: Met. Phys. **4**, 1170.
Hartman-Boutron, F., 1965, Phys. Kondens. Mater. **4**, 114.
Hashemifar, S. J., P. Kratzer, and M. Scheffler, 2005, Phys. Rev. Lett. **94**, 096402.
Hedin, L., 1965, Phys. Rev. **139**, 796.
Heinze, S., M. Bode, A. Kubetzka, O. Pietzsch, X. Nie, S. Blügel, and R. Wiesendanger, 2000, Science **288**, 1805.
Helmholdt, R. B., R. A. de Groot, F. M. M. G. van Engen, and K. H. J. Buschow, 1984, J. Magn. Magn. Mater. **43**, 249.
Herring, C., 1966, *Magnetism* (Academic, New York), Vol. 4.
Heusler, F., 1903, Verh. Dtsch. Phys. Ges. **5**, 219.
Hewson, A. C., 1993, *The Kondo Problem to Heavy Fermions* (Cambridge University Press, Cambridge).
Hirsch, J. E., 1983, Phys. Rev. B **28**, 4059.
Hohenberg, P., and W. Kohn, 1964, Phys. Rev. **136**, B864.
Hordequin, C., E. Lelivre-Bernab, and J. Pierre, 1997, Physica B **234-236**, 602.
Hordequin, C., J. P. Nozieres, and J. Pierre, 1998, J. Magn. Magn. Mater. **183**, 225.
Hordequin, C., J. Pierre, and R. Currat, 1997, Physica B **234-236**, 605.
Hordequin, C., D. Ristoiu, L. Ranno, and J. Pierre, 2000, Eur. Phys. J. B **16**, 287.
Hoshino, K., T. Kurikawa, H. Takeda, A. Nakajima, and K. Kaya, 1995, J. Phys. Chem. **99**, 3053.
Huang, D. J., C. F. Chang, H. T. Jeng, G. Y. Guo, H. J. Lin, W. B. Wu, H. C. Ku, A. Fujimori, Y. Takahashi, and C. T. Chen, 2004, Phys. Rev. Lett. **93**, 077204.
Huang, D. J., L. H. Tjeng, J. Chen, C. F. Chang, W. P. Wu, S. C. Chung, A. Tanaka, G. Y. Guo, H. J. Lin, S. G. Shyu, C. C. Wu, and C. T. Chen, 2003, Phys. Rev. B **67**, 214419.
Hubbard, J., 1963, Proc. R. Soc. London, Ser. A **A276**, 238.
Hybertsen, M. S., M. Schlüter, and N. E. Christensen, 1989, Phys. Rev. B **39**, 9028.
Irkhin, V. Y., 1987, Fiz. Met. Metalloved. **64**, 260.
Irkhin, V. Y., and Y. P. Irkhin, 1994, Phys. Status Solidi B **183**, 9.
Irkhin, V. Y., and Y. P. Irkhin, 2007, *Electronic Structure, Correlation Effects and Physical Properties of d- and f-Metals and their Compound* (Cambridge International Science, Cambridge).
Irkhin, V. Y., and M. I. Katsnelson, 1983, Sov. Phys. Solid State **25**, 1947.
Irkhin, V. Y., and M. I. Katsnelson, 1984, Fiz. Tverd. Tela (Leningrad) **26**, 3055.
Irkhin, V. Y., and M. I. Katsnelson, 1985a, Zh. Eksp. Teor. Fiz. **88**, 522 [Sov. Phys. JETP **61**, 306 (1985)].
Irkhin, V. Y., and M. I. Katsnelson, 1985b, J. Phys. C **18**, 4173.
Irkhin, V. Y., and M. I. Katsnelson, 1988, Fiz. Met. Metalloved. **66**, 41.
Irkhin, V. Y., and M. I. Katsnelson, 1990, J. Phys.: Condens. Matter **2**, 7151.
Irkhin, V. Y., and M. I. Katsnelson, 1994, Usp. Fiz. Nauk **164**, 705 [Phys. Usp. **37**, 659 (1994)].
Irkhin, V. Y., and M. I. Katsnelson, 1996, Phys. Rev. B **53**, 14008.
Irkhin, V. Y., and M. I. Katsnelson, 2001, Eur. Phys. J. B **19**, 401.
Irkhin, V. Y., and M. I. Katsnelson, 2002, Eur. Phys. J. B **30**, 481.
Irkhin, V. Y., and M. I. Katsnelson, 2005a, Eur. Phys. J. B **43**, 479.
Irkhin, V. Y., and M. I. Katsnelson, 2005b, Phys. Rev. B **72**, 054421.
Irkhin, V. Y., and M. I. Katsnelson, 2006, Phys. Rev. B **73**, 104429.
Irkhin, V. Y., M. I. Katsnelson, and A. V. Trefilov, 1989, Physica C **160**, 397.
Irkhin, V. Y., M. I. Katsnelson, and A. V. Trefilov, 1994, Zh. Eksp. Teor. Fiz. **105**, 1733 [JETP **78**, 936 (1994)].
Irkhin, V. Y., and A. V. Zarubin, 2000, Eur. Phys. J. B **16**, 463.
Irkhin, V. Y., and A. V. Zarubin, 2004, Phys. Rev. B **70**, 035116.
Irkhin, V. Y., and A. V. Zarubin, 2006, J. Magn. Magn. Mater. **300**, 246.
Ishida, S., S. Akazawa, Y. Kubo, and J. Ishida, 1982, J. Phys. F: Met. Phys. **12**, 1111.
Ishida, S., S. Fujii, S. Kashiwagi, and S. Asano, 1995, J. Phys. Soc. Jpn. **64**, 2152.
Ishida, S., J. Ishida, S. Asano, and J. Yamashita, 1976a, J. Phys. Soc. Jpn. **41**, 1570.
Ishida, S., J. Ishida, S. Asano, and J. Yamashita, 1976b, J. Phys. Soc. Jpn. **41**, 1570.
Ishida, S., Y. Kubo, J. Ishida, and S. Asano, 1980, J. Phys. Soc. Jpn. **48**, 814.
Ishigaki, A., and T. Moriya, 1996, J. Phys. Soc. Jpn. **65**, 3402.
Itoh, H., T. Ohsawa, and J. Inoue, 2000, Phys. Rev. Lett. **84**, 2501.
Jansen, M., R. Hagenmayer, and N. Korber, 1999, C.R. Acad. Sci., Ser. IIc: Chim **2**, 591.

Jarrell, M., 1992, Phys. Rev. Lett. **69**, 168.
Jarrell, M., and J. E. Gubernatis, 1996, Phys. Rep. **269**, 134.
Jarrett, H. S., W. H. Cloud, R. J. Bouchard, S. R. Butler, C. G. Frederick, and J. L. Gillson, 1968, Phys. Rev. Lett. **21**, 617.
Ji, Y., G. J. Strijkers, F. Y. Yang, C. L. Chien, J. M. Byers, A. Anguelouch, G. Xiao, and A. Gupta, 2001, Phys. Rev. Lett. **86**, 5585.
Jo, M.-H., N. D. Mathur, J. E. Evetts, and M. G. Blamire, 2000a, Appl. Phys. Lett. **77**, 3803.
Jo, M.-H., N. D. Mathur, N. K. Todd, and M. G. Blamire, 2000b, Phys. Rev. B **61**, R14905.
Jonker, J., and G. H. V. Santen, 1950, J. Magn. Magn. Mater. **16**, 337.
Joss, W., L. N. Hall, G. W. Crabtree, and J. J. Vuillemin, 1984, Phys. Rev. B **30**, 5637.
Judd, B. R., 1963, *Operator Techniques in Atomic Spectroscopy* (McGrow-Hill, New York).
Kajueter, H., and G. Kotliar, 1996, Phys. Rev. Lett. **77**, 131.
Kämper, K. P., W. Schmitt, G. Güntherodt, R. J. Gambino, and R. Ruf, 1987, Phys. Rev. Lett. **59**, 2788.
Kanamori, J., 1963, Prog. Theor. Phys. **30**, 276.
Kaplan, T. A., S. D. Mahanti, and Y.-S. Su, 2001, Phys. Rev. Lett. **86**, 3634.
Karla, I., J. Pierre, A. P. Murani, and M. Neumann, 1999, Physica B **271**, 294.
Karla, I., J. Pierre, and B. Ouladdiaf, 1998, Physica B **253**, 215.
Karla, I., J. Pierre, and R. V. Skolozdra, 1998, J. Alloys Compd. **265**, 42.
Kato, H., T. Okuda, Y. Okimoto, Y. Tomioka, Y. Takenoya, A. Ohkubo, M. Kawasaki, and Y. Tokura, 2002, Appl. Phys. Lett. **81**, 328.
Katsnelson, M. I., and D. M. Edwards, 1992, J. Phys.: Condens. Matter **4**, 3289.
Katsnelson, M. I., and A. I. Lichtenstein, 1999, J. Phys.: Condens. Matter **11**, 1037.
Katsnelson, M. I., and A. I. Lichtenstein, 2000, Phys. Rev. B **61**, 8906.
Katsnelson, M. I., and A. I. Lichtenstein, 2002, Eur. Phys. J. B **30**, 9.
Katsnelson, M. I., and A. V. Trefilov, 1990, Z. Phys. B: Condens. Matter **80**, 63.
Keizer, R. S., S. T. B. Goennenwein, T. M. Klapwijk, G. Miao, G. Xiao, and A. Gupta, 2006, Nature (London) **439**, 825.
Kino, H., F. Aryasetiawanx, I. Solovyev, T. Miyake, T. Ohno, and K. Terakura, 2003, Physica B **329-333**, 858.
Kisker, E., G. Baum, A. H. Mahan, W. Raith, and B. Reihl, 1978, Phys. Rev. B **18**, 2256.
Kisker, E., C. Carbone, C. F. Flipse, and E. F. Wassermann, 1987, J. Magn. Magn. Mater. **70**, 21.
Kleiber, M., M. Bode, R. Ravlić, and R. Wiesendanger, 2000, Phys. Rev. Lett. **85**, 4606.
Kobayashi, K. I., T. Kimura, H. Sawada, K. Terakura, and Y. Tokura, 1998, Nature (London) **395**, 677.
Kobayashi, K.-I., T. Kimura, Y. Tomioka, H. Sawada, K. Terakura, and Y. Tokura, 1999, Phys. Rev. B **59**, 11159.
Kohn, W., and L. J. Sham, 1965, Phys. Rev. **140**, A1133.
Korotin, M. A., V. I. Anisimov, D. I. Khomskii, and G. A. Sawatzky, 1998, Phys. Rev. Lett. **80**, 4305.
Kotliar, G., S. Y. Savrasov, K. Haule, V. S. Oudovenko, O. Parcollet, and C. A. Marianetti, 2006, Rev. Mod. Phys. **78**, 865.
Kübler, J., 1984, Physica B & C **127B**, 257.
Kübler, J., 2000, *Theory of Itinerant Electron Magnetism* (Calderon Press, Oxford).
Kübler, J., 2003, Phys. Rev. B **67**, 220403.
Kübler, J., A. R. William, and C. B. Sommers, 1983, Phys. Rev. B **28**, 1745.
Kubo, K., and N. Ohata, 1972, J. Phys. Soc. Jpn. **33**, 21.
Kubo, R., 1957, J. Phys. Soc. Jpn. **12**, 570.
Kulatov, E., and I. I. Mazin, 2003, J. Phys.: Condens. Matter **2**, 343.
Kurmaev, E. Z., A. Moewes, S. M. Butorin, M. I. Katsnelson, L. D. Finkelstein, J. Nordgren, and P. M. Tedrow, 2003, Phys. Rev. B **67**, 155105.
Kurtulus, Y., R. Dronskowski, G. D. Samolyuk, and V. P. Antropov, 2005, Phys. Rev. B **71**, 014425.
Laad, M. S., L. Craco, and E. Müller-Hartmann, 2001, Phys. Rev. B **64**, 214421.
Leighton, C., *et al.*, 2007, J. Phys.: Condens. Matter **19**, 315219.
Leonov, I., A. N. Yaresko, V. N. Antonov, and V. I. Anisimov, 2006, Phys. Rev. B **74**, 165117.
Lewis, S. P., P. B. Allen, and T. Sasaki, 1997, Phys. Rev. B **55**, 10253.
Lezaic, M., 2006, unpublished.
Lezaic, M., P. Mavropoulos, J. Enkovaara, G. Bihlmayer, and S. Blugel, 2006, Phys. Rev. Lett. **97**, 026404.
Liang, S., and H. Pang, 1995, Europhys. Lett. **32**, 173.
Lichtenstein, A. I., and M. I. Katsnelson, 1998, Phys. Rev. B **57**, 6884.
Liechtenstein, A. I., M. I. Katsnelson, V. P. Antropov, and V. A. Gubanov, 1987, J. Magn. Magn. Mater. **67**, 65.
Lichtenstein, A. I., M. I. Katsnelson, and G. Kotliar, 2001, Phys. Rev. Lett. **87**, 067205.
Liu, B.-G., 2003, Phys. Rev. B **67**, 172411.
Lutovinov, V. S., and M. Y. Reizer, 1979, Zh. Eksp. Teor. Fiz. **77**, 707.
Luttinger, J. M., and J. C. Ward, 1960, Phys. Rev. **118**, 1417.
MacDonald, A. H., T. Jungwirth, and M. Kasner, 1998, Phys. Rev. Lett. **81**, 705.
Mackintosh, A. R., and O. K. Andersen, 1980, in *Electrons at the Fermi Surface*, edited by M. Springford (Cambridge University Press, London).
Maeno, Y., H. Hashimoto, K. Yoshida, S. Nishizaki, T. Fujita, J. G. Bednorz, and F. Lichtenberg, 1994, Nature (London) **372**, 532.
Mahan, G. D., 1990, *Many-Particle Physics* (Plenum Press, New York).
Matar, S., G. Demazeau, J. Sticht, V. Eyert, and J. Kübler, 1992, J. Phys. I **2**, 315.
Mavropoulos, P., I. Galanakis, V. Popescu, and P. H. Dederichs, 2004, J. Phys.: Condens. Matter **16**, S5759.
Mavropoulos, P., M. Ležaić, and S. Blügel, 2005, Phys. Rev. B **72**, 174428.
Mazin, I. I., 2000, Appl. Phys. Lett. **77**, 3000.
Mazin, I. I., D. J. Singh, and C. Ambrosch-Draxl, 1999, Phys. Rev. B **59**, 411.
McCann, E., and V. I. Fal'ko, 2002, Phys. Rev. B **66**, 134424.
McCann, E., and V. I. Fal'ko, 2003, Phys. Rev. B **68**, 172404.
McMahan, A. K., R. M. Martin, and S. Satpathy, 1988, Phys. Rev. B **38**, 6650.
Miao, G. X., P. LeClair, A. Gupta, G. Xiao, M. Varela, and S. Pennycook, 2006, Appl. Phys. Lett. **89**, 022511.
Millis, A. J., H. Monien, and D. Pines, 1990, Phys. Rev. B **42**, 167.
Min, B. I., T. Oguchi, H. J. F. Jansen, and A. J. Freeman, 1986,

Phys. Rev. B **33**, 324.
Min, B. I., M. S. Park, and J. H. Park, 2004, J. Phys.: Condens. Matter **16**, S5509.
Mizuguchi, M., H. Akinaga, T. Manago, K. Ono, M. Oshima, M. Shirai, M. Yuri, H. J. Lin, H. H. Hsieh, and C. T. Chen, 2002, J. Appl. Phys. **91**, 7917.
Moodera, J. S., and D. M. Mootoo, 1994, J. Appl. Phys. **76**, 6101.
Mori, H., 1965, Prog. Theor. Phys. **34**, 399.
Moriya, T., 1963, J. Phys. Soc. Jpn. **18**, 516.
Moriya, T., 1985, *Spin Fluctuations in Itinerant Electron Magnetism* (Springer, Berlin).
Moriya, T., 1994, *Spectroscopy of Mott Insulators and Correlated Metals* (Springer, Berlin).
Mortonx, S. A., G. D. Waddill, S. Kim, I. K. Schuller, S. A. Chambers, and J. G. Tobin, 2002, Surf. Sci. **513**, L451.
Mott, N. F., 1974, *Metal-Insulator Transitions* (Taylor & Francis, London).
Mott, N. F., 1980, Philos. Mag. B **B42**, 327.
Nadgorny, B., 2007, J. Phys.: Condens. Matter **19**, 315209.
Nadgorny, B., I. I. Mazin, M. Osofsky, R. J. Soulen, P. Broussard, R. M. Stroud, D. J. Singh, V. G. Harris, A. Arsenov, and Y. Mukovskii, 2001, Phys. Rev. B **63**, 184433.
Nagaev, E. L., 1983, *Physics of Magnetic Semiconductors* (Mir, Moscow).
Nagaev, E. L., 2001, Phys. Rep. **346**, 387.
Nagao, K., M. Shirai, and Y. Miura, 2004, J. Phys.: Condens. Matter **16**, S5725.
Nagaoka, Y., 1966, Phys. Rev. **147**, 392.
Nakano, H., 1957, Prog. Theor. Phys. **17**, 145.
Nanda, B. R. K., and I. Dasgupta, 2003, J. Phys.: Condens. Matter **15**, 7307.
Nazmul, A. M., S. Sugahara, and M. Tanaka, 2002, Appl. Phys. Lett. **80**, 3120.
Norman, M. R., and A. J. Freeman, 1986, Phys. Rev. B **33**, 8896.
Nozieres, P., 1964, *Theory of Interacting Fermi Systems* (Benjamin, New York).
Obermeier, T., T. Pruschke, and J. Keller, 1997, Phys. Rev. B **56**, R8479.
Öğüt, S., and K. M. Rabe, 1995, Phys. Rev. B **51**, 10443.
Ohno, H., 1998a, Science **281**, 951.
Ohno, H., 1998b, J. Magn. Magn. Mater. **200**, 110.
Okabayashi, J., M. Mizuguchi, K. Ono, M. Oshima, A. Fujimori, H. Kuramochi, and H. Akinaga, 2004, Phys. Rev. B **70**, 233305.
Orgassa, D., H. Fujiwara, T. C. Schulthess, and W. H. Butler, 1999, Phys. Rev. B **60**, 13237.
Orgassa, D., H. Fujiwara, T. C. Schulthess, and W. H. Butler, 2000, J. Appl. Phys. **87**, 5870.
Otto, M. J., R. A. M. van Woerden, P. J. van der Valk, J. Wijngaard, C. F. van Bruggen, and C. Haas, 1989, J. Phys.: Condens. Matter **1**, 2351.
Ozdogan, K., I. Galanakis, E. Sasioglu, and B. Aktas, 2006, J. Phys.: Condens. Matter **18**, 2905.
Paessler, R., 1999, Phys. Status Solidi B **216**, 975.
Park, J. H., E. Vescovo, H. J. Kim, C. Kwon, R. Ramesh, and T. Venkatesan, 1998, Nature (London) **392**, 794.
Park, M. S., S. K. Kwon, and B. I. Min, 2001, Phys. Rev. B **64**, 100403.
Pickett, W. E., 1998, Phys. Rev. B **57**, 10613.
Pickett, W. E., S. C. Erwin, and E. C. Ethridge, 1998, Phys. Rev. B **58**, 1201.
Pickett, W. E., and H. Eschrig, 2007, J. Phys.: Condens. Matter **19**, 315203.
Pickett, W. E., and D. J. Singh, 1996, Phys. Rev. B **53**, 1146.
Pierre, J., and I. Karla, 2000, J. Magn. Magn. Mater. **217**, 74.
Pierre, J., I. Karla, and K. Kaczmarska, 1999, Physica B **261**, 845.
Porta, P., M. Marezio, J. P. Remeika, and P. D. Dernier, 1972, Mater. Res. Bull. **7**, 157.
Pourovskii, L. V., M. I. Katsnelson, and A. I. Lichtenstein, 2005, Phys. Rev. B **72**, 115106.
Pourovskii, L. V., M. I. Katsnelson, and A. I. Lichtenstein, 2006, Phys. Rev. B **73**, 060506.
Prinz, G. A., 1998, Science **282**, 1660.
Rabe, M., J. Pommer, K. Samm, B. Oezyilmaz, C. Koenig, M. Fraune, U. Ruediger, G. Guentherodt, S. Senz, and D. Hesse, 2002, J. Phys.: Condens. Matter **14**, 7.
Rahman, M. M., M. Kisaku, T. Kishi, D. Matsunaka, W. A. Dino, H. Nakanishi, and H. Kasai, 2004, J. Phys.: Condens. Matter **16**, S5755.
Ramesha, K., R. Seshadri, C. Ederer, T. He, and M. A. Subramanian, 2004, Phys. Rev. B **70**, 214409.
Rengade, M. E., 1907, Ann. Chim. Phys. **11**, 348.
Ristoiu, D., J. P. Nozieres, C. N. Borca, B. Borca, and P. A. Dowben, 2000, Appl. Phys. Lett. **76**, 2349.
Roesler, M., 1965, Phys. Status Solidi **8**, K31.
Roth, L. M., 1969a, Phys. Rev. **184**, 451.
Roth, L. M., 1969b, Phys. Rev. **186**, 428.
Rozenberg, M. J., 1997, Phys. Rev. B **55**, R4855.
Rubtsov, A. N., V. V. Savkin, and A. I. Lichtenstein, 2005, Phys. Rev. B **72**, 035122.
Rusz, J., L. Bergqvist, J. Kudrnovsky, and I. Turek, 2006, Phys. Rev. B **73**, 214412.
Rybchenko, S. I., Y. Fujishiro, H. Takagi, and M. Awano, 2006, Appl. Phys. Lett. **89**, 132509.
Sakuma, A., 2002, J. Phys. Soc. Jpn. **71**, 2534.
Sakuraba, Y., M. Hattori, M. Oogane, Y. Ando, H. Kato, A. Sakuma, T. Miyazaki, and H. Kubota, 2006, Appl. Phys. Lett. **88**, 192508.
Sakuraba, Y., M. Hattori, M. Oogane, H. Kubota, Y. Ando, A. Sakuma, and T. Miyazaki1, 2007, J. Phys. D **40**, 1221.
Sakuraba, Y., T. Miyakoshi, M. Oogane, Y. Ando, A. Sakuma, T. Miyazaki, and H. Kubota, 2006, Appl. Phys. Lett. **89**, 052508.
Salamon, M. B., and M. Jaime, 2001, Rev. Mod. Phys. **73**, 583.
Sandratskii, L. M., 1998, Adv. Phys. **47**, 91.
Sandratskii, L. M., 2001, Phys. Rev. B **64**, 134402.
Sandratskii, L. M., and P. Bruno, 2003, Phys. Rev. B **67**, 214402.
Sanyal, B., L. Bergqvist, and O. Eriksson, 2003, Phys. Rev. B **68**, 054417.
Sasioglu, E., I. Galanakis, L. M. Sandratskii, and P. Bruno, 2005, J. Phys.: Condens. Matter **17**, 3915.
Sasioglu, E., L. M. Sandratskii, and P. Bruno, 2005, J. Appl. Phys. **98**, 063523.
Sasioglu, E., L. M. Sandratskii, P. Bruno, and I. Galanakis, 2005, Phys. Rev. B **72**, 184415.
Savkin, V. V., A. N. Rubtsov, M. I. Katsnelson, and A. I. Lichtenstein, 2005, Phys. Rev. Lett. **94**, 026402.
Savrasov, S. Y., and G. Kotliar, 2004, Phys. Rev. B **69**, 245101.
Schaf, J., K. L. Dang, P. Veillet, and I. A. Campbell, 1983, J. Phys. F: Met. Phys. **13**, 1311.
Schlottmann, P., 2003, Phys. Rev. B **67**, 174419.
Schwarz, K., 1986, J. Phys. F: Met. Phys. **16**, L211.
Senateur, J. P., A. Ronault, R. Fruchart, and D. Fruchart, 1972,

J. Solid State Chem. **5**, 226.
Shirai, M., 2003, J. Appl. Phys. **93**, 6844.
Shirai, M., T. Ogawa, I. Kitagawa, and N. Suzuki, 1998, J. Magn. Magn. Mater. **177-181**, 1383.
Shirakawa, H., E. J. Louis, A. G. MacDiarmid, C. K. Chiang, and A. J. Heeger, 1977, J. Chem. Soc., Chem. Commun. **16**, 578.
Silin, V. P., and A. Z. Solontsov, 1984, Fiz. Met. Metalloved. **58**, 1080.
Singley, E. J., C. P. Weber, D. N. Basov, A. Barry, and J. M. D. Coey, 1999, Phys. Rev. B **60**, 4126.
Skomski, R., 2007, J. Phys.: Condens. Matter **19**, 315202.
Skomski, R., and P. A. Dowben, 2002, Europhys. Lett. **58**, 544.
Sokolov, O. B., V. I. Grebennikov, and E. A. Turov, 1977, Phys. Status Solidi B **83**, 383.
Solovyev, I., N. Hamada, and K. Terakura, 1996, Phys. Rev. B **53**, 7158.
Solovyev, I. V., and M. Imada, 2005, Phys. Rev. B **71**, 045103.
Sorantin, P. I., and K. Schwarz, 1992, Inorg. Chem. **31**, 567.
Soulen, R. J., J. M. Byers, M. S. Osofsky, B. Nadgorny, T. Ambrose, S. F. Cheng, P. R. Broussard, C. T. Tanaka, J. Nowak, J. S. Moodera, A. Barry, and J. M. D. Coey, 1998, Science **282**, 85.
Soulen, R. J., *et al.*, 1999, J. Appl. Phys. **85**, 4589.
Springford, M., 1980, *Electrons at the Fermi Surface* (Cambridge University Press, Cambridge).
Stagarescu, C. B., X. Su, D. E. Eastman, K. N. Altmann, F. J. Himpsel, and A. Gupta, 2000, Phys. Rev. B **61**, R9233.
Suzuki, K., and P. M. Tedrow, 1998, Phys. Rev. B **58**, 11597.
Tkachov, G., E. McCann, and V. I. Fal'ko, 2001, Phys. Rev. B **65**, 024519.
Tomioka, Y., T. Okuda, Y. Okimoto, R. Kumai, K. I. Kobayashi, and Y. Tokura, 2000, Phys. Rev. B **61**, 422.
Toropova, A., G. Kotliar, S. Y. Savrasov, and V. S. Oudovenko, 2005, Phys. Rev. B **71**, 172403.
Troyer, M., and U.-J.Wiese, 2005, Phys. Rev. Lett. **94**, 170201.
Tsujioka, T., T. Mizokawa, J. Okamoto, A. Fujimori, M. Nohara, H. Takagi, K. Yamaura, and M. Takano, 1997, Phys. Rev. B **56**, R15509.
Turzhevskii, S. A., A. I. Lichtenstein, and M. I. Katsnelson, 1990, Fiz. Tverd. Tela (Leningrad) **32**, 1952 [Sov. Phys. Solid State **32**, 1138 (1990)].
Ueda, K., and T. Moriya, 1975, J. Phys. Soc. Jpn. **38**, 32.
Ukraintsev, V. A., 1996, Phys. Rev. B **53**, 11176.
Ulmke, M., 1998, Eur. Phys. J. B **1**, 301.
Vaitheeswaran, G., V. Kanchana, and A. Delin, 2005, Appl. Phys. Lett. **86**, 032513.
van der Marel, D., and G. A. Sawatzky, 1988, Phys. Rev. B **37**, 10674.
van Engen, P. G., K. H. J. Buschow, R. Jongebreur, and M. Erman, 1983, Appl. Phys. Lett. **42**, 202.
van Leuken, H., and R. A. de Groot, 1995, Phys. Rev. B **51**, 7176.
Verwey, E., 1939, Nature (London) **144**, 327.
Viret, M., L. Ranno, and J. M. D. Coey, 1997, Phys. Rev. B **55**, 8067.
Vollhardt, D., N. Blumer, K. Held, and M. Kollar, 1999, Adv. Solid State Phys. **38**, 383.
von der Linden, W., and D. M. Edwards, 1991, J. Phys.: Condens. Matter **3**, 4917.
Vonsovsky, S. V., 1974, *Magnetism* (Wiley, New York).
Vonsovsky, S. V., and M. I. Katsnelson, 1989, *Quantum Solid State Physics* (Springer, Berlin).
Walz, F., 2002, J. Phys.: Condens. Matter **14**, R285.
Wang, L., K. Umemoto, R. M. Wentzcovitch, T. Y. Chen, C. L. Chien, J. G. Checkelsky, J. C. Eckert, E. D. Dahlberg, and C. Leighton, 2005, Phys. Rev. Lett. **94**, 056602.
Watts, S. M., S. Wirth, S. von Molnár, A. Barry, and J. M. D. Coey, 2000, Phys. Rev. B **61**, 9621.
Weht, R., and W. E. Pickett, 1999, Phys. Rev. B **60**, 13006.
Wessely, O., *et al.*, 2003, Phys. Rev. B **68**, 235109.
Wiesendanger, R., H.-J. Güntherodt, G. Güntherodt, R. J. Gambino, and R. Ruf, 1990, Phys. Rev. Lett. **65**, 247.
Wijngaard, J. H., C. Haas, and R. A. de Groot, 1989, Phys. Rev. B **40**, 9318.
Wijngaard, J. H., C. Haas, and R. A. de Groot, 1992, Phys. Rev. B **45**, 5395.
Wurmehl, S., G. H. Fecher, H. C. Kandpal, V. Ksenofontov, C. Felser, H.-J. Lin, and J. Morais, 2005, Phys. Rev. B **72**, 184434.
Xiang, H. J., J. Yang, J. G. Hou, and Q. Zhu, 2006, J. Am. Chem. Soc. **128**, 2310.
Xie, W.-H., B.-G. Liu, and D. G. Pettifor, 2003, Phys. Rev. B **68**, 134407.
Xie, W.-H., Y.-Q. Xu, B.-G. Liu, and D. G. Pettifor, 2003, Phys. Rev. Lett. **91**, 037204.
Yablonskikh, M. V., Y. M. Yarmoshenko, V. I. Grebennikov, E. Z. Kurmaev, S. M. Butorin, L.-C. Duda, J. Nordgren, S. Plogmann, and M. Neumann, 2001, Phys. Rev. B **63**, 235117.
Yamasaki, A., 2006, unpublished.
Yamasaki, A., L. Chioncel, A. I. Lichtenstein, and O. K. Andersen, 2006, Phys. Rev. B **74**, 024419.
Yanase, A., and K. Siratori, 1984, J. Phys. Soc. Jpn. **53**, 312.
Yarmoshenko, Y. M., M. I. Katsnelson, E. I. Shreder, E. Z. Kurmaev, A. Slebarski, S. Plogmann, T. Schlathoelter, J. Braun, and M. Neumann, 1998, Eur. Phys. J. B **2**, 1.
Zener, C., 1951, Phys. Rev. **82**, 403.
Zhang, J., F. Ye, H. Sha, P. Dai, J. A. Fernandez-Baca, and E. W. Plummer, 2007, J. Phys.: Condens. Matter **19**, 315204.
Zhao, B.-H., H.-Q. Nie, K.-Y. Zhang, K. A. Chao, and R. Micnas, 1987, Phys. Rev. B **36**, 2321.
Zhao, G. L., J. Callaway, and M. Hayashibara, 1993, Phys. Rev. B **48**, 15781.
Zhao, J. H., F. Matsukura, K. Takamura, E. Abe, D. Chiba, and H. Ohno, 2001, Appl. Phys. Lett. **79**, 2776.
Zhao, K., J. Feng, Y. Huang, J. gao Zhao, H. Lu, X. Han, and W. Zhan, 2006, Appl. Phys. Lett. **88**, 052506.
Zhao, K., J. F. Feng, Y. H. Huang, J. G. Zhao, H. B. Lu, X. F. Han, and W. S. Zhan, 2005, Chin. Phys. **14**, 2595.
Zhao, Y.-J., and A. Zunger, 2005, Phys. Rev. B **71**, 132403.
Ziebeck, K. R. A., and P. J. Webster, 1974, J. Phys. Chem. Solids **35**, 1.
Ziese, M., 2002, Rep. Prog. Phys. **65**, 143.
Zurek, E., O. Jepsen, and O. K. Andersen, 2005, ChemPhysChem **6**, 1934.
Zutic, I., J. Fabian, and S. D. Sarma, 2004, Rev. Mod. Phys. **76**, 323.